AN INVESTIGATION OF RESIDUAL FUEL OIL ASH DEPOSIT FORMATION AND REMOVAL IN COOLED GAS TURBINE NOZZLES

by

John Clisby Blanton

Dissertation submitted to the Graduate Faculty of the
Virginia Polytechnic Institute and State University
in partial fulfillment of the requirements for the degree of

DOCTOR OF PHILOSOPHY

in

Mechanical Engineering

APPROVED:

W. F. O'Brien, Jr., Chairman

H. L. Moses

N. S. Eiss

A. M. Squires

J. L. Lytton

July, 1981

Blacksburg, Virginia

ACKNOWLEDGEMENTS

This dissertation represents the culmination of four years of research efforts by the author. The names of all those who have contributed in some way to these efforts are too numerous to mention here, but there are a number who deserve special recognition.

The author wishes to thank the members of his advisory committee for their contributions, and particular thanks go to his major professor, Dr. W. F. O'Brien, Jr., and to the department head,

.

There were many people at the General Electric Company in Schenectady, New York, who made invaluable contributions and deserve some recognition. Special thanks go to , ,

, , and . Without the support of these and many others, the experimental portion of this dissertation could not have been successful.

is acknowledged for the typing of the draft and final versions of the manuscript.

Last, but not least, the author wishes to thank his wife, , and his parents, , for their love, support (both emotional and financial), and continued encouragement throughout the years spent in pursuit of the master's and doctoral degrees.

TABLE OF CONTENTS

LIST OF FIGURES

LISTS OF TABLES

LIST OF SYMBOLS

English Symbols

A	area
a,b	constants in linearized throat area equations (4.4, 4.5)
c	specific heat
h	convective heat transfer film coefficient
k	thermal conductivity
L	vane cord length
$\dot{m}$	mass flow rate
NAIN	nozzle area index number, eq. (4.1)
Nu	Nusselt number
p	pressure
Pr	Prandtl number
$\dot{Q}$	heat transfer rate or heat load
R	specific gas constant
Re	Reynold's number
T	temperature
t	time
v	velocity

Greek Symbols

γ	specific heat ratio
μ	absolute viscosity
ρ	mass density

ϕ	dimensionless surface temperature, eq. (4.11)
Ω	resistance to heat transfer, eq. (4.13)

Subscripts

as	at the ash surface
cw	cooling water
g	gas
L	based on vane chord length
in	at the inlet
ms	at the metal surface
SF	suction face of nozzle vane
total	for the entire nozzle sector
03	stagnation property at nozzle inlet

Superscripts

( )*	at the nozzle throat
( )'	approximate quantity

1. INTRODUCTION

As supplies of light distillate petroleum fuels available for electric power generation are diminished, an increasing emphasis is being placed on fuels flexibility. This development has had a particularly sharp impact on the combustion turbine industry. The relatively low thermal efficiency of simple-cycle, heavy-duty combustion turbine engines has resulted in a low priority being placed on the procurement of clean fuels (e.g., light distillates and/or natural gas) for their consumption. The highest priority for clean fuel consumption has been assigned to consumer applications, such as transportation and home heating. Other applications, in particular electric power generation, are being gradually converted to alternative fuels. It is becoming apparent that for the heavy-duty combustion turbine industry to survive, two objectives must be met: (1) engine cycle efficiencies must be improved to become more competitive with other heat engines for power generation, and (2) the capabilities for utilization of alternative fuels must be fully realized and exploited.

A particular class of alternative fuels which appears to have abundant near-term availability is the heavy residual petroleum fuel (grade no. 6 fuel oil, or Bunker fuel). This fuel has been used for years in steam generating units and with varying success in combustion turbine engines (a detailed background will follow in a later section). The major problem encountered in the use of this class of fuel is that in the untreated state it contains metallic contaminants, in particular

sodium and vanadium, which are extremely corrosive to hot gas path alloys. State-of-the-art fuel treatment techniques have all but eliminated the corrosion problem, but have resulted in the creation of another problem. Corrosion inhibitors, added to the fuel, result in the formation of high-melting point ash species in the combustion products. This ash tends to form deposits on gas path surfaces. In steam generating units this results in decreased heat transfer to the working substance and necessitates cleaning of the surfaces periodically. This is not a major operational problem, however, as the deposit formation rates tend to be low enough that ash cleaning can be performed during regular shutdowns.

In combustion turbine engines, however, the ash deposits result in significant output power losses. The gas velocities in the hot gas path sections may be more than two orders of magnitude higher than those experienced in steam generating units. These high velocities result in higher ash deposit rates caused by ash particle impaction and other mechanisms. The output power losses due to the ash formation result from two effects: (1) a decrease in the mass flow capacity of the engine due to physical and aerodynamic plugging at the gas path passage throats, and (2) a decrease in the specific work output of the turbine due to a reduction in the efficiency (cascade losses). It should be pointed out that aerodynamic losses are extremely important in combustion turbines, whereas in steam generating units aerodynamics are relatively unimportant.

The current trend in combustion turbine engine design practice is

towards higher turbine inlet temperatures. The resulting increases in engine power output and simple-cycle thermal efficiency are strong incentives to continue this practice to the greatest possible extent. The major limitation in a conventional combustion turbine is the ability of the hot gas path components to withstand the combination of the high stress and high temperature conditions. Present state-of-the-art prime mover combustion turbine engines operate with maximum turbine inlet temperatures on the order of 1400 K. More advanced turbine cooling techniques, such as transpiration cooling, water cooling, etc., are being developed toward the goal of increasing this to 1900 K or higher.

An unfortunate consequence of the increasing gas temperatures in combustion turbine engines is the effect on the ash deposition when residual fuels are used. The rate of formation of ash deposits has been observed to increase dramatically with increased gas temperatures. In addition, the physical characteristics of the ash deposited from higher temperature gases differ markedly from the deposits formed at lower temperatures. In general the high temperature deposits are structurally harder and are more difficult to clean from the gas path surfaces. As a result, the problems previously described with ash deposits in combustion turbine engines are greatly intensified in advanced-design engines.

One concept for decreasing the ash deposition when ash-bearing fuels are used in high gas temperature conditions is the water-cooled turbine. In has been speculated that by maintaining gas path surfacetemperatures at 800 K and below the ash particles cannot form sufficiently strong

bonds to adhere to the surface.

The subject of the present dissertation is an investigation of ash deposit formation and removal in advanced-design combustion turbine engines. The principle experimental work focuses on water-cooled hardware of the type being evaluated for advanced-design high-temperature engines. The following are the basic objectives of the dissertation:

1. Assimilate data regarding field experience with the use of residual fuel oil in combustion turbine engines.
2. Assimilate data regarding experimental research with residual fuel oil use in laboratory gas turbine "simulators".
3. Evaluate the relation of laboratory "simulator" data to actual field experience.
4. Speculate on the impact of near-term advanced turbine designs on the use of residual fuel oil in combustion turbine engines.
5. Obtain and analyze experimental data involving residual fuel oil ash deposition in a turbine simulator using advanced-design turbine hardware.
6. Examine and discuss ash deposit rate data with respect to known previous experiments, and compare the results of the new tests with respect to parameter variation.
7. Examine in detail data from ash removal incidents, both localized and general, and use the observations to speculate on the ash deposit character and on-line cleanability in advanced-design turbines.

8. Examine in detail local heat transfer measurements and relate the observations to the ash deposit data.
9. Develop and demonstrate a technique for using existing field experience and turbine simulator data to predict the performance of advanced-design combustion turbine engines using residual fuels.
10. Make conclusions and recommendations regarding advanced-design turbine engines and residual fuel oil ash deposit formation and removal.

2. BACKGROUND

A listing of some of the more important properties of typical combustion turbine engine liquid fuels is given in Table 1 [1]*. The heavy residual fuel oil is of primary interest in this investigation. Note the high viscosity and specific gravity for the heavy residual oil as well as the high levels of ash and trace metal contaminants. It is because of these properties that difficulties arise in combustion turbine engine operation using these fuels.

The high viscosity of the residual oil results in numerous problems in fuel handling and combustion. In general, the stored fuel must be heated (usually with steam) before it can be pumped through the treatment and handling systems [2]. Proper atomization of residual fuel oil in the combustion chamber can be a serious problem. In some cases this problem is overcome by using high pressure air atomization [3]. The combustion flame resulting from the burning of residual oil has a much greater radiation strength than a clean flame. This results in higher combustion system hardware temperatures [2]. These and other problems related to fuel handling and combustion require appropriate attention but may usually be overcome without serious difficulty.

The more serious problems encountered with the use of residual fuel oil in combustion turbine engines involve the deleterious effects of the combustion products on the turbine hot gas path. These effects

---

*Numbers in brackets indicate references listed at the end of the dissertation.

TABLE 1

Properties of Typical Combustion Turbine Liquid Fuels

	True Distillates		Ash-bearing Fuels	
Fuel Type	Kerosene	No. 2 Distillate	Blended Residuals and Crudes	Heavy Residuals
Specific Gravity, 100 F (38 C)	0.78/0.83*	0.82/0.88	0.80/0.92	0.92/1.05
Viscosity, cSt, 100 F (38 C)	1.4/2.2	2.0/4.0	2/100	100/1800
Gross Heating Value, kJ/kg	44,790/45,840	43,950/45,840	43,950/45,630	42,490/43,950
Gross Heating Value, Btu/lb	19,300/19,700	19,000/19,600	19,000/19,400	18,300/18,900
Sulfur, %	0.01/0.1	0.1/0.8	0.2/3	0.5/4
Nitrogen, %	0.002/0.01	0.005/0.06	0.06/0.2	0.05/0.9
Hydrogen, %	12.8/14.5	12.2/13.2	12.0/13.2	10/12.5
Ash (Fuel as delivered), ppm	1/5	2/50	25/200	100/1000
Ash (Inhibited), ppm	-	-	25/250	100/7000
Trace Metal Contaminants (Untreated)				
Sodium	0/0.5	0/1	1/100	1/350
Vanadium, ppm	0/0.1	0/0.1	0.1/80	5/400
Lead, ppm	0/0.5	0/1	0/1	0/25
Calcium, ppm	0/1	0/2	0/10	0/50

*The slash (/) is intended to define the possible range of the parameter.

are generally divided into three categories for study: (1) erosion, (2) corrosion, and (3) deposition.

Erosion by particle impaction has been observed in combustion turbines operating on coal and coal-derived fuels [4,5], where particulate matter of size 5-10 μm and above are present. In the combustion of residual oil, particulate matter are generally in the submicron range and thus erosion has not been found to be a problem.

Corrosion in the turbine gas path is due primarily to the formation of vanadium pentoxide (V_2O_5) and sodium sulfate (Na_2SO_4) in the combustion products [6,7]. Sodium is present in the fuel as sodium chloride and is volatilized during the combustion process, combining with sulfur trioxide and water vapor as follows [8]:

$$2NaCl + SO_3 + H_2O \rightarrow Na_2SO_4 + 2HCl \qquad (2.1)$$

Since sodium chloride is water-soluble, it can be removed effectively from the fuel by water-washing and centrifuging the mixture [2,3].

Vanadium is present in the fuel in so-called "porhyrin" complexes [7], which are not water-soluble and cannot be removed from the fuel economically. The formation in vanadium pentoxide is described by:

$$2VO(OH)_3 \rightarrow V_2O_5 + 3H_2O \qquad (2.2)$$

In order to inhibit the formation of vanadium pentoxide in the combustion products, a chemical additive is introduced to the fuel which combines with the vanadium during the combustion process to form high melting point compounds. It has been found that magnesium, added to the

fuel at a 3-to-1 weight ratio to vanadium, provides adequate inhibition [3,6,7]. The magnesium combines with free oxygen to form magnesium oxide, which then combines with sulfur trioxide and vanadium compounds in the following reactions [9,10]:

$$Mg + \frac{1}{2} O_2 \rightarrow MgO\ (s) \tag{2.3}$$

$$MgO + SO_3 \rightarrow MgSO_4\ (s) \tag{2.4}$$

$$3MgO + V_2O_5 \rightarrow 3MgO \cdot V_2O_5\ (s) \tag{2.5}$$

$$2MgO + V_2O_5 \rightarrow 2MgO \cdot V_2O_5\ (s) \tag{2.6}$$

The compounds denoted by (s) are high-melting point solid species which form particulate matter in the combusion products. All have been shown to be stable compounds in an equilibrium calculation of the combustion reaction [10], and all have been identified in ash samples taken from combustion turbine engines burning residual fuel oil [3].

Effective fuel treatment of the residual oil prior to combustion in the turbine engine will effectively control corrosion [2]. The remaining problem which must then be faced is that of ash deposition. Note that all of the ash components of eqs. (2.3-2.6) are the result of the magnesium inhibitor added to the fuel. The ash deposition problem is thus one which is created by the solution to the corrosion problem.

As a combustion turbine engine is operated on a treated residual fuel, the ash particles tend to adhere to the turbine aerodynamic surfaces, resulting in a deterioration of the engine performance. To the operator of the engine there would be three noticeable indications:

(1) an increase in the compressor discharge pressure, (2) a decrease in the engine power output, and (3) an increase in the engine heat rate. The engine deterioration is due to the combined result of two effects [11]. The first and most obvious effect is the physical and aerodynamic restriction of the turbine passage throats. This restriction, or fouling, results in the increased compressor discharge pressure. The second effect causing engine performance deterioration is a decrease in the turbine efficiency (increased irreversibility) due to increased frictional losses, boundary layer separation, and increased secondary flow activity. These effects may all be characterized by total pressure losses relative to the turbine blade rows (cascade losses).

As a result of the turbine performance deterioration due to the ash deposit formation, the length of uninterrupted engine operation is limited. It has been observed, in some cases, that simply shutting the turbine engine down will result in a substantial deposit removal [2,3]. Combustion turbine engines used for intermittent and/or peaking applications would thus require less maintenance for active cleaning of the ash deposits. In other applications, where ash deposition rates are high or where continuous operation is desired, some method for cleaning the deposits must be applied. Cleaning procedures which have evolved through field experiences include off-line washing of the deposits and on-line removal by injection of abrasive material. The effectiveness of the cleaning procedures depends on the nature of the ash deposits themselves.

Ash deposit formation and removal in combustion turbine blade

passages has been studied extensively in pressurized turbine simulator test facilities [3,9,12-18]. These facilities generally involved the expansion of high-temperature, high-pressure combustion products through a stationary turbine nozzle cascade (one or more throats). The goal is to duplicate the hot gas path temperatures, pressures, and aerodynamics as closely as deemed necessary without the expenditures required for full engine tests. Turbine simulators have proved to be a very valuable tool in the investigation of turbine fouling or gas flow restriction as well as supplying information regarding ash character and cleanability. Unfortunately, data cannot be obtained from simulator experiments relating to cascade losses because the extreme gas path conditions prohibit the use of the necessary instrumentation. This makes it difficult to predict with certainty the overall performance deterioration in a full-scale engine from turbine simulator data alone. A comparison of turbine simulator data to actual engine performance will be discussed in a later section.

Past and on-going turbine simulation experiments involve not only simulated turbine conditions but also the use of a simulated fuel. These fuels are created by introducing additives to a no. 2 distillate fuel oil in the amounts necessary to achieve the desired contaminant levels. This enables accurate monitoring and control of the containment levels in the fuel and elminates the handling and treatment problems associated with the actual residual fuel. Both water-soluble [3,13-15,17,18] and oil-soluble [9,12,16] additives have been used successfully. A listing of some of the chemical additives used is given in

Table 2.

A few of the more important observations which have been made in turbine simulator tests are summarized below:

1. For a fixed geometry gas path, the major variables that have been studied are the gas temperature and pressure, the gas path surface temperature, and the contaminant levels in the fuel.
2. An increase in gas temperature with the other variables held constant results in an increase in the rate at which ash deposits form [13-15,18]. This effect has also been observed in full-scale engines [2].
3. The effect of changes in the gas path surface temperature has not been fully investigated. It has generally been thought that the deposit rates will be lower on cooled surfaces [3,19] due to decreased "sticking" effectiveness, but some investigators have found disagreement or conflicting results [15,16,18]. It has been speculated that deposit rates could be enhanced by cooling due to thermophoresis [20]. The effect of surface temperature is one of the subjects of the present investigation.
4. The effect of changes in gas pressure has not been fully investigated. There appears to be no change in the chemistry of the ash deposits formed at six atmospheres [18], and at three atmospheres [9,12], compared to those formed in an actual engine at twelve atmospheres [3].
5. The effect of increasing in equal proportions the contaminants in

TABLE 2

Additives for Residual Fuel Simulation

Contaminant Simulated	Additive	Contaminant Content, %wt	Solubility
Sulfur	Carbon Disulfide (CS_2)	84.2	Oil
Vanadium	Vanadium Napthenate	3	Oil
Vanadium	Vanadyl Sulfate ($VOSO_4$)	34.7	Water
Magnesium	KONTOL® KI-81	15	Oil
Magnesium	Magnesium Sulfate ($MgSO_4$)	20.2	Water
Sodium	Sodium Sulfonate	3	Oil
Sodium	Sodium Chloride	39.3	Water
Calcium	Calcium Napthenate	4	Oil

the fuel is to increase the ash load in the combustion products and thus increase the deposits proportionately. The ratios of the contaminant levels to each other are of critical importance to the character of the ash formed, particularly the sodium-to-vanadium (Na/V) ratio, the magnesium-to-vanadium (Mg/V) ratio, and the sulfur trioxide (SO_3) mole fraction [10].

6. The temperature at the gas-surface interface has a significant influence on the chemistry of the ash formed. Depending on the amount of sulfur in the fuel, the deposits formed at cooler surfaces will be predominantly soft, water-soluble magnesium sulfate ($MgSO_4$). At hotter surfaces, hard, insoluble magnesium oxide (MgO) will form. Since the deposit layer forming on a cooled surface has in insulating effect, the outer surface will become hotter and the potential for the formation of a layered deposit exists (see Fig. 1). This phenomena has been observed in turbine simulator experiments [3,13,18], and predicted using an equilibrium analysis of the combustion products [10]. This would tend to support the assumption that thermochemical equilibrium exists in the thermal boundary layer on the gas path surface.

7. The cleanability of the ash deposits has been observed to be directly related to the ash chemistry. The soft, water-soluble $MgSO_4$ deposits may be readily removed but the hard, insoluble MgO deposits are generally not readily responsive to on- or off-line cleaning procedures [13,14]. Ash cleanability is one of the subjects of the present investigation.

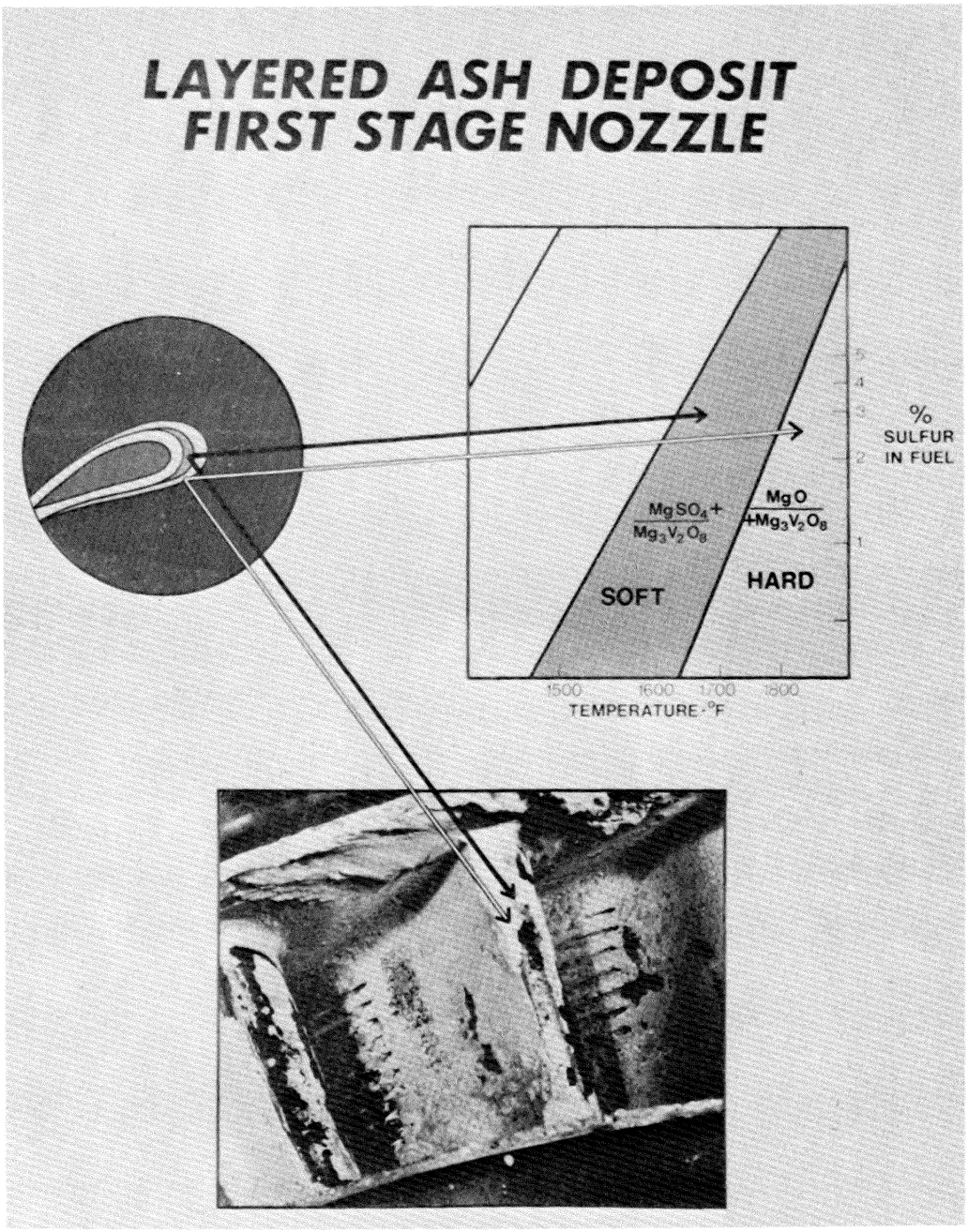

FIGURE 1

Layered Ash Deposit [3]

As previously mentioned, turbine engine designers are continuously striving to operate at higher gas temperatures for increased power output and higher engine efficiency. Materials currently used for hot gas path hardware can withstand temperatures of up to about 1150 K. For turbine inlet temperatures above this value, the gas path hardware must be cooled in some manner to prevent damage.

Consider as an example of a state-of-the-art heavy-duty combustion turbine engine the General Electric Company model MS7001E [21]. Development of this model was begun in 1973, and at design conditions (on no. 2 distillate fuel) the turbine firing temperature* is 1358 K. A three-stage turbine is used, and the first-stage nozzle and the first- and second-stage bucket row hardware are cooled by air extracted from the compressor. Special care was taken in the placement of the film-cooling holes in the first-stage nozzle in an attempt to minimize hole plugging by deposits [3]. This phenomenon has been observed in aircraft engine-type nozzle cooling hole arrangements [16] and in applications with coal-derived fuels [22].

For operation on residual fuel the MS7001E is derated from its design condition to a firing temperature of 1283 K, which reduces the power output from 75 to 65 MW. This compromise reduces the ash deposit formation rate and minimizes the formation of tenacious MgO deposits [14].

The next generation of combustion turbine engines will be designed for firing temperatures of approximately 1450 K, and eventually tem-

*General Electric defines the "turbine firing temperature" as the average stagnation gas temperature entering the first-stage rotor.

peratures of 1900 K and higher are projected [23]. To achieve these temperature levels, more advanced turbine cooling schemes are being developed.

One scheme which has been put forward for cooling of turbine hardware is the use of air transpiration-cooled materials. A semi-porous skin material is used through which cooling air uniformly (in theory) flows [24]. The boundary layer "blowing" would also seem to be an ideal way to protect the gas path surface from particle impingment [25]. At present the transpiration-cooled turbine has yet to be demonstrated at the prototype scale on any fuel.

Another scheme of turbine cooling is to increase the cooling coverage on a present-design aircraft engine-type arrangement. These designs feature a large number of small air-exit holes placed over much of the gas path surface, particularly at the airfoil leading edge [26,27]. This arrangement may have adequate high temperature resistance but would not be suitable for residual oil operation because of cooling hole plugging [16].

One turbine cooling scheme which appears to offer promising application to both high gas temperature design and use with residual fuel oil is a water-cooled turbine [15,17-19,23]. This particular scheme offers several advantages over conventional and near-term air-cooled designs: (1) very low surface temperatures allow for a wider choice of materials for optimum strength and corrosion resistance, and (2) no gas path coolant exit holes are exposed to possible blockage by deposits.

The evaluation of the water-cooled turbine during operation on residual fuel oil is one of the subjects of the present investigation.

3. DESCRIPTION OF EXPERIMENTS

3.1 Test Facilities

3.1.1 Turbine Simulator

The ash deposition experiments performed in support of the present investigation were carried out in a research vehicle known as the "turbine simulator", located at the General Electric Company's Corporate R R & D Center in Schenectady, NY. The construction of the simulator and performance of the experiments were carried out under the personal supervision and direction of the author.

The principle design features of the turbine simulator are shown in the schematic diagram of Fig. 2. The basic design philosophy of the simulator is to, given the constraints of the test system, kinematically and dynamically simulate as closely as possible the combustion and expansion processes of a full-scale engine combustor and first-stage turbine nozzle. The physical size limitation of the simulator is set by the available capacity of the existing air supply system. This particular simulator is designed to accommodate turbine nozzle cascade segments having throat cross-sectional areas of approximately $48(10^{-4})$ to $53(10^{-4})$ m^2. The design pressure for the combustion system is 6 atmospheres, which for a turbine inlet temperature of 1310 K results in a gas flow rate of approximately 3.2 kg/sec. This air flow and pressure matches approximately the full capacity of the test system air supply.

In order to accommodate the limitations of the air supply system,

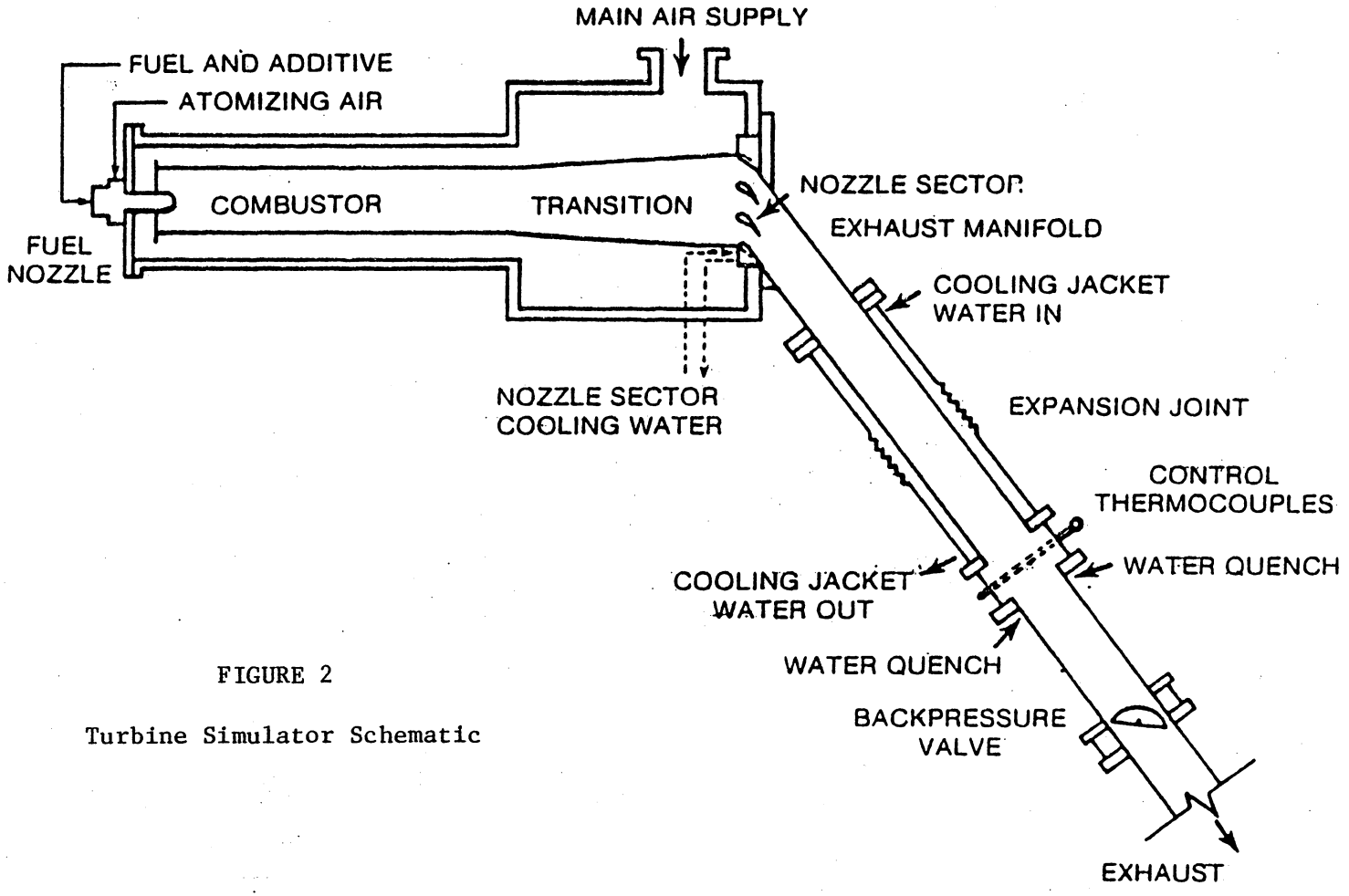

FIGURE 2

Turbine Simulator Schematic

the combustion pressure has been compromised. In a full-scale engine the compressor discharge pressure is considerably higher than 6 atmospheres. The MS7001E, for example, operates at 11.5 atmospheres [21]. This compromise was made in view of the fact that the turbine inlet temperature is the most important parameter in the ash deposition experiment and thus must be simulated as closely as possible. The reduction in pressure to 6 atmospheres is assumed to have no affect on the ash formation and deposition. Data from previous investigations, discussed in chapter 2, support this assumption.

The air flow pattern in the turbine simulator closely approximates the actual engine arrangement. Main air (simulating the compressor discharge) is delivered to the simulator at 6 atmospheres pressure and 561 K temperature from the air supply system. This air enters the top of the pressure vessel (see Fig. 2) and flows back into the combustor casing around the combustor liner. The primary air for combustion is metered through circular holes in the head end of the liner and secondary air enters through dilution holes and film-cooling slots along the length of the liner. An air-atomizing fuel nozzle is used and is located at the liner head end. Atomizing air is supplied to the nozzle at a maximum pressure of 12 atmospheres.

The combustion products leave the liner and enter a special curved transition piece. This reduces the flow cross-section from a circular to an annular segment shape, with an area reduction of approximately 2-to-1. The transition is of a "goose-neck" shape, such that the nozzle cascade is not directly exposed to the incandescence of the flame zone.

The nozzle cascade segments are especially fabricated for the turbine simulator from General Electric Company model MS3002 (11,000 hp) first-stage nozzle castings. Each segment consists of three (3) throat passages formed by four (4) nozzle vanes. The combustion products enter axially and are turned approximately 70-75 degrees, resulting in a flow area reduction of approximately 3.5-to-1. In testing the flow at the nozzle throat is sonic, assured by maintaining a greater-than-critical pressure ratio across the cascade (approximately 2-to-1).

In the testing done in support of the present program, two turbine nozzle cascade segments were used. An advanced air-cooled sector, fabricated for a previous test program, was used to provide baseline data for comparison with data from the tests using the second nozzle. The air-cooled sector utilized film cooling on the pressure and suction faces as well as both endwalls. This arrangement closely simulates the cooling scheme used on the MS7001E engine first-stage nozzle. The second nozzle cascade, especially fabricated for this program, was a monolithic, water-cooled design. The nozzle vanes and endwall sections were separately cast in Inconel alloy 718, machined and STEM*-drilled, and then assembled by electron-beam welding. A photograph of the finished nozzle sector is shown in Fig. 3. The nozzle mounting assembly and associated water distribution plumbing is shown in Fig. 4.

A cross-sectional schematic showing the overall geometric features of the nozzle cascade sector is shown in Fig. 5. This design is typical

---

* Shaped Tube Electrode Machining

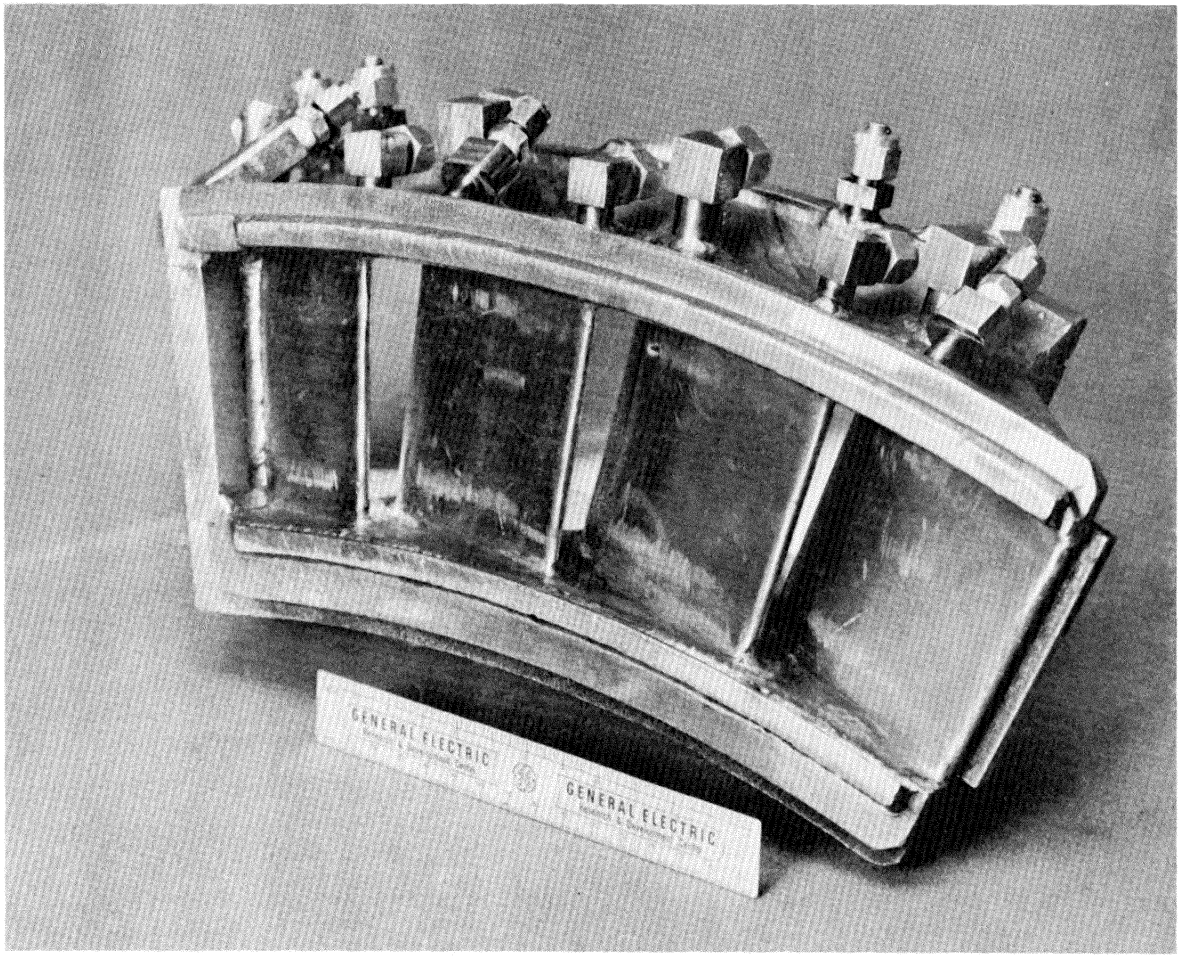

FIGURE 3

Watter-Cooled Nozzle Cascade Sector

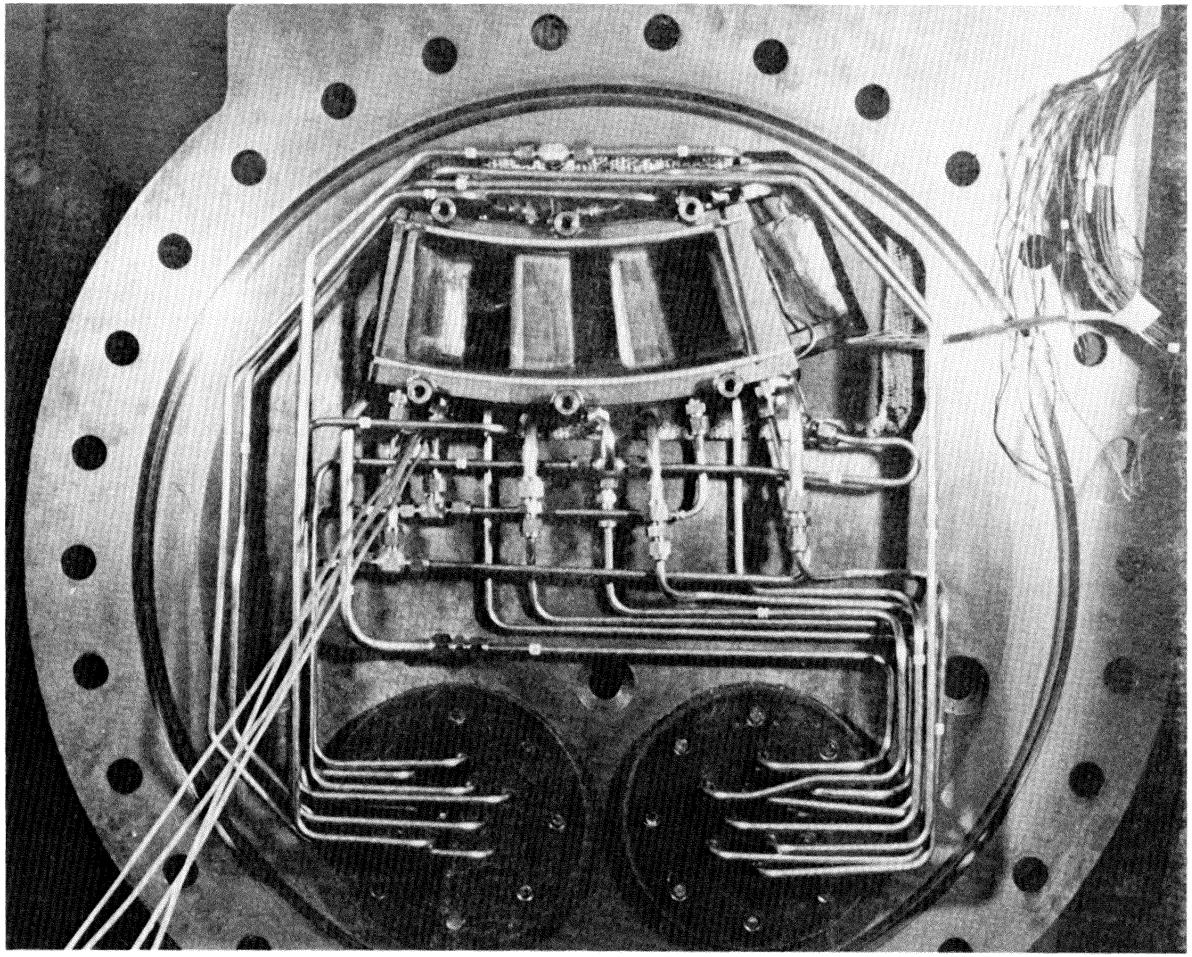

FIGURE 4

Nozzle Sector Mounting Assembly

WATER-COOLED NOZZLE
INSTRUMENTATION & AIRFOIL IDENTIFICATION

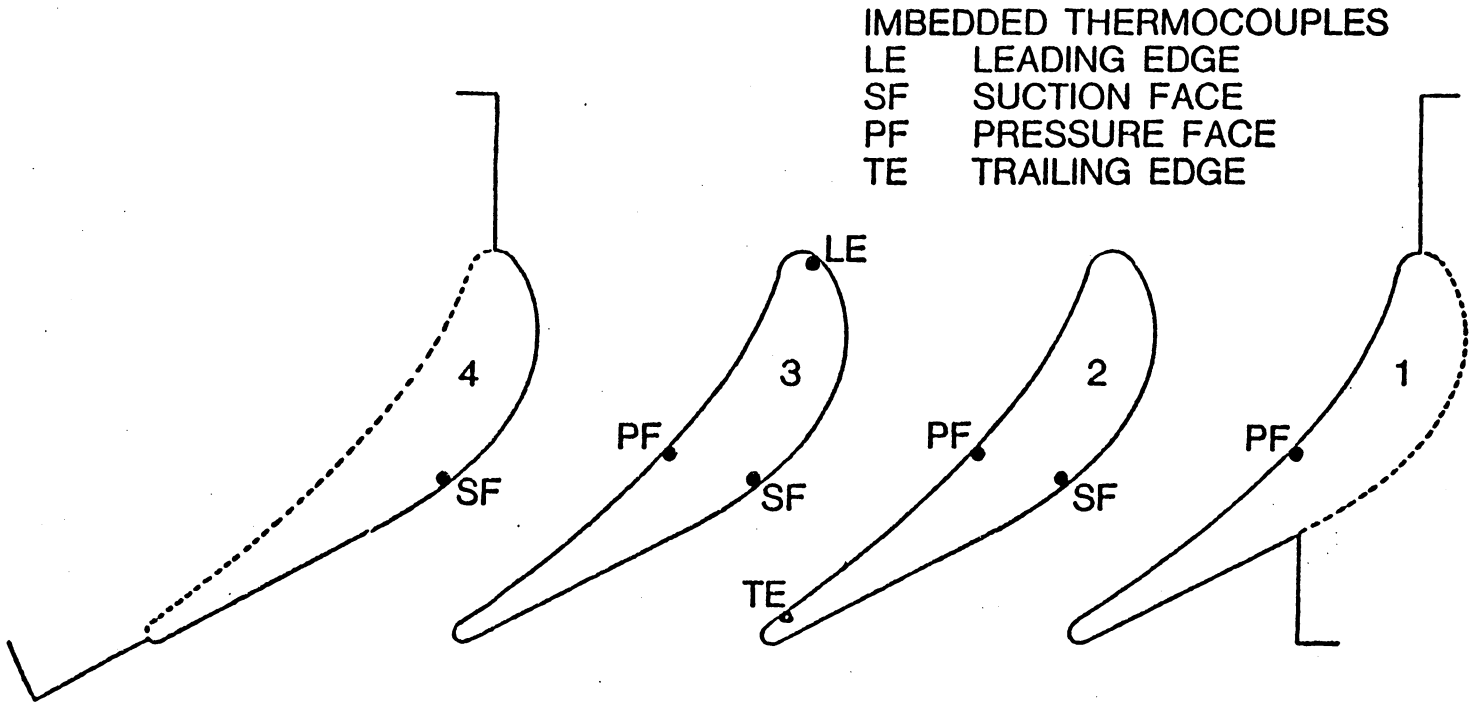

FIGURE 5

Nozzle Sector Cross Section Schematic

for low-reaction, highly-loaded first-stage nozzles on heavy-duty combustion turbine engines.

Exit gases from the nozzle are expanded into a water-cooled exhaust pipe and subsequently pass through a special section containing exhaust "control" temperature thermocouples. At the aft end of the section, the exhaust gases are quenched by the introduction of water. The quenched gases pass through a remotely-actuated butterfly valve used to control the system backpressure.

Figure 6 is a photograph of the turbine simulator test cell. Clearly visible are the turbine simulator, the main air supply line, the exhaust pipe, and both the air- and water-cooled nozzle sectors and mounting assemblies.

3.1.2 Support Systems

Air Supply

High pressure air is supplied to the turbine simulator by two 660-KW reciprocating air compressors. The nozzle segments and operating conditions selected for the turbine simulator were matched to the output capabilities of these compressors. Each compressor is equipped with inter- and after-coolers so that the compressor discharge air can be maintained at near-ambient temperature.

A non-vitiating gas-fired preheater is used to heat the high-pressure supply air to the desired combustor inlet temperature. This preheater is placed under automatic control during a long-term to

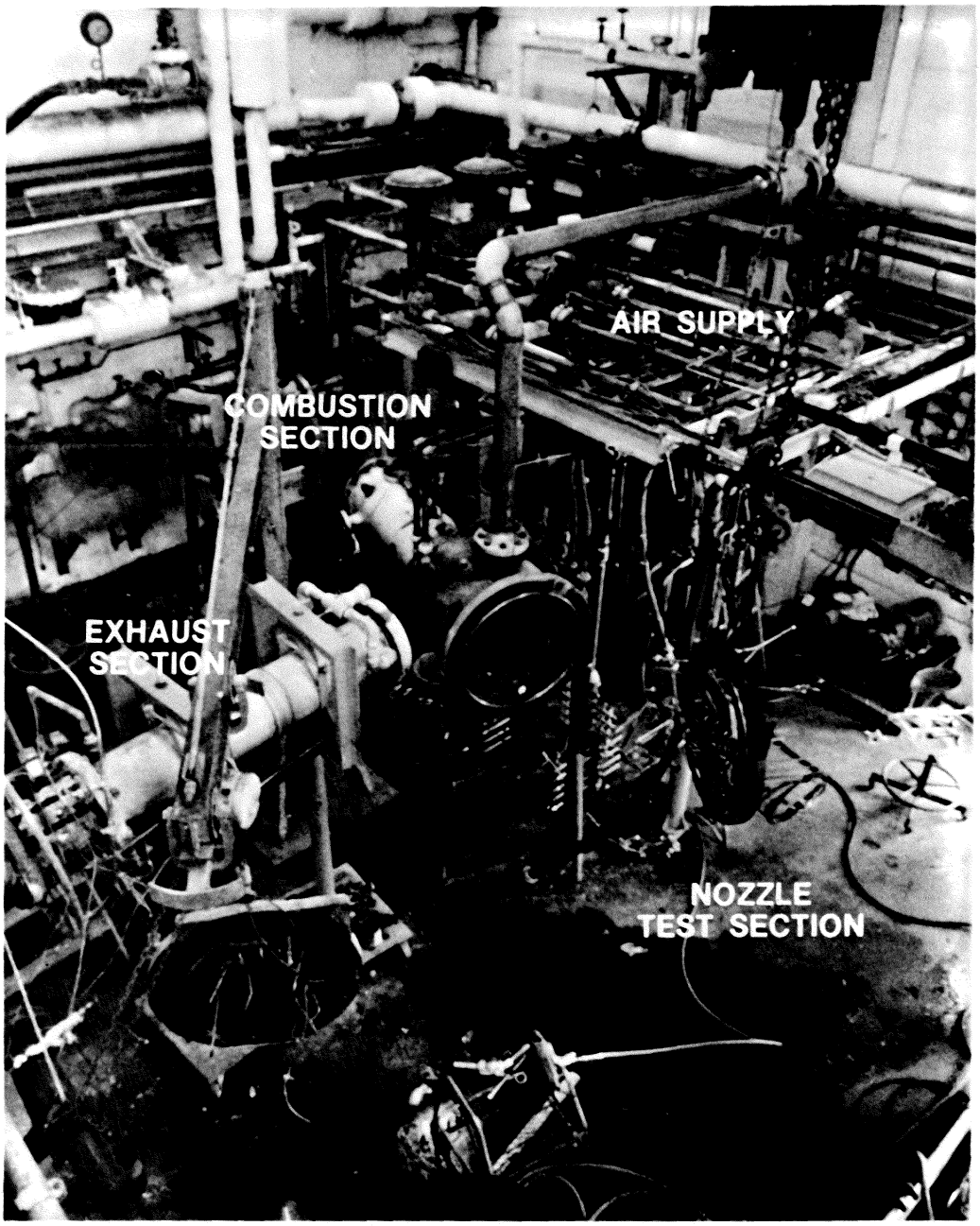

FIGURE 6

Turbine Simulator Test Cell

maintain constant air supply temperatures.

The nozzle coolant air for the air-cooled nozzle tests is extracted from the main air supply line downstream of the preheater and upstream of the main control value for the turbine simulator. This coolant air thus closely simulates the conditions in an actual engine. In an MS7001E, for example, the coolant air is extracted from between the 16th and 17th (next-to-last and last) compressor stages [21].

The fuel atomizing air is extracted from the main air supply upstream of the preheater and is thus approximately at room temperature.

Figure 7 is a schematic showing the turbine simulator support systems.

Water Supply

Coolant water used in the tests involving the water-cooled nozzle sector is supplied to the turbine simulator facility from a closed-circuit system at a pressure of approximately 6.9 MPa. The water is metered to the rig through ten (10) individual supply lines to the four nozzle vanes and to the inner and outer endwalls of the three throat passages. The four vanes are each on separate circuits and the endwalls are partially manifolded together such that there are nine (9) individual return lines from the nozzle sector. The supply lines are those on the lower right in Fig. 4 and the return lines are those on the lower left.

The closed-circuit water supply system consist of a high-pressure

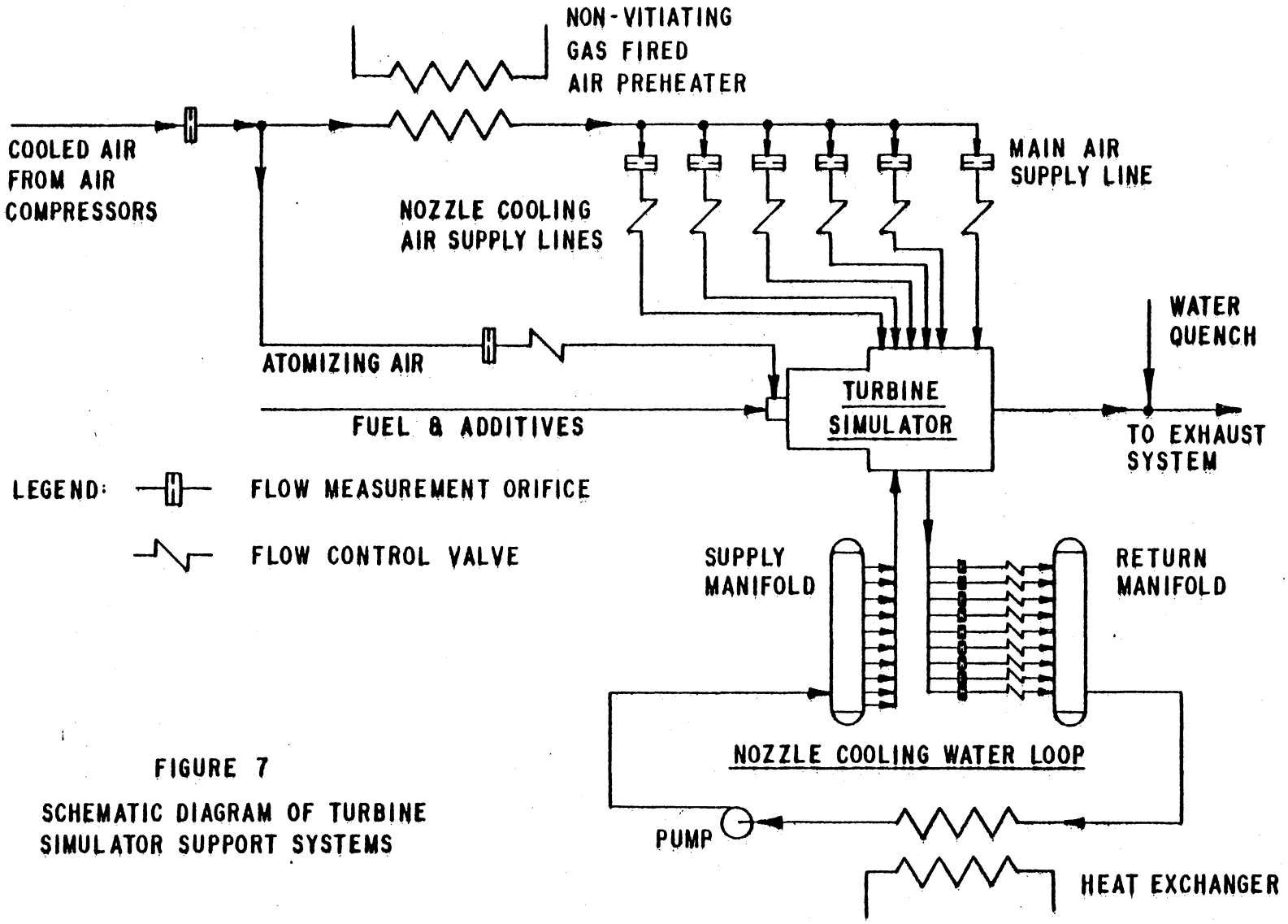

FIGURE 7

SCHEMATIC DIAGRAM OF TURBINE
SIMULATOR SUPPORT SYSTEMS

delivery pump, low-pressure boost pump, and two heat exchangers. One heat exchanger, located on the return line, is used to remove the heat added to the coolant water in the nozzle sector. The second heat exchanger, located on the supply line, was intended for use in pre-heating the supply water. This option was not exercised in this program. A demineralizer was also installed in the circuit. The nominal flow rate for the water circuit is approximately 60 ℓ/min.

Fuel Supply

A simulated residual fuel was used in all testing in the turbine simulator. A no. 2 distillate was doped with various oil- and water-soluble additives to achieve the desired contaminant levels. Water-soluble additives were used for sodium, magnesium, and vanadium. Oil-soluble additives were used for sulfur and calcium (see Table 2).

A schematic of the fuel supply and additive system is shown in Fig. 8.

Test Control

During long-term tests involving the turbine simulator and the various support systems the entire test operation is placed under automatic control. The actual control elements are remotely-controlled valves on the natural gas supply to the air preheater and on the fuel flow to the turbine simulator. The control variables are the preheater discharge air temperature and the turbine simulator exhaust gas

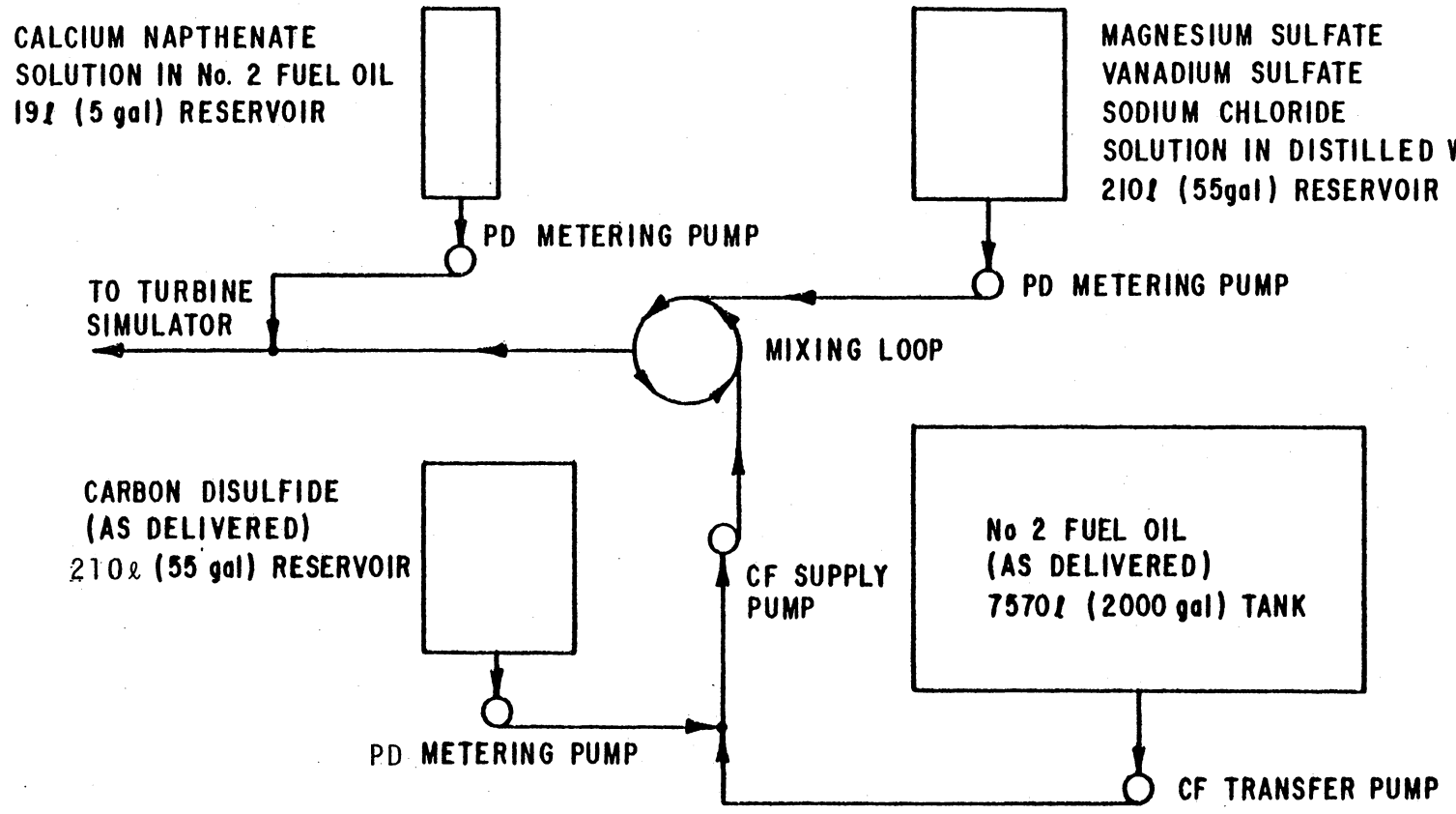

LEGEND: PD - POSITIVE DISPLACEMENT
CF - CENTRIFUGAL

FIGURE 8

SCHEMATIC DIAGRAM OF
FUEL AND ADDITIVE SYSTEM

temperature, respectively. The test operator selects the dead band and the control response rate for each controller.

The critical operational and research data are monitored continuously on-line by a computer-based data-acquisition system (described below). In several cases certain variables are specially monitored and compared against maximum and/or minimum values input by the test operator. Alarm and abort sequences can be enabled to protect test hardware (and personnel), should an emergency situation arise.

Data Acquisition

The turbine simulator and support systems are heavily instrumented to provide data for both operational and research purposes. In all cases, remote transducers were used to gather data. The transducer signals were collected, conditioned, converted to engineering units, and stored by a computer-based data acquisition system. A simplified schematic diagram of the system is shown in Fig. 9. The raw test data were reduced on-line by a computer program which executed for each data sample taken. All raw and reduced data were available for on-line display at CRT terminals or data for the entire test could be plotted on-line for inspection.

All temperature data were taken using chromel-alumel (type K) thermocouples. An electric uniform temperature reference (UTR) was used for temperature compensation. Some of the more important temperatures measured were air and water temperatures at flow-measurement orifices (for density and viscosity calculation) and in coolant inlet and return

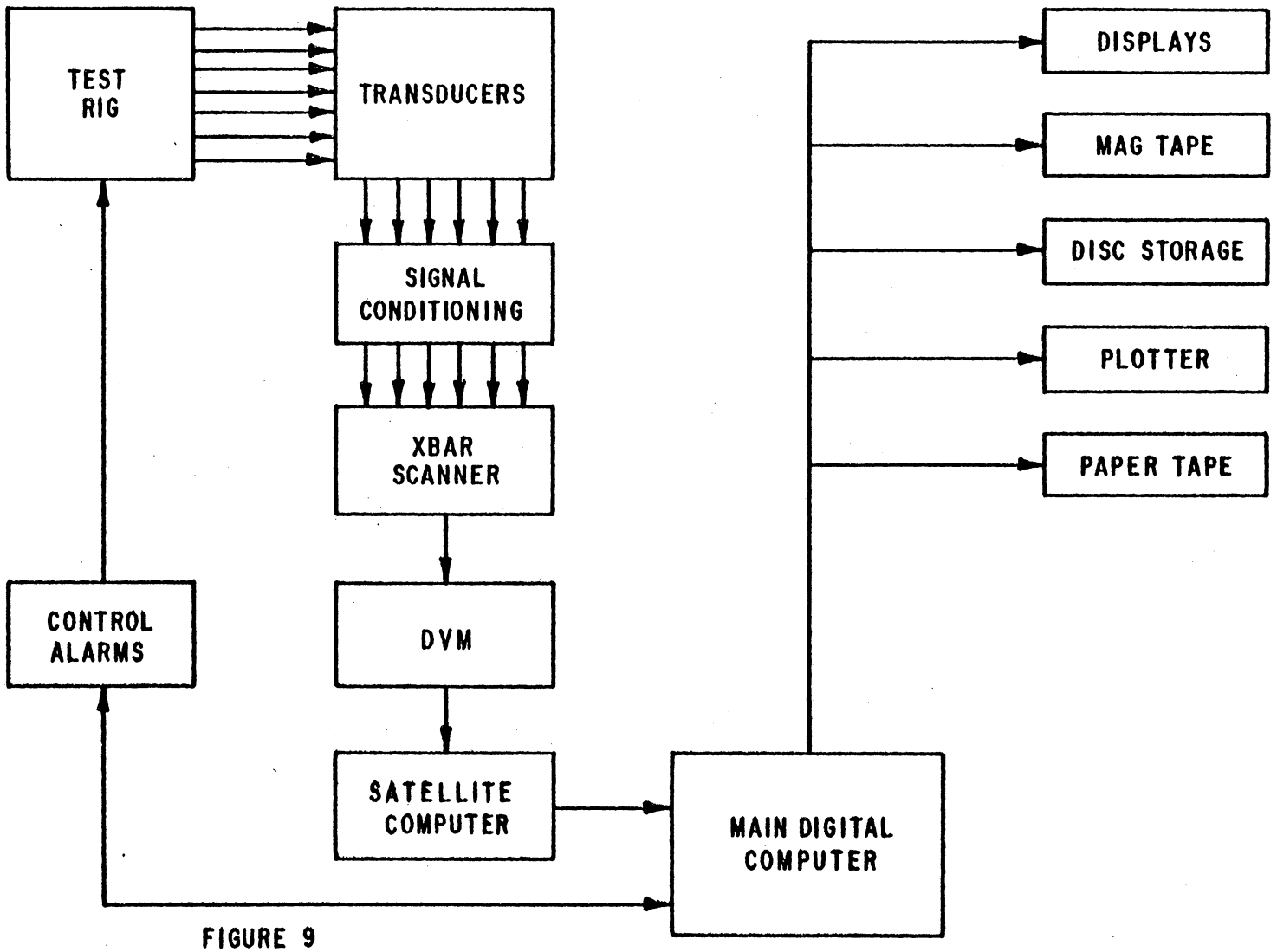

FIGURE 9
SCHEMATIC OF DATA AQUISITION SYSTEM

lines for heat transfer calculations. The air preheater outlet temperature and the simulator exhaust temperature were provided with multiply redundant measurement because of their importance as control variables. Surface metal thermocouples were installed in the turbine nozzle cascade sector to measure hot gas path surface temperatures. The combustor liner was also provided with thermocouples, mainly as a protective measure.

Fluid pressures were measured using strain-gage pressure transducers. Three scanning valve systems, two for air and one for water, were available and were used for most measurements. Individual, dedicated transducers were used for a number of the more critical pressure measurements to provide redundancy. In addition, several differential pressure (dp) transducers were provided for situations where a particularly accurate measurement of pressure difference was required, e.g., fluid flow measurement orifices.

The fuel flow rate is an extremely important measurement in that it is used in the calculation of the combuster exit temperature. The fuel flow was measured using a turbine flow meter.

In addition to the various transducer data mentioned above, a substantial amount of data was taken manually during the tests by the operating personnel. A number of pressures, temperatures, fluid levels, and rotameter readings were taken. These data were valuable as a check on the proper operation of the data acquisition system. The fuel additives were monitored closely to insure proper contaminant levels were achieved. One very important manual data measurement was an

on-line, free oxygen gas analysis of the exhaust products. This information provided an additional means for computing the fuel/air ratio.

3.2 Test Plans

There were several overall objectives identified for the turbine simulator test program planned in support of the present investigation. The General Electric Company has proposed the program* as a demonstration that water-cooling will lead to increased engine availability in heavy-fuels applications because of lower rates of ash deposit formation and/or enhanced cleanability of deposits. To accomplish this, it was proposed to fabricate a water-cooled turbine nozzle cascade segment to be tested in the turbine simulator facility. The results, in terms of ash deposit formation rate and cleanability, would be compared to results of baseline tests performed using a state-of-the-art, air-cooled nozzle.

From a more fundamental standpoint, this test program provided the opportunity to investigate the effect of various operational parameters on ash deposit formation and removal. The effect of gas temperature was already well-known, but effect of parameters such as gas path surface temperature and gas pressure had received little attention in the prior work. Although the number of tests available restricted performance of a comprehensive investigation, some consideration for

---

*Water-Cooled Gas Turbine Development Program
Contract RP 234-3 Task 6.0 Funded by the Electric Power Research Institute (EPRI)

evaluation of the effect of these parameters was given during the planning of the test program.

The test schedule as initially planned included six (6) tests. The first four of these served as a two-point investigation of the effect of gas temperature variation in both the air- and the water-cooled nozzle test sections. The initial pair of tests were performed at an engine firing temperature of 1283 K, a value typical of the rated full-load condition of current-design combustion turbine engines intended for residual fuel oil application. The remaining four tests were performed at a 1394 K engine firing temperature, representative of next-generation engines. The first two of these tests would complete the gas temperature investigation. The second two were included to investigate ash cleaning procedures, calcium variation, etc., to be specified at a later date. All six tests were performed at the standard simulator conditions of 6 atmospheres chamber pressure and 561 K combustor inlet temperature.

Two (2) additional tests were included in the test program. These tests were performed at a chamber pressure of 3 atmospheres, with all other conditions the same as for the previous four tests. The first of these tests was performed with the water-cooled nozzle sector; the second test used the air-cooled nozzle. These tests were intended not as an investigation of the pressure effect but primarily to study the effect of very low gas path surface temperatures. The lower gas pressure resulted in a decreased gas-side heat transfer film coefficient and substantially lower surface temperatures.

4. DATA ANALYSIS

4.1 Throat Plugging Data Reduction

The single most important parameter used to characterize ash accumulation is the cascade mass flow capacity, referred to by the General Electric Company as the nozzle area index number (NAIN), given by the equation

$$NAIN = \dot{m}_g \frac{\sqrt{T_{03}}}{P_{03}} \tag{4.1}$$

Note that eq (4.1) is a simplified version of the relation for the throat area of a frictionless, adiabatic, sonic nozzle, given by the equation [28]

$$A^* = \frac{\dot{m}_g}{P_{03}} \frac{RT_{03}}{\gamma} \left(\frac{\gamma+1}{2}\right)^{\frac{\gamma+1}{\gamma-1}}{}^{1/2} \tag{4.2}$$

In a turbine simulator test where ash deposits are fouling the gas path, a quantitative assessment of the degree and rate of blockage can be gained by observing changes in the above quantities. Either quantity may be used, however, eq. (4.2) is preferred as variation of gas properties for testing at variable temperatures is accounted for. Also, the interpretation of the throat area A* as a meaningful physical parameter give this quantity additional preference.

It should be pointed to that in operation the turbine nozzle sector is neither frictionless nor adiabatic. The throat area A* will thus not represent the actual physical throat area of the turbine nozzle, but will be smaller due to the constricting effect of the hydrodynamic

boundary layers. From this it is clear that decreases in A* will not only indicate physical blockage due to ash layers formed in the turbine passage throats, but also aerodynamic blockage due to increasing boundary layer thickness, secondary flows, and/or flow separation. In this respect the value of A* as a blockage parameter is not diminished, as the aerodynamic blockage is just as important thermodynamically as the physical blockage, i.e., they both result in the same effect in the actual turbine. From an engine operation standpoint, however, the throat area A* variation will not completely characterize performance degradation, as no information is conveyed regarding the turbine stage efficiency. Here the aerodynamic effects dominate over the physical blockage in causing performance losses. This point will be discussed in greater detail in chapter 7.

The heat transfer which occurs in the turbine passage will also have an affect on the applicability of the throat area A* as a blockage parameter. Since the combustion gas has a Prandtl number less than unity, the thermal boundary layer will, in theory, be slightly thicker than the hydrodynamic boundary layer. This means the heat transfer effects will extend into the region of nominally frictionless flow. The effect, however, will be slight since the Prandtl number is near unity. In addition, the heat transfer is decreased during operation due to the thermal barrier insulating effect of the ash deposit layers. In evaluating data for the present test program, the effect of convective heat transfer on the variation of the throat area A* will be neglected.

The mass flow of combustion products, $\dot{m}_g$ in eq. (4.2), was determined by summing the measured compressor delivery air flow rate and the fuel flow rate. The air mass flow was measured using a sharp-edged pipe orifice and appropriate pressure and temperature transducers. The fuel flow, as mentioned previously, was measured using a turbine flow meter. The nozzle inlet stagnation pressure p_{03} was taken to be equal to the static pressure measured in the combustor liner head end (recirculation region). The nozzle inlet stagnation temperature was calculated from the measured air and fuel flow data and the combustor inlet temperature. The accuracy of this calculation was verified by a thermocouple probe upstream of the nozzle sector and an analysis of the free oxygen in the exhaust products. The critical variables for the air flow and nozzle inlet temperature calculations were input to an on-line calculation program which executes for every sampling of the test data. The throat area, given by eq. (4.2), was also calculated by the program.

The rate of ash deposit formation or fouling in a turbine nozzle expressed in terms of the percentage decrease in NAIN or A* per 100 hours of operation. Thus, in terms of throat area A*, the following relation was used to express ash plugging rates between time t_1 and t_2 in a test:

$$\frac{d}{dt}\left[\frac{A^*}{A^*(0)}\right] = \frac{A^*(t_1) - A^*(t_2)}{t_2 - t_1} \times \frac{1}{A^*(0)} \times 100 \times 100\% \qquad (4.3)$$

In previous turbine simulator tests, the nozzle throat area has been observed to decrease at a more or less constant rate [13,14]. To make

an objective evaluation of the rate of ash deposition, it has thus become the practice to fit a straight line through the data obtained during periods of ash accumulation. The plugging rate is then obtained by using the negative of the slope of this line in place of the term in brackets in eq. (4.3).

When some event occurs which results in the removal of ash deposits from the nozzle, there will be an increase in the throat area A*. This increase will appear in the data as a step discontinuity in the throat area A*, followed by a resumption in fouling with decreasing A*. The magnitude of the recovery may be quantified in several ways. In the present analysis area increase will be expressed as a percentage of the throat area change from the original, clean nozzle value up to that point in the test. The magnitude of the area increase will be evaluated not from discrete data points but from the linear approximations which best fit the data before and after the recovery. In this manner irregularities in the data are accounted for and a more objective evaluation of the recovery is obtained.

As an example, consider a test during which ash fouling data is obtained over two separate periods of uninterupted ash fouling separated by an incident of ash removal. Let t_1 and t_2 be the times at the start and end of the first period and t_2 and t_3 be the endpoints of the second period. The area recovery occurs at time t_2. Using the least squares method [29] of analysis of the discrete data, the following linear approximations are obtained:

$$A^*(t) = a_{12} + b_{12}t \; ; \qquad t_1 \leq t < t_2 \tag{4.4}$$

$$A^*(t) = a_{23} + b_{23}t \; ; \qquad t_2 < t \leq t_3 \tag{4.5}$$

The ash plugging rates (expressed a per cent plugging per 100 hours) for each period would be

$$t_1 < t < t_2 : \quad \frac{d}{dt}(A^*) = (-b_{12}) \times \frac{10^5}{A^*(0)} \quad \% \text{ per 100 hrs} \tag{4.6}$$

$$t_2 < t < t_3 : \quad \frac{d}{dt}(A^*) = (-b_{23}) \times \frac{10^5}{A^*(0)} \quad \% \text{ per 100 hrs} \tag{4.7}$$

The per cent recovery occurring at time t_2 is

$$\overline{\Delta A^*} = \frac{A^*(t_2+) - A^*(t_2-)}{A^*(0) - A^*(t_2-)} \times 100\% = \frac{a_{23} + b_{23}t_2 - a_{12} - b_{12}t_2}{A^*(0) - a_{12} - b_{12}t_2} \times 100\% \tag{4.8}$$

4.2 Heat Transfer Data Reduction

In the case of the water-cooled nozzle cascade sector a large amount of data were accumulated which could be applied towards an analysis of heat transfer phenomena in the nozzle sector. A number of imbedded surface metal thermocouples had been installed in the nozzle to monitor the metal temperatures. The location of these thermocouples at mid-span on the nozzle vanes is shown in Fig. 5.

The water coolant flow rates and temperatures are measured for each of the nine return lines from the turbine simulator. The total inlet flow rate and temperature are also measured. This allows not only a

closure check on the water flow rate, but also the overall nozzle heat transfer to be determined. Because of the manner in which the water circuits were interconnected in the nozzle sector, the only individual circuits which could be analyzed are the four airfoil circuits. The endwall circuits had common connections and could not be isolated for heat balance calculations.

The overall heat transfer to the turbine nozzle sector is calculated using

$$\dot{Q}_{total} = \sum_{j=1}^{9} \dot{m}_{cw,j}\, c_{cw}\, (T_{cw,j} - T_{cw,in}) \tag{4.9}$$

where the subscript j refers to the jth return circuit. The heat transfer to the individual vanes are calculated using

$$\dot{Q}_j = \dot{m}_{cw,j}\, c_{cw}\, (T_{cw,j} - T_{cw,in}) \tag{4.10}$$

Using the nozzle vane metal temperatures a measure of the local heat transfer characteristics of the airfoils can be determined. The dimensionless surface temperature at the location of a particular thermocouple is given by

$$\phi = \frac{T_{ms} - T_{cw,in}}{T_g - T_{cw,in}} \tag{4.11}$$

where the free stream gas temperature is the same as the turbine inlet stagnation temperature T_{03}. Note that the dimensionless surface temperature as defined can take on values from 0 to 1 with 1 representing an

uncooled (adiabatic) vane and 0 representing a perfectly cooled vane.

To aid in the analysis of local heat transfer to the free standing turbine vanes a simple one-dimensional heat transfer network was devised. A schematic diagram of this network is shown in Fig. 10. Note that three nodes or stations are defined in the network. The first of these, at the low temperature end, represents the coolant water flowing through the 17 individual radial water passages. The temperature of this node is taken to be the average coolant temperature, defined by:

$$T_{cw,avg} = \frac{1}{2} (T_{cw,j} + T_{cw,in}) \tag{4.12}$$

The second node represents the airfoil metal surface. Its temperature is given by the imbedded surface metal thermocouple. Heat transfer between the first and second nodes is by forced convection in the water channels and conduction through the airfoil structure. The third node represents the surface of the ash deposit layer (should one exist). Heat transfer between the second and third nodes is by conduction. For a clean nozzle, $T_{as} = T_{ms}$. The fourth and final node represents the hot gas free stream. Its temperature is taken to be the same as the turbine inlet stagnation temperature T_{03}. Heat transfer between the third and fourth nodes is by forced convection.

The overall resistance to heat transfer between the endpoints of the network (i.e., the hot gas and the coolant water) is given by

$$\Omega_j = \left(\frac{T_g - T_{cw,avg}}{\dot{Q}}\right)_j \tag{4.13}$$

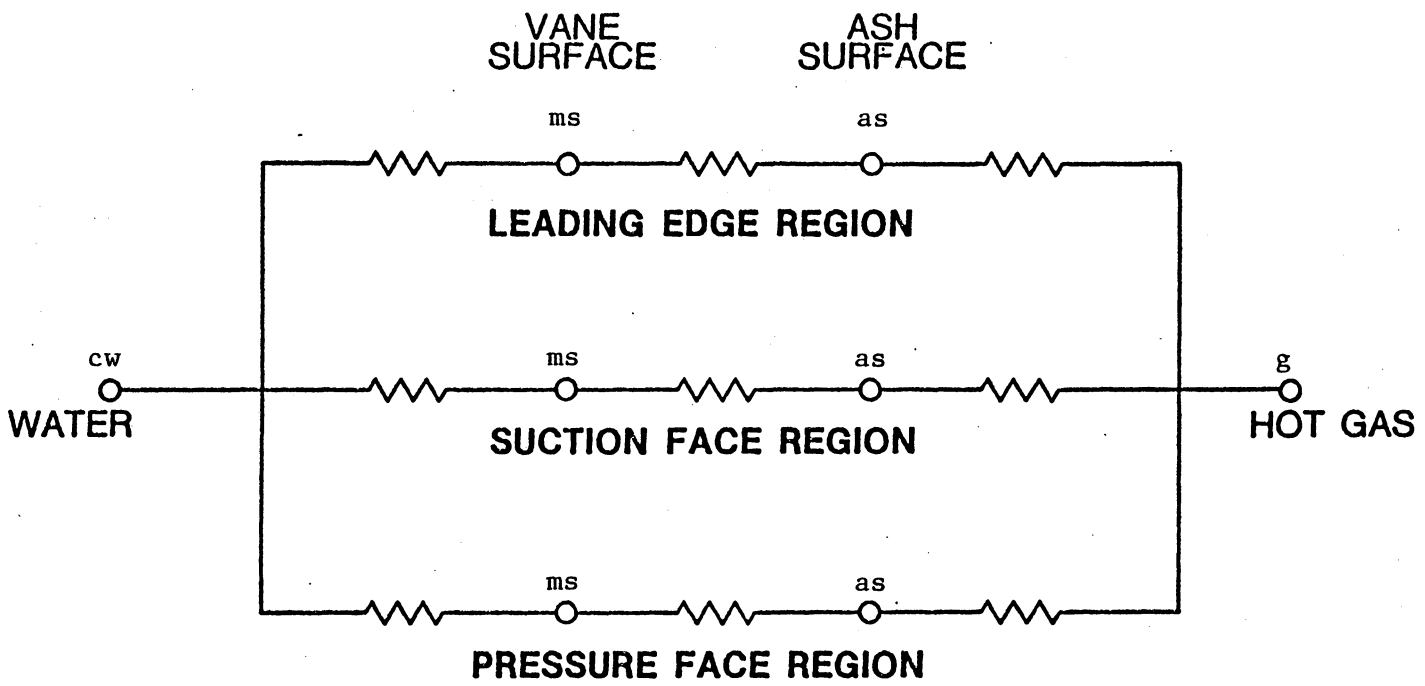

FIGURE 10

One-Dimensional Heat Transfer Analysis Network

This resistance is the overall equivalent resistance of the various one-dimensional parallel paths through which heat is transferred in the vane as modeled.

The effect of the ash deposit formation can best be characterized by observing changes in the surface resistance of the vanes. This includes the resistance between the second and fourth nodes (metal surface to hot gas). Consider, as an example, the surface resistance of the suction face of vane 2 (see Fig. 5 for vane nomenclature). This resistance is given by the expression

$$\Omega_{SF,2} = \left(\frac{T_g - T_{ms}}{\dot{Q}}\right)_{SF,2} \tag{4.14}$$

In the present experiment, eq. (4.14) cannot be evaluated as insufficient data are available for calculation of the heat flow through the individual branches of the network of Fig. 10. This difficulty will be avoided by simply using the overall vane heat transfer, eq. (4.10), in place of the individual branch heat flow in eq. (4.14). Thus

$$\Omega'_{SF,2} = \frac{(T_g - T_{ms})_{SF,2}}{\dot{Q}_2} \tag{4.15}$$

The prime (') in eq. (4.15) indicates the resistance is an approximate quantity. The branch surface resistance defined by eq. (4.15) will not represent a meaningful numerical value from an absolute standpoint. It does, however, present a useful parameter for characterizing relative changes in the surface resistance of a vane region during the course of

an experiment. Of course, some potential for error is introduced through the use of this analysis procedure should some significant shift in the relative heat flow distribution occur during an experiment.

The transfer of heat against the resistance defined by eq. (4.14), or similar expressions for other network branches, includes conduction through the ash layer (should one exist) and forced convection from the gas free-stream. Several factors are expected to influence the resistance. Conduction through the ash layer represents the simplest part of the problem, as the resistance of the ash layer is a function only of the thermal conductivity and thicknenss of the ash deposit. The forced convection problem is somewhat more complicated, however. Since in many multiple-mode heat transfer problems the convective film resistance is dominant, this facet will receive considerable attention in the analysis.

Dimensional analysis of the forced-convection heat transfer phenomena has shown [30] that expressions of the form

$$Nu_L = Nu_L\ (Re_L,\ Pr) \tag{4.16}$$

are useful in correlating experimental data. The Nusselt number is defined by

$$Nu_L = \frac{hL}{k_g} \tag{4.17}$$

where L is the characteristic length scale of the experiment. Equations (4.15) and (4.17) can be combined using Newton's law of cooling to

yield, with slight modification,

$$Nu_L = \frac{\dot{Q}_j}{(T_g - T_{ms})\, k_g\, L} \tag{4.18}$$

Equation (4.18) defines a dimensionless heat transfer conductance coefficient which, in theory, should reasonably correlate heat transfer data from the turbine simulator experiments.

The Reynold's number used in correlating turbine blade heat transfer data is generally based on the nozzle exit velocity and the airfoil chord length [31]. Again, modeling the turbine nozzle as a sonic isentropic nozzle, the following form is obtained

$$Re_L = \frac{\rho^* V^* L}{\mu^*} \tag{4.19}$$

where the characteristic length L, which also appears in eq. (4.18), is taken to be the airfoil chord length. Using isentropic flow relations [28], eq. (4.19) can be reduced to

$$Re_L = \frac{P_{03} L}{\mu^*} \quad \frac{\gamma}{RT_{03}} \left(\frac{2}{\gamma+1}\right)^{\frac{\gamma+1}{\gamma-1}} \quad 1/2 \tag{4.20}$$

The viscosity μ^* in eq. (4.20) is evaluated at the throat static temperature T^*, determined using

$$T^* = \left(\frac{2}{\gamma+1}\right) T_{03} \tag{4.21}$$

Again, since the turbine nozzle is not isentropic, the actual Reynold's number would be slightly less than the value given by eq. (4.20). The

theoretical Reynold's number will in any case be used in correlating the heat transfer and aerodynamic data. One of the advantages of using this form is the case of calculation; note the value of Re_L depends only on the turbine inlet temperature and pressure.

5. RESULTS

5.1 Operational Data

A listing of the turbine simulator test series performed in support of the present investigation is shown in Table 3. Note that seven full-length tests were performed. Four of the tests involved use of the water-cooled nozzle sector. Test number 4 also was performed using the water-cooled sector, but difficulties were encountered which cut short the test before any ash deposit data were obtained.

The nominal operating conditions for each of the tests are listed in Table 3. The turbine inlet temperatures are given in the table, but in the actual planning of the test program the turbine firing temperature is the parameter that is varied. Tests 1 and 2 were planned for a firing temperature of 1283 K and the remainder of the tests were to be performed at 1394 K. The actual range of conditions attained during the tests are also given in Table 3.

The simulated fuel used in the entire test series contained contaminants which simulated levels found in a typical residual oil specified by the program sponsor (E.P.R.I.). Contaminant specifications for the fuel are given in Table 4. These specifications are for the full prototype engine condition, which implies a combustor pressure of approximately 12 atmospheres. Since the turbine simulator is operated at a lower pressure, the mass flux of combustion products (and thus ash particles) through the nozzle will be lower by a proportional amount. In order to correct for this, the fuel contaminant levels in any given

TABLE 3

Nominal and Actual Test Conditions

Test	Type*	Turbine Inlet Temperature degrees Kelvin				Turbine Inlet Pressure atmospheres				Nominal Metal Temperatures degrees Kelvin (estimated)		Test Duration hrs
		Nominal	Actual			Nominal	Actual					
			avg	min	max		avg	min	max	avg	max	
1	AC	1305	1318	1300	1336	6.0	6.0	5.6	6.3	1090	1140	53.8
2	WC	1313	1311	1337	1247	6.0	6.5	6.1	6.7	670	780	64.7
3	AC	1429	1398	1454	1319	6.0	6.7	6.1	7.4	1140	1200	88.2
4	WC	1428	-	-	-	6.0	-	-	-	730	840	6.0
5	WC	1428	1421	1393	1448	6.0	6.3	5.8	6.7	730	840	48.4
6	WC	1428	1418	1245	1457	6.0	6.0	5.4	6.2	730	840	22.3
7	WC	1436	1433	1347	1456	3.0	3.1	3.0	3.1	590	700	61.5
8	AC	1425	1481	1434	1527	3.0	3.3	3.2	3.5	1000	1060	38.6

*Type designation: AC - air-cooled nozzle; WC - water-cooled nozzle

TABLE 4

Fuel Contaminant Specifications

Contaminant	Actual Engine Level - 12 atm ppm	Simulated Test Level - 6 atm ppm	Simulated Test Level - 3 atm ppm
Sodium	1	2	4
Vanadium	100	200	400
Magnesium	300	600	1200
Calcium	10	20	40
Sulfur	0.5%	1.0%	2.0%

test were adjusted upward to provide the same mass flux of ash particles through the nozzle as would be found in a full-size engine. These adjusted values are also given in Table 4. Some exceptions to this practice occurred in the latter two tests; these cases will be examined in more detail in the following section.

A brief description of each test follows.

5.2 Test Descriptions

Test Number One

This was the first test in the new turbine simulator and thus served as a system checkout as well as an ash deposit test. The air-cooled turbine nozzle cascade sector was used. The nominal turbine firing (nozzle exit) temperature was 1283 K, which for the air coolant flows used corresponded to a nozzle inlet temperature of approximately 1305 K. The combustor pressure was intended to be 6 atmospheres, and during the test was observed to vary from 5.6 to 6.3 atmospheres.

The duration of this test was approximately 54 hours. There was one uncontrolled shutdown of the test due to a malfunction of the flame detection system after approximately 27 1/2 hours of testing. The test was also terminated by a uncontrolled shutdown due to an operator error.

Following the final shutdown a test of off-line cleanability of the ash deposit was made. Water at a flow rate of approximately 28 ℓ/min was introduced through the fuel nozzle with an air flow of approximately 1 kg/sec. This would simulate the cranking conditions of a combustion

turbine engine. After a wash cycle of approximately 30 minutes and another 30 minutes soak period, the simulator was fired to the full test conditions for 10 minutes, then shut down and secured.

Test Number Two

The thermodynamic conditions for the second test were the same as for test number 1. In this case, however, the water-cooled nozzle cascade sector was used. For the nominal firing temperature of 1283 K and the expected nozzle heat transfer a turbine inlet temperature of 1313 K was required. The combustor pressure ran somewhat high in this test, varying from 6.1 to 6.7 atmospheres.

The duration of test number 2 was approximately 65 hours. There were no interruptions in the test operation and the simulator was shut down in a controlled manner. Approximately 45 hours into the test a malfunction in the fuel control resulted in a momentary increase in the firing temperature estimated to be of the order of 50 K.

At the termination of fired testing a water-wash/soak/refire sequence was performed using the same procedure as used in the previous test.

Test Number Three

This test, as well as all successive tests, was performed at a nominal firing temperature of 1394 K. The air-cooled nozzle sector was used, with film-cooling flow rates such that a turbine inlet temperature

of 1429 K was required. The combustor pressure was again somewhat high, ranging from 6.1 to 7.4 atmospheres.

Test number 3 was the longest of the test series at approximately 88 hours duration. A controlled shutdown was performed at a point 27 hours into the test to correct a problem with the additive system. This was the only interruption in the test, although an incident occurred 71 hours into the test due to an equipment malfunction which resulted in a momentary firing temperature increase. Henceforth incidents of increased firing temperature will be referred to as "thermal excursions".

A water-wash sequence was again performed at the conclusion of this test.

Test Number Four

This test was the first attempt to operate the water-cooled nozzle sector at the higher firing temperature (1394 K). A water system failure terminated the test after only six hours of operation.

Test Number Five

Test 5 was the first of two successive tests performed using the water-cooled nozzle sector at a 1394 K firing temperature and a nominal combustor pressure of 6 atmospheres. The actual combustor pressure varied from 5.8 to 6.7 atmospheres. The required turbine inlet temperature was 1428 K.

The duration of this test was approximately 48 hours. There were

no interuptions of continuous operation, although thermal excursions occurred at two points, approximately 10 and 36 hours into the test. A error in the preparation of additives was made which resulted in no sodium additive being introduced to the fuel after a point 19 hours into the test. The impact of this omission will be discussed in a later section.

After the ash deposit formation test, a water-wash sequence was performed.

Test Number Six

This was a short test (22.5 hours duration) used to verify the ash plugging results of test number five and to investigate on-line ash cleaning. The nominal test conditions were the same as for test five. The combustor pressure in test six varied from 5.4 to 6.2 atmospheres.

The first 18 hours of the test were used to establish the ash deposition rate. At that point an attempt at on-line ash deposit removal was attempted. A charge of approximately 4.5 kg of no. 16 mesh (maximum 1.5 mm) crushed walnut shells were injected into the combustor through a secondary air dilution hole using an external compressed air source. A second charge was injected 30 minutes later.

The test was terminated in an uncontrolled fashion due to a failure of the water system high pressure pump. For this test no attempt was made to water-wash the deposit.

Test Number Seven

Test 7 and 8 were added to the program as an investigation of the effect of reducing surface temperatures at the 1394 K firing temperature level. To accomplish this, the nominal combustor pressure was decreased from 6 to 3 atmospheres. The resulting lower hot gas path heat transfer coefficients yielded a reduction in surface metal temperatures (on the clean nozzle) of greater than 100 K.

This test used the water-cooled nozzle sector. The test duration was 61.5 hours, with no operational interruptions. This and the following test were the most involved of the series in terms of the number of on-line investigations and the amount of data gathered. Nutshell cleanings were attempted at three points and a brief investigation of the effect of atomizing air pressure variation was performed near the end of the test. The additive levels were also varied from the nominal engine levels in this and the following test.

Test Number Eight

This test was intended to duplicate the conditions of test number 7 except that in this case the air-cooled nozzle sector was used. The test duration was 39.2 hours. The same additive level schedule was followed. Two nutshell cleanings were attempted along with a third abrasive cleaning using coke instead of nutshells.

5.3 Ash Deposit Formation and Removal

The nozzle throat area histories for the seven full-length tests (1-3, 5-8) are shown in Figs. 11-18. The throat areas were calculated using eq. (4.2) and plotted against the real test time in hours. In each case the throat area was normalized using the value calculated for the clean nozzle at the beginning of the test. A test-by-test description of the throat area results follows.

Figure 11 shows the throat area history for test number 1. This test was performed using the air-cooled nozzle sector at a turbine firing temperature of 1283 K (see Table 3 for other conditions). Note that there are two periods of relatively steady ash deposit formation separated by an area increase which occurred between 27.3 and 29.5 hours into the test. This corresponds to the period directly after the sudden shutdown (test hours do not accumulate during shutdowns). The area increase was the result of the high thermal stresses experienced by the ash deposit during the sudden shutdown and subsequent restart. Some of the deposits fractured, spalled, and were swept away from the nozzle surface.

The throat area data before and after the recovery were analyzed using the least squares method to determine the best linear fit. The results are shown as solid lines in Fig. 11. The ash plugging rates for the two periods, as defined by eqs. (4.6) and (4.7), were 16.6 and 17.7 per cent per 100 hours, respectively. The throat area recovery, defined by eq. (4.8), was 27.5 per cent.

A water wash/soak/refire sequence was performed after the post-test

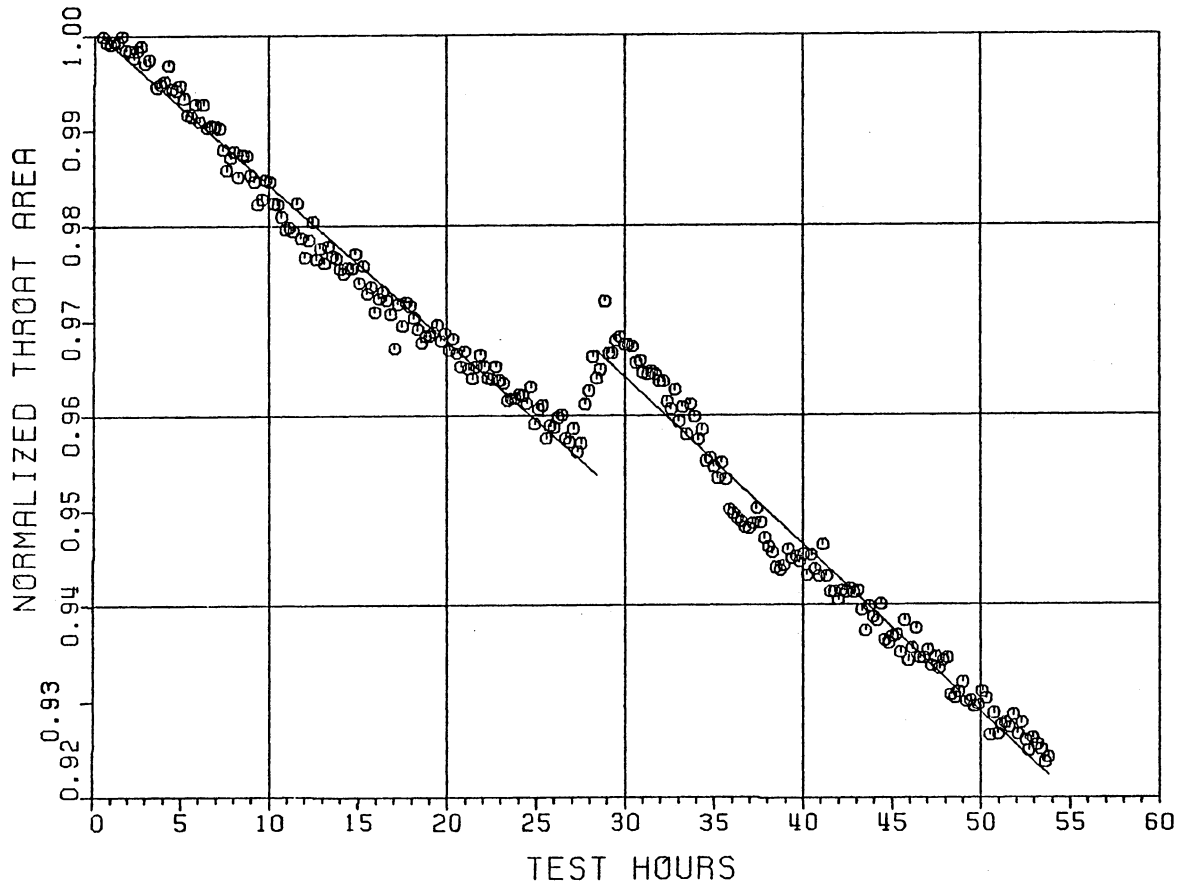

FIGURE 11
NOZZLE THROAT AREA HISTORY FOR TEST NUMBER 1

ash sampling and inspection were completed. An area recovery of approximately 90 per cent was obtained. Subsequent inspection of the nozzle revealed some light deposit remaining on the nozzle surfaces.

The film cooling air supplied to the nozzle sector was monitored very closely during this and all of the air-cooled tests. It was very interesting to note that in all tests there was no decrease in the coolant flow whatsoever. The implication is that despite the formation of a deposit layer on the nozzle vane surfaces, the film cooling air holes were not plugged at all. The deposit layer was in some cases observed to completely cover the film holes, but the cooling air was able to penetrate the layer by forming small "worm holes" in the deposit.

The nozzle throat area history for test number 2 is shown in Fig. 12. This test was performed under the same turbine firing conditions as test number 1, except that the water-cooled turbine nozzle sector was used. Note that two distinct periods of relatively steady throat area reduction are present separated by a pronounced recovery at a point 45.4 hours into the test. The straight-line approximations of the throat area data, obtained by linear regression analysis, are included as before as solid lines. The ash plugging rates for the two periods were 11.4 and 13.6 per cent per 100 hours, respectively. The throat area recovery at the 45.4 hour point was 43.3 per cent.

The sharp increase in the nozzle throat area is indicative of ash removal from the nozzle surface. In this particular case the ash removal was due to an accidental increase in the nozzle inlet temperature,

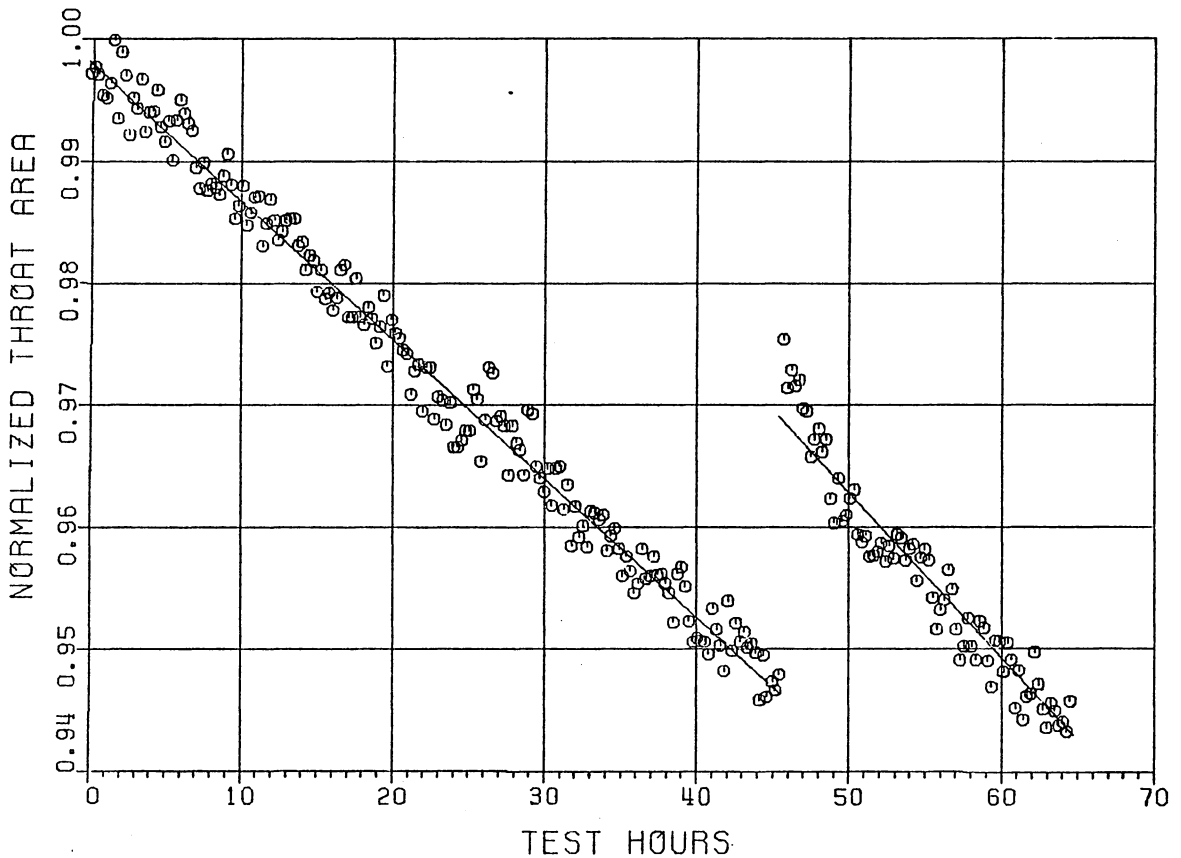

FIGURE 12
NOZZLE THROAT AREA HISTORY FOR TEST NUMBER 2

resulting in a spalling of the ash deposit layer caused by the sudden thermal stresses. The firing temperature increase was caused by a sudden accidental increase in the fuel flow rate resulting from a fuel control malfunction.

Following shutdown of the turbine simulator for inspection and sampling of the ash deposits, the rig was reassembled and a water wash/soak/refire sequence was performed. A 100 per cent recovery of the nozzle throat area was obtained, indicating complete removal of the ash from the nozzle sector. A visual inspection later verified this.

In test number 3 the air-cooled turbine nozzle sector was used. The turbine firing temperature was increased to 1394 K, consistent with the objectives of the near-term advanced cooling program. The nozzle throat area history for this test is shown in Fig. 13. Note the extreme amount of throat area plugging in this test. The throat area reduction at the conclusion of the test was in excess of 20 per cent. The throat area history was somewhat irregular, although clearly a near-linear reduction is observed. The throat area recovery 71 hours into the test was the result of a thermal excursion. Plugging rates before and after the excursion were 24.3 and 35.6 per cent per 100 hours. The throat area recovery caused by the thermal excursion was 22.5 per cent. As before, the solid lines plotted with the data represent the least-squares "best fit".

The thermal excursion which occurred 71 hours into the test was the result of a sudden decrease in the combustion air flow to the turbine simulator. The full air flow was restored very quickly, but gas

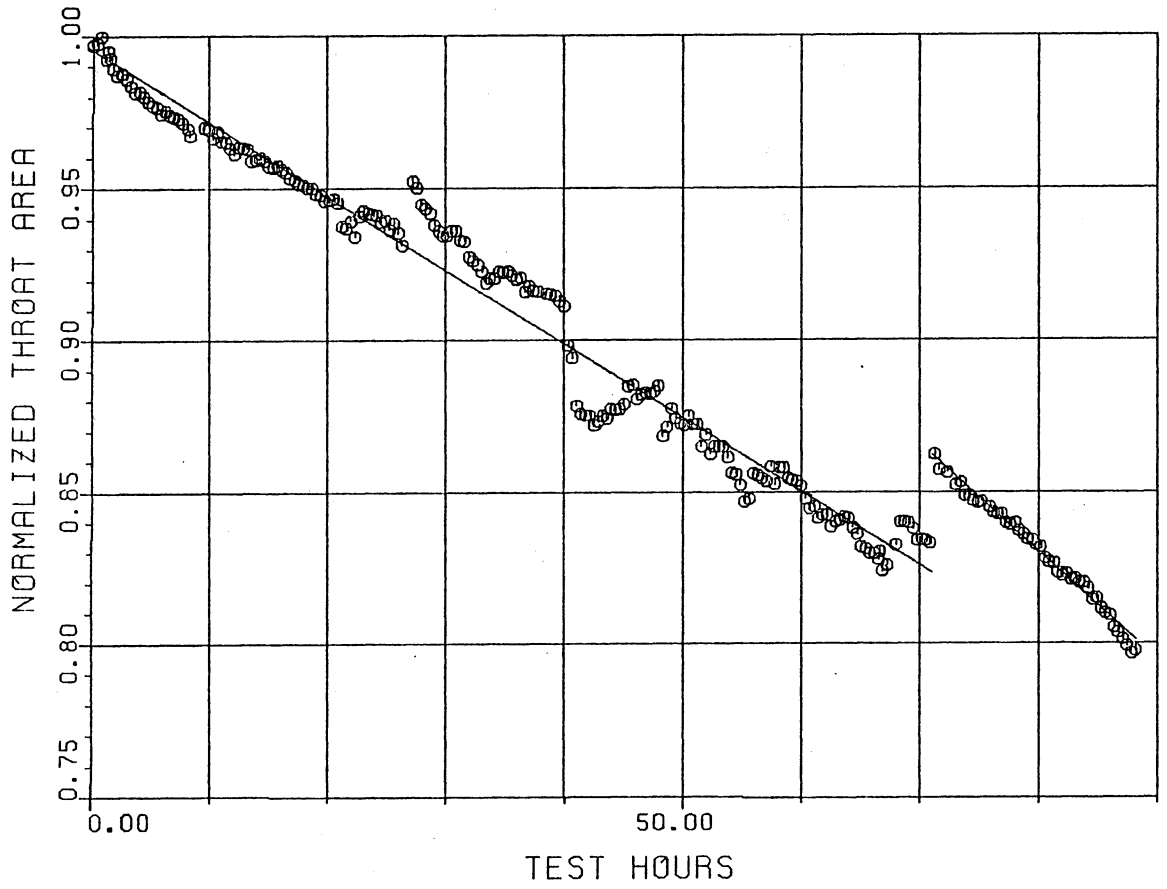

FIGURE 13
NOZZLE THROAT AREA HISTORY FOR TEST NUMBER 3

temperatures approaching 1800 K may have been reached for a period of one to two seconds (the temperature estimate is based on observations of air pressure gages for the main air flow orifice in the test control room). The high gas temperature affected ash removal by thermal shock.

Immediately following the test the turbine simulator was partially disassembled so that a visual inspection of the ash deposit could be made and ash samples taken. The rig was then reassembled for a water wash/soak/refire sequence. The nozzle throat area recovery was evaluated at approximately 90 per cent. A later visual inspection revealed a substantial amount of ash remaining on the nozzle, particularly on the pressure surfaces.

Test number 4 was the first attempt to operate the turbine simulator with the water-cooled turbine nozzle sector at the higher firing temperature of 1394 K. As mentioned previously, an equipment failure forced an early termination of the test. No useful data relative to ash deposition were obtained from this test.

Figure 14 shows the nozzle throat area history for test number 5. This test was performed at the higher firing temperature level of 1394 K, using the water-cooled turbine nozzle sector. Note that there are 3 distinct periods of uninterrupted operation with ash deposition, separated by throat area recovery phenomena 9.9 and 35.9 hours into the test. The straight-line regression approximations of the throat area are displayed in Fig. 14 as straight lines. The ash plugging rates for the three periods were 31.3, 42.5, and 69.9 per cent per 100 hours, respectively. The throat area recoveries were 67.7 and 54.9 per cent,

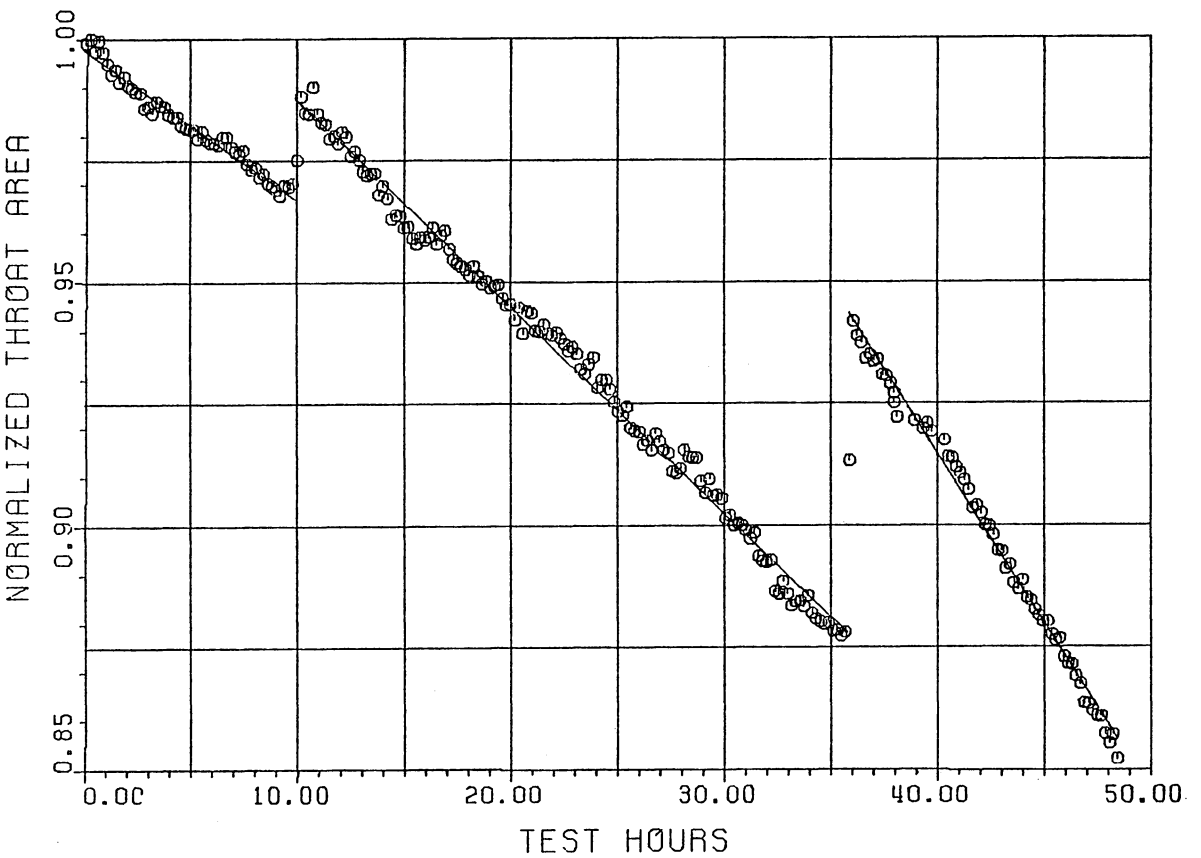

FIGURE 14
NOZZLE THROAT AREA HISTORY FOR TEST NUMBER 5

respectively.

The two nozzle throat area increases were both due to similar phenomena. In each case the turbine inlet temperature was allowed to increase accidentally, causing a loss of ash deposit through spalling. The nature of the gas temperature increase was, however, entirely different for the two instances. The first, which occurred 9.9 hours into the test, was the result of a sudden accidental increase in the fuel flow rate. This incident was similar to the thermal excursion which occured in test number 2. The second excursion, which occurred 35.9 hours into the test, was the result of a sudden decrease in the air flow supplied to the turbine simulator (such as occurred in test number 3). This resulted in an increased fuel-to-air ratio and thus a higher combustion temperature rise. The resulting increase in turbine inlet temperature was accompanied by a decrease in gas pressure. This characteristic is the major difference between this and the former temperature excursion, which occurred at essentially constant pressure. Henceforth thermal excursions of the former type will be referred to as "Type I" thermal excursions. The latter-type will be designated "Type II".

Following rig shutdown, a water wash/soak/refire sequence was performed as before. Nozzle throat area recovery was evaluated and found to be 100 per cent (the same as in test number 2). Visual inspection verified that no ash deposit remained on the nozzle.

The nozzle throat area history for test number 6 is shown in Fig. 15. The nominal firing conditions for this test were the same as for

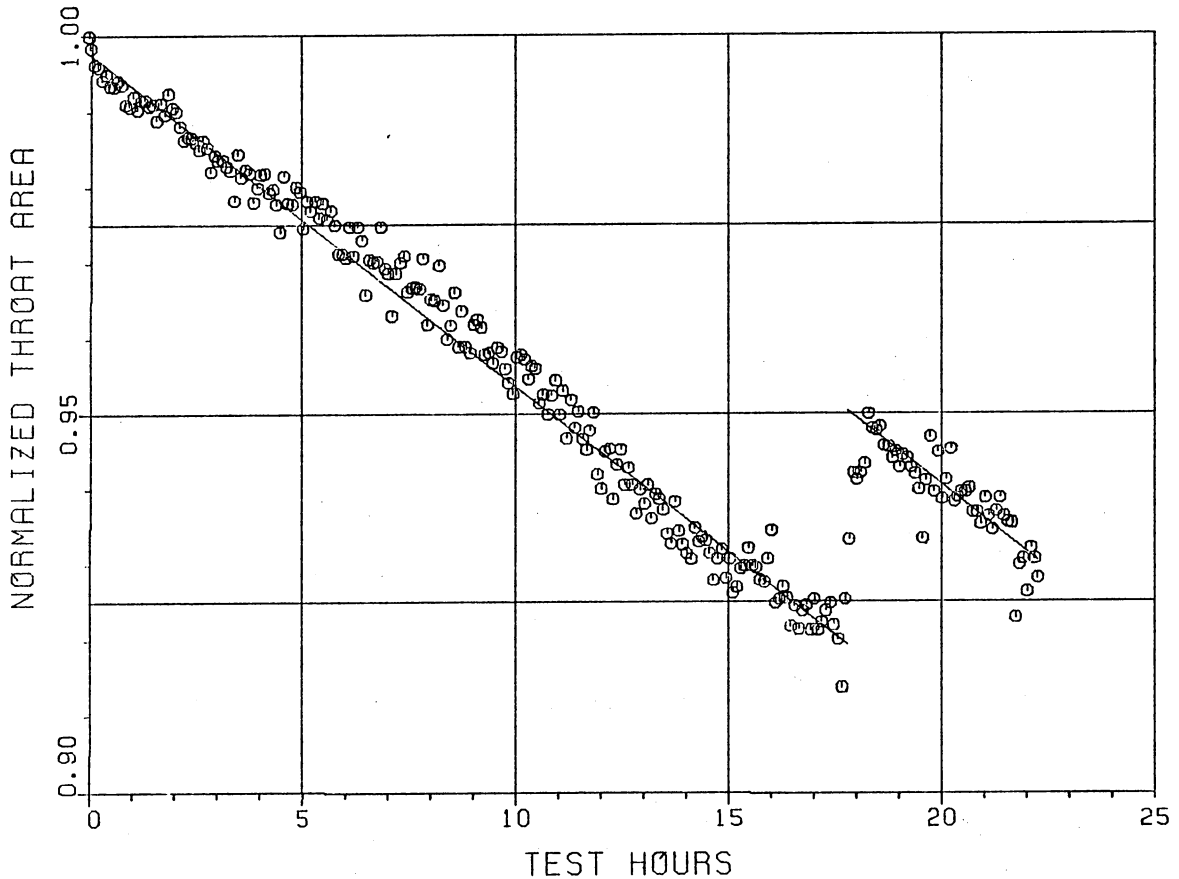

FIGURE 15
NOZZLE THROAT AREA HISTORY FOR TEST NUMBER 6

test number 5. Note that one large recovery event occurred at a point approximately 17.8 hours into the test. As mentioned previously, this recovery was due to an attempt to intentionally affect cleaning of the ash deposits by the injection of crushed walnut shells into the hot gas stream at full load conditions. The nutshell injection was actually performed in two stages with a 30 minute period between the injections. The 17.8 hour recovery point thus represents the approximate time of the nutshell injections.

The ash deposition rates for the periods before and after the throat area recovery were 44.5 and 44.8 per cent per 100 hours, respectively. The throat area recovery resulting from the nutshell injections was 39.0 per cent.

In test number 7, the firing temperature was the same as for the previous four tests (1394 K), but the gas pressure was reduced by a factor of 2 to obtain lower surface metal temperatures. The contaminant additive levels were doubled (see Table 4) over a portion of the test to compensate for the reduced gas flow rate. The nozzle throat area history for this test is shown in Fig. 16. Note that there were numerous periods of ash deposition with several recovery events. Over the first 26.4 hours of testing, some difficulty was experienced with the contaminant additive system, so that data obtained during this period has questionable significance. The additive levels achieved during this period were estimated to be approximately 30 per cent of simulated full engine levels. A large throat area increase occurred 22.5 hours into the test, the reason for which is unknown. Up to this point the ash deposit

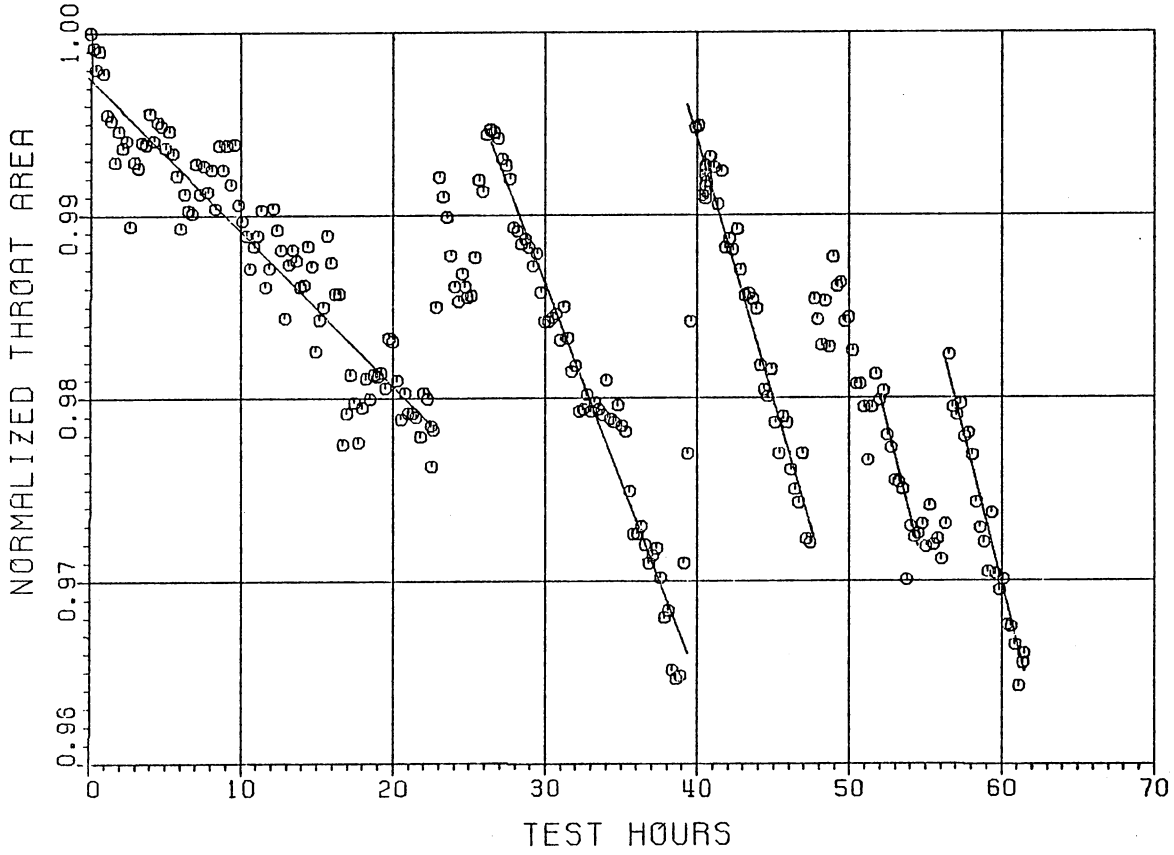

FIGURE 16
NOZZLE THROAT AREA HISTORY FOR TEST NUMBER 7

rate was approximately 8.5 per cent per 100 hours. From 26.4 hours until the end of the test, no further problems were encountered with the additive system. The nozzle was nutshelled at this point. From 26.4 hours to 39.4 hours ash accumulated at an approximate rate of 21.6 per cent per 100 hours. Nutshell injection resulted in a 95 per cent recovery (based on the nozzle area at 26.4 hours), after which ash was allowed to deposit under the same firing conditions until 47.7 hours into the test. The ash deposition rate for this period was approximately 28.4 per cent per 100 hours. A third nutshelling at this point resulted in 58 per cent area recovery. For the period of testing discussed above (26.4 to 47.7 hours), the fuel contaminant additives were introduced at a rate which simulated 50 per cent of the full engine levels. For the remainder of the testing, the additive levels were adjusted to 100 per cent of the engine levels. From 47.7 to 52.0 test hours much scatter was observed in the throat area data (see Fig. 16). The ash deposit rate was 16.4 per cent per 100 hours, calculated by linear regression. At 52.0 hours the atomizing air (A/A) pressure was increased from 4.2 to 6.0 atmospheres (A/A pressure ratio increase from 1.4 to 2.0). The ash deposition rate was observed to increase dramatically to 32.7 per cent per 100 hours. At 54.5 test hours the atomizing air pressure was decreased back to 4.2 atmospheres (A/A pressure ratio 1.4). Over the next 1.8 hours there was considerable scatter in the data, although it appears that little or no decrease in throat area was occuring. At 56.3 test hours the atomizing air pressure was decreased to 3.6 atomspheres (A/A pressure ratio 1.2). At this point a recovery in nozzle throat

area of 37.0 per cent was observed. The atomizing air pressure was then reset to the original value of 4.2 atmospheres for the remainder of the test. The ash deposition rate for the final test period (shut down at 61.5 hours) was 34.4 per cent per 100 hours.

The nozzle throat area history for test number 8 is shown in Fig. 17. Test conditions were the same as for test number 7, including a period of reduced additive levels to simulate the period over which additive system difficulties were encountered in the pervious test. This period extended to 16.4 hours into the test. The ash deposit formation rate to this point was 23.4 per cent per 100 hours. The nozzle was then nutshelled and a 59.7 per cent recovery was observed. The additive rates were then adjusted to 50 per cent of simulated engine level. From 16.4 to 33.0 hours a deposition rate was observed of 39.2 per cent per 100 hours. The nozzle was nutshelled at this point for a second time, resulting in a 72.2 per cent recovery in throat area. The additive levels were then boosted to full simulated engine levels for the remainder of the test. The ash deposit rate from this point (33.0 hours) up to 38.6 hours increased to 51.0 per cent per 100 hours. Abrasive cleaning by coke injection was then attempted. Insufficient data were obtained after the cleaning to objectively evaluate the resulting recovery, but it appears to be of the order of 30 to 60 per cent.

5.4 Heat Transfer

The heat transfer data that are reported here are measured using

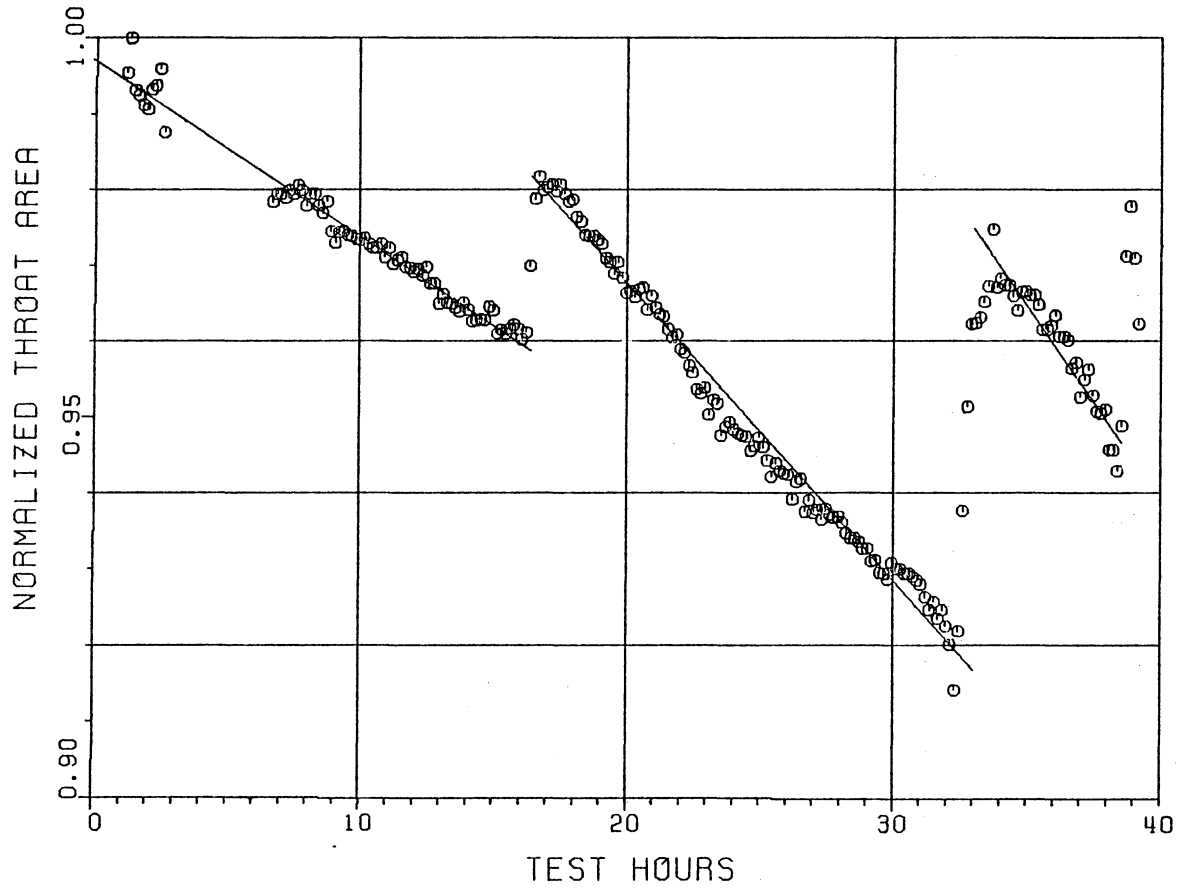

FIGURE 17
NOZZLE THROAT AREA HISTORY FOR TEST NUMBER 8

the water-cooled turbine nozzle sector. Data are thus reported only from tests 2, 5, 6, and 7.

The nozzle heat load history for test number 2 is shown in Fig. 18. The heat load value was determined using eq. (4.9), and normalized using the maximum value for the clean nozzle at the beginning of the test. Note that the heat load follows the same general trend observed for the throat area, that is, generally decreasing, with sharp increases where ash removal occurs. There is more scatter in the heat load data, however, than in the throat area data. Since both heat load and throat area follow the same trends during a test, it is reasonable to expect some correlation to exist between the two. Figure 19 shows the nozzle heat load plotted versus the throat area. Note that there is considerable scatter in the data. Much of this scatter is due to the unsteadying influence of the thermal excursion event 45.4 hours into the test. Examining the data in separate parts clearly reveals this. Figure 20 shows the same data as Fig. 19, except points from 0-45 hours and from 50-64.7 hours are plotted using different symbols. The intermediate points between 45 to 50 hours are eliminated. This procedure differentiates between the two periods of the test and eliminates the unsteadyness in the "recovery" or "nonequilibrium" period following the loss of ash deposit. Note that the clear correlation between the heat load and throat area is now evident. The data appear to follow a linear relation both before and after the ash loss, with a shift in the magnitude of the relation occuring at the recovery point.

Selected vane surface metal temperature histories for test number 2

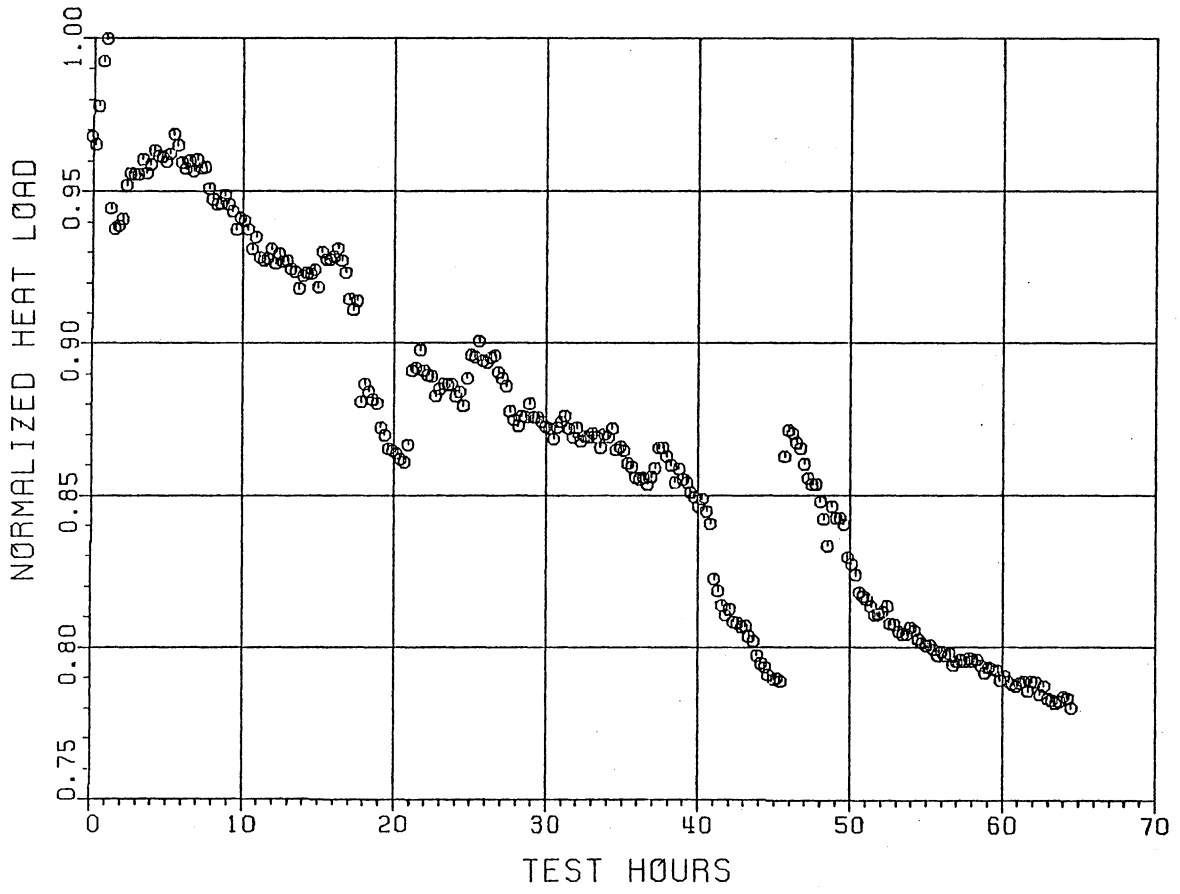

FIGURE 18
NOZZLE HEAT LOAD HISTORY FOR TEST NUMBER 2

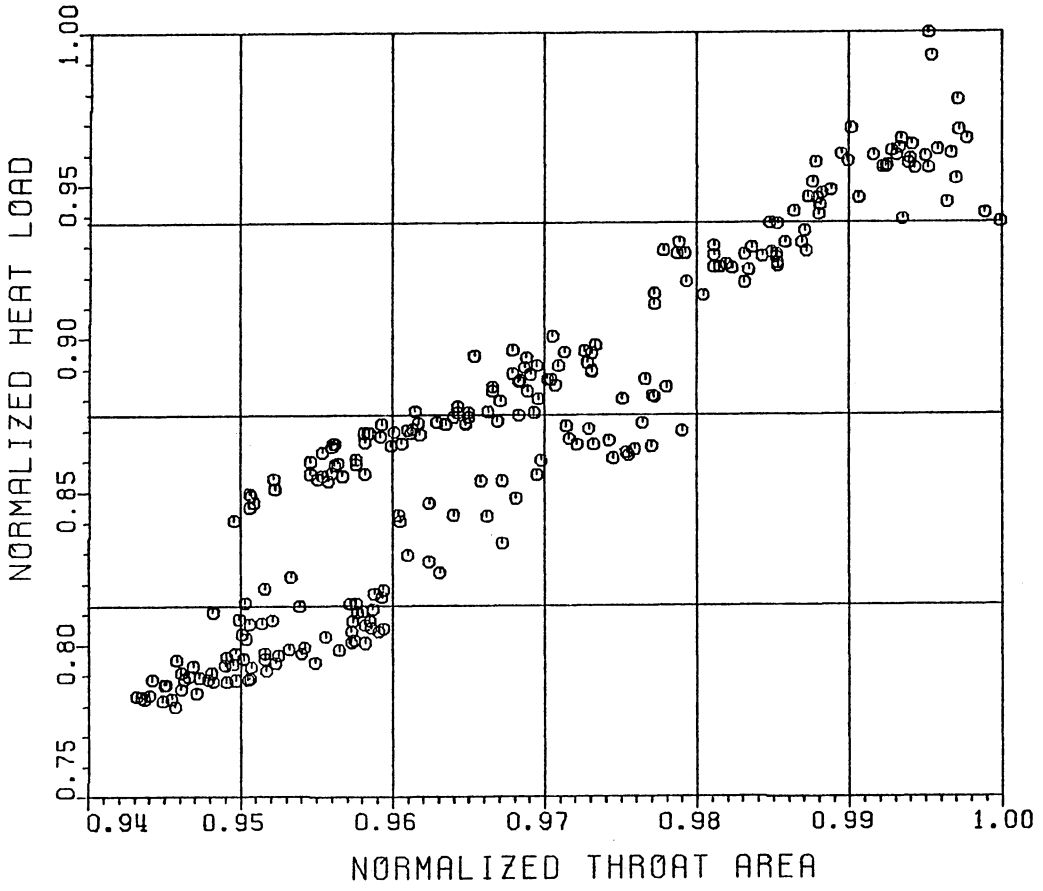

FIGURE 19
NOZZLE HEAT LOAD VARIATION WITH
THROAT AREA FOR TEST NUMBER 2

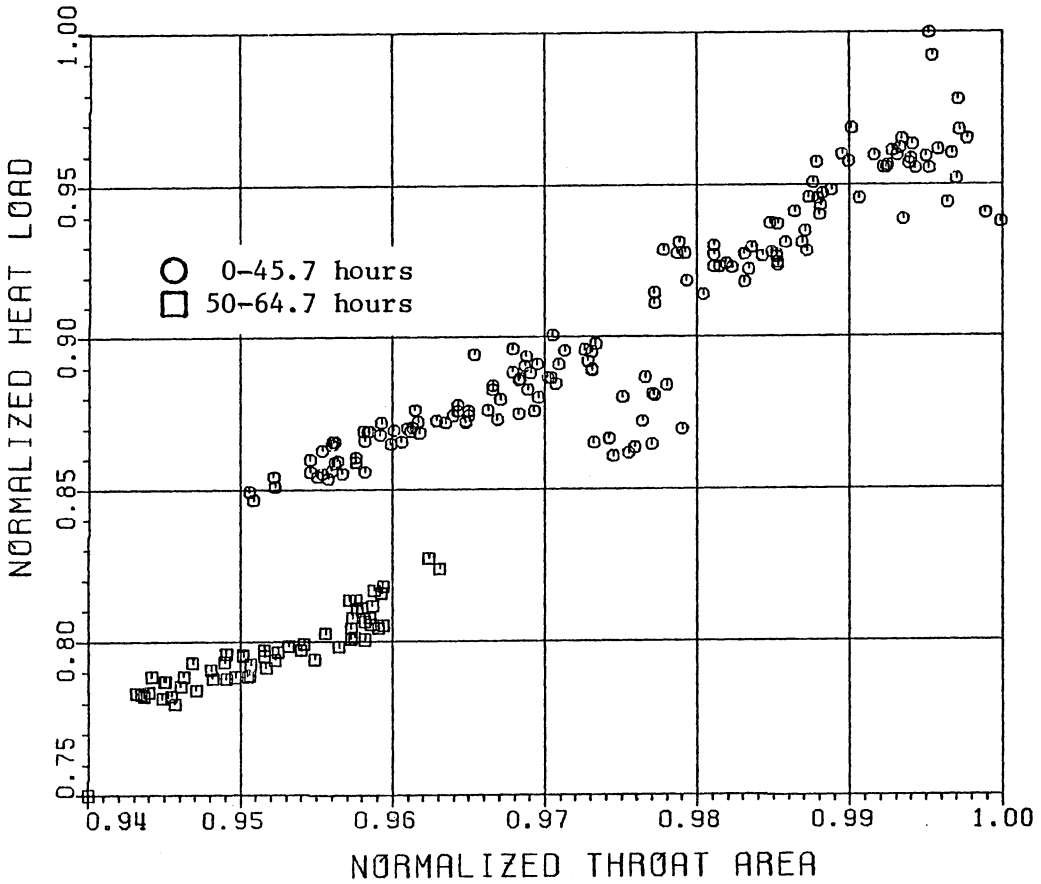

FIGURE 20
NOZZLE HEAT LOAD VARIATION WITH
THROAT AREA FOR TEST NUMBER 2

are shown in Figs. 21-24. The data are for the suction and pressure faces of vanes 2 and 3, the two free-standing vanes (see Fig. 5). The temperatures are non-dimensionalized using eq. (4.11), to account for variations in gas and cooling water temperatures. Note that in each case except for the suction face of vane 3, the temperature increased somewhat during the first 5-8 hours, then decreased steadily until broken by sharp increases indicating ash loss. In the case of the suction faces (Figs. 21, 23) very little, if any, perturbation in temperature was noted at the 45.4 hours ash removal. There is, however, an indication of a disturbance at a point 24.8 hours into the test. Suction face temperature on both vanes 2 and 3 increased significantly. The pressure face data (Figs. 22, 24) clearly show the thermal excursion ash removal at 45.4 hours, but do not show the disturbance noted in the suction face data earlier in the test. The nominal gas temperature for this test was 1311 K, the nominal cooling water temperature was 294 K, and thus the full scale of the dimensionless vane temperature is 1017 K (1830 F), or approximately 102 K (183 F) per division.

The dimensionless vane surface metal temperature provides a simple measure of the local influence of the ash deposition on the nozzle vanes. A deeper insight into the ash deposition/hot gas path heat transfer phenomena can be gained by making use of the combined surface metal temperature and heat load data acquired. The dimensionless heat transfer conductance, defined by eq. (4.18), is a measure of the combined thermal resistance of the ash deposit layer and the ash/gas path surface. As indicated by eq. (4.16), this parameter is a function of

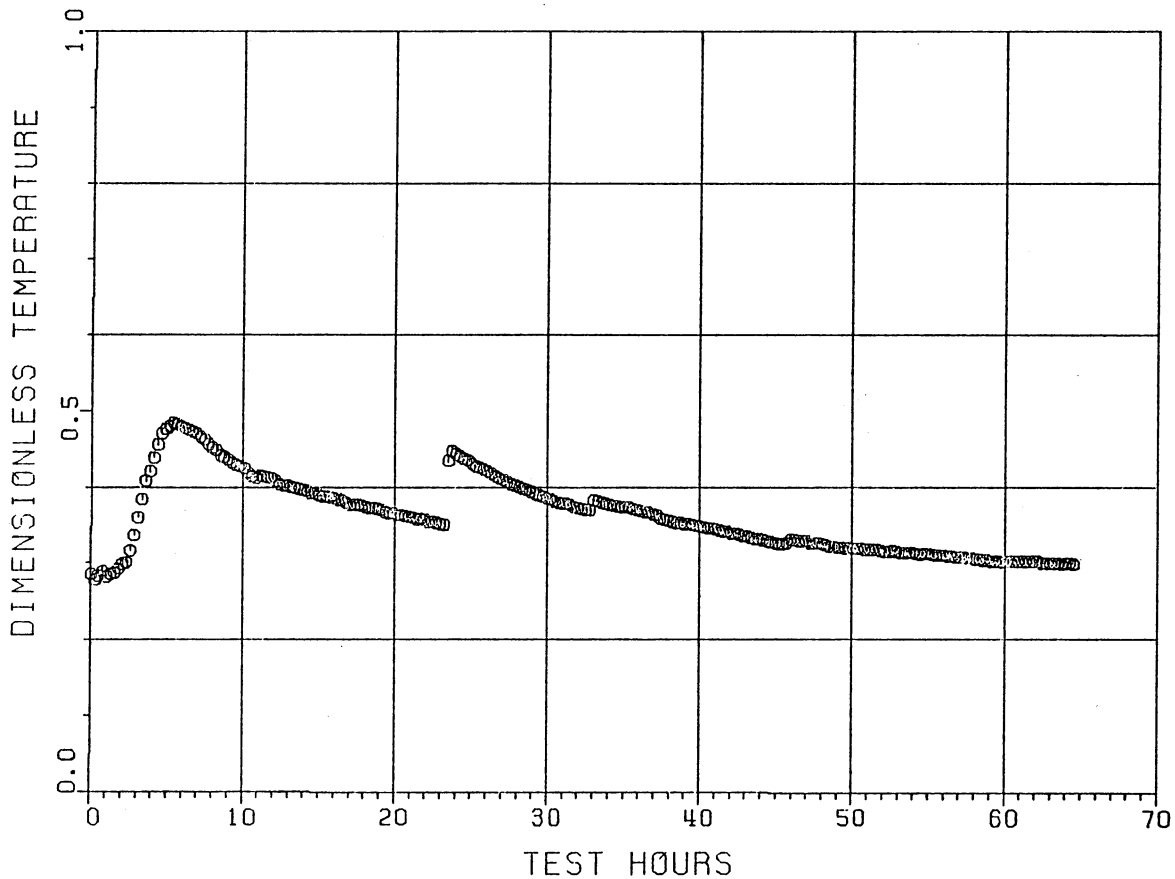

FIGURE 21
VANE 2 SUCTION FACE SURFACE TEMPERATURE
HISTORY FOR TEST NUMBER 2

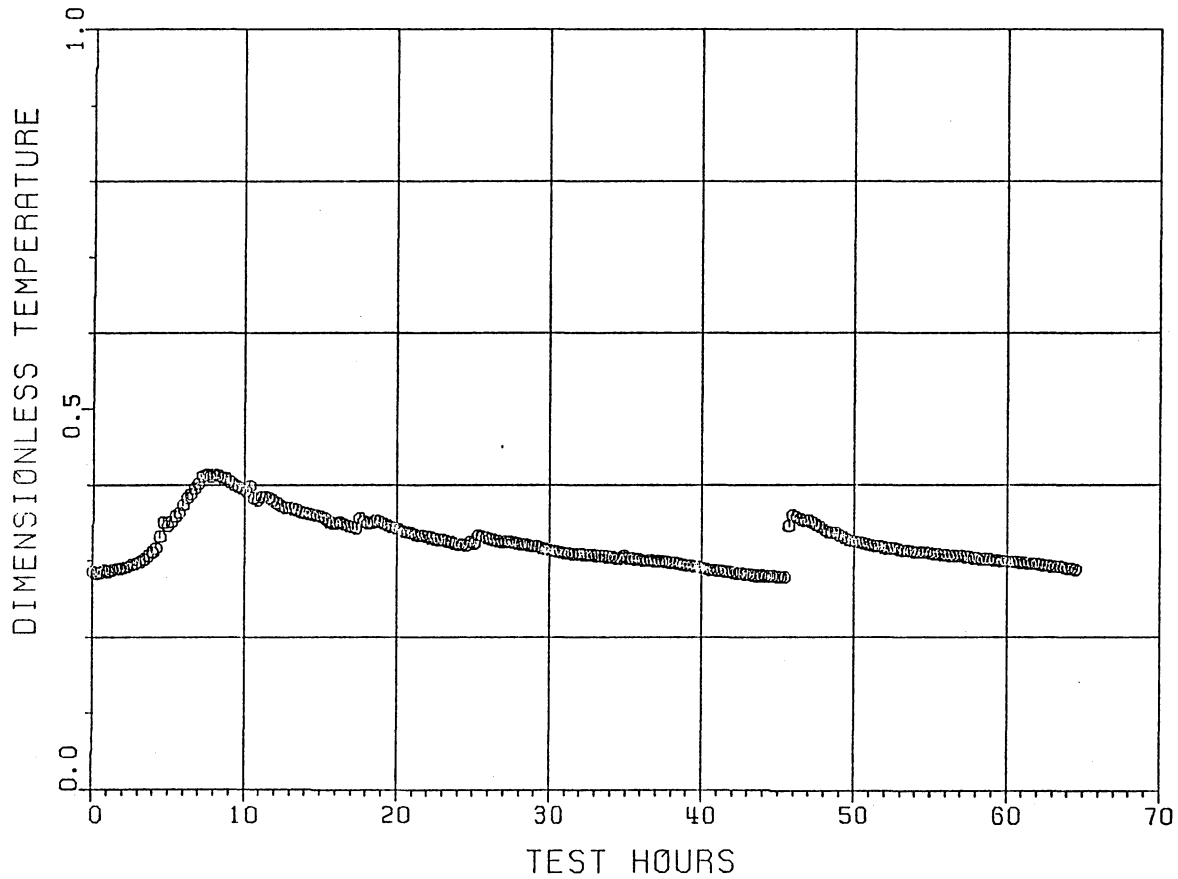

FIGURE 22
VANE 2 PRESSURE FACE SURFACE TEMPERATURE
HISTORY FOR TEST NUMBER 2

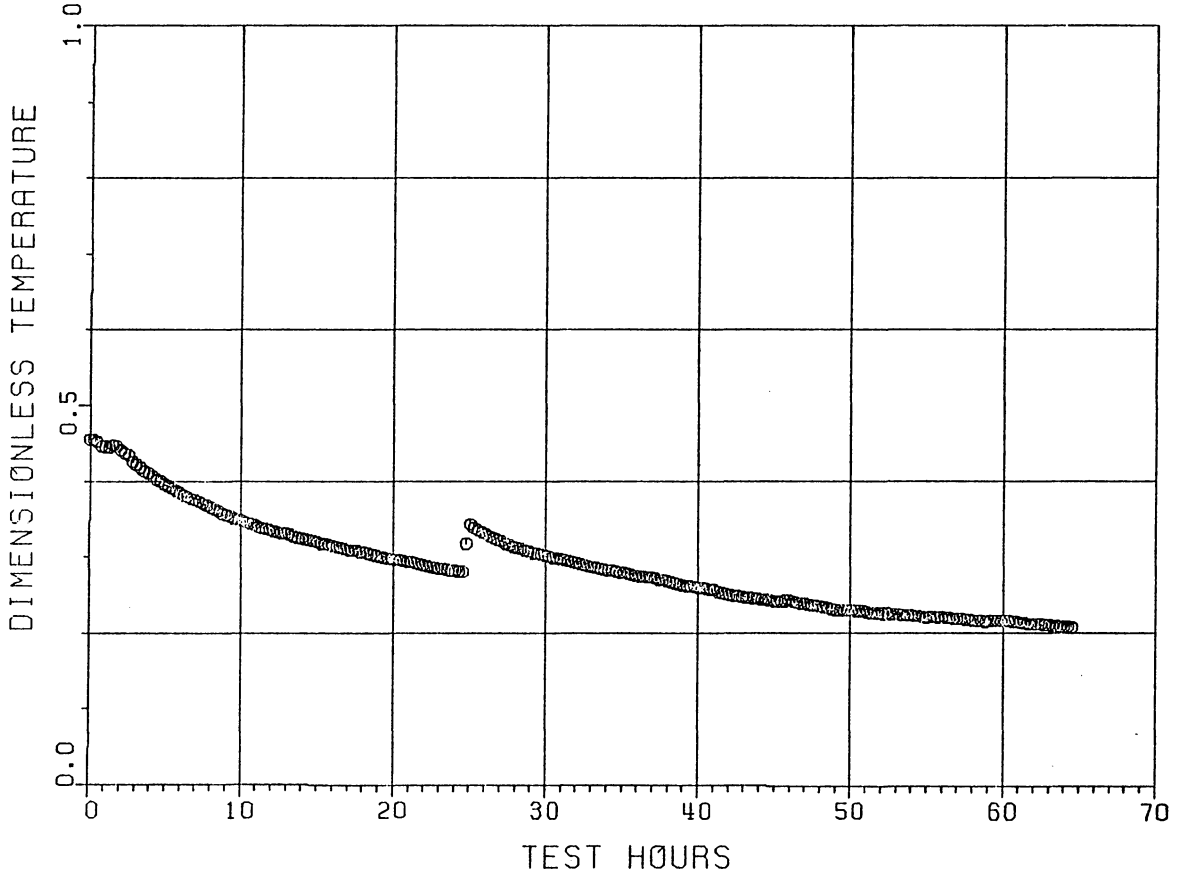

FIGURE 23
VANE 3 SUCTION FACE SURFACE TEMPERATURE
HISTORY FOR TEST NUMBER 2

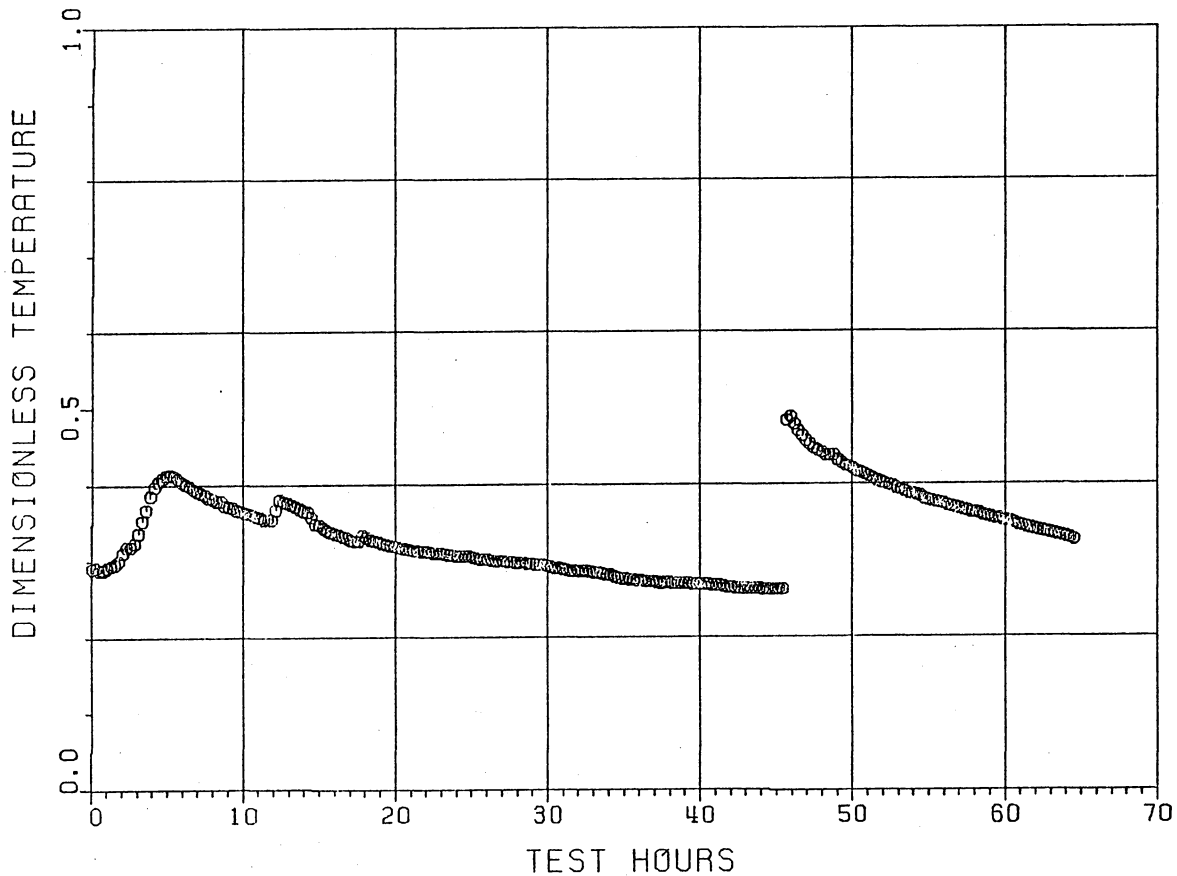

FIGURE 24
VANE 3 PRESSURE FACE SURFACE TEMPERATURE
HISTORY FOR TEST NUMBER 2

the airfoil Reynold's number, defined by eq. (4.20). The airfoil Reynold's number history for test number 2 is shown in Fig. 25. The nominal Reynold's number for the test is 3.5 (10^6), but variations of up to 5.8 per cent were experienced due to changes in test conditions because of plugging. The effect of these Reynold's number variations on the dimensionless heat transfer conductance can be examined using data taken in turbine simulator experiments with a clean nozzle sector using clean fuel. Such experiments were run prior to test number 7, with a Reynold's number variation of 1.5 (10^6) to 3.7 (10^6). The results are shown in Figs. 26-29 for the suction and pressure faces of vanes 2 and 3. Note that in each case, a near linear variation of the dimensionless heat transfer conductance with Reynold's number is observed. By dividing the computed value of the heat transfer coefficient by the airfoil Reynold's number, a correction is thus made for Reynold's number variations in a test. (It is assumed that Reynold's number variations do not affect heat transfer through the ash layer in a test.)

The corrected dimensionless heat transfer conductances for test number 2 are shown in Figs. 30-33. Note that some differences exist in trends observed in the surface temperature data alone. An increase in seen in the heat transfer on the suction faces at the 45.4 hour point which was not observed in the surface temperatures. The slight perturbation in the suction side temperatures at 24.8 hours can also be seen on the pressure face heat transfer coefficeints. The corrected dimensionless heat transfer coefficent thus appears to convey more information than the surface temperatures alone.

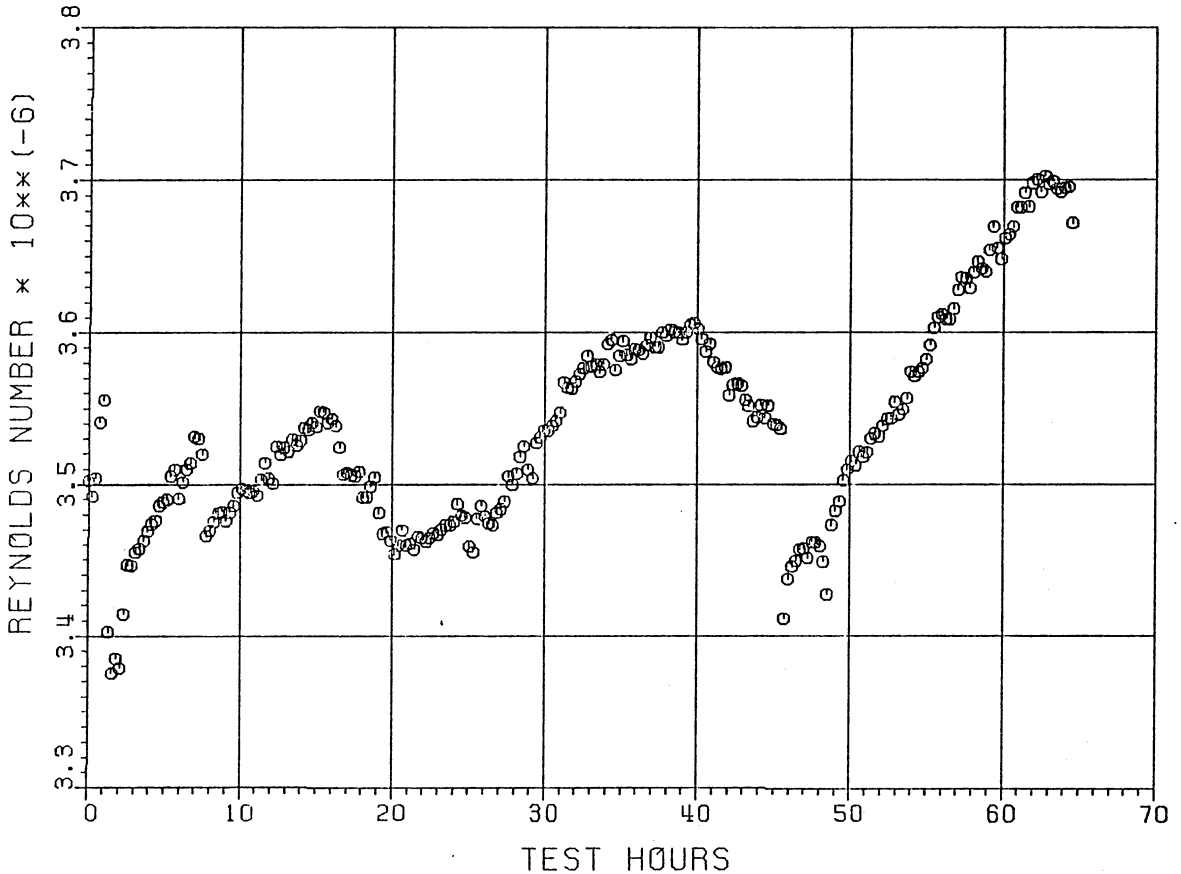

FIGURE 25
REYNOLDS NUMBER HISTORY FOR TEST NUMBER 2

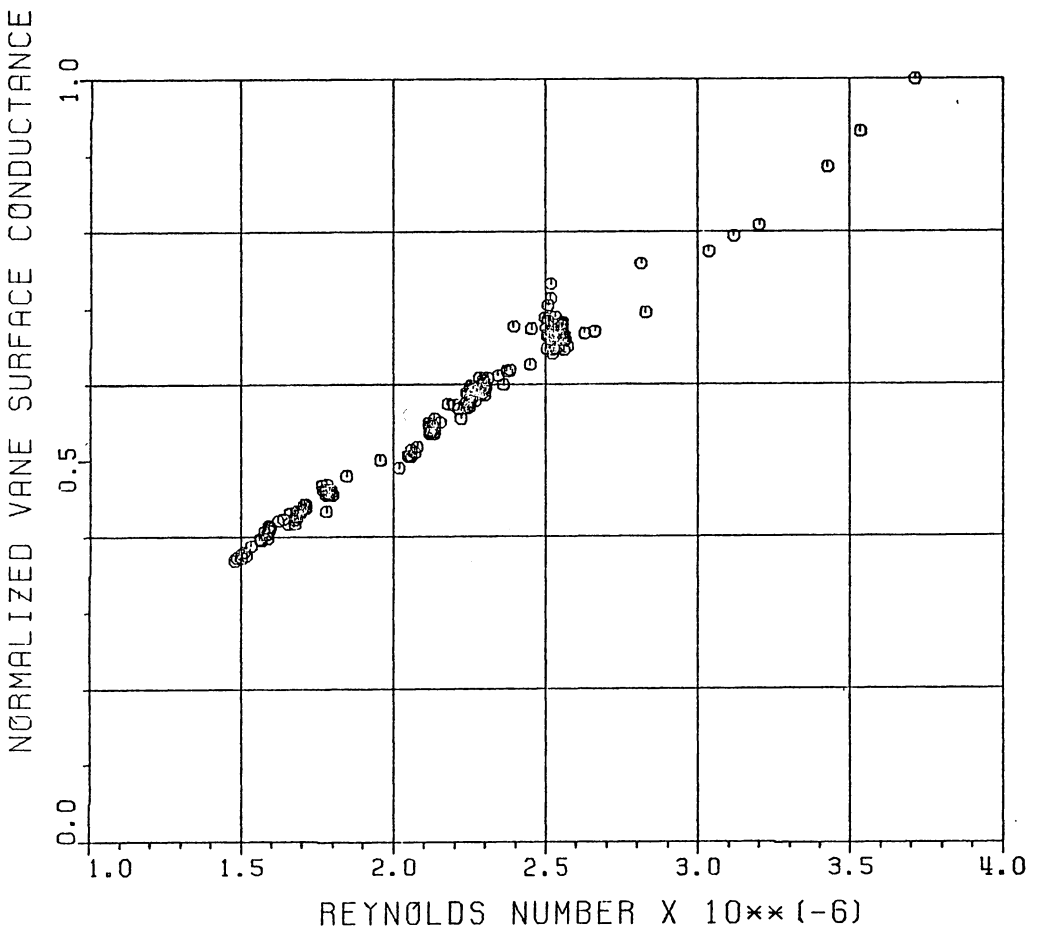

FIGURE 26
VANE 2 SUCTION FACE SURFACE CONDUCTANCE VARIATION
WITH REYNOLDS NUMBER FOR CLEAN NOZZLE SECTOR

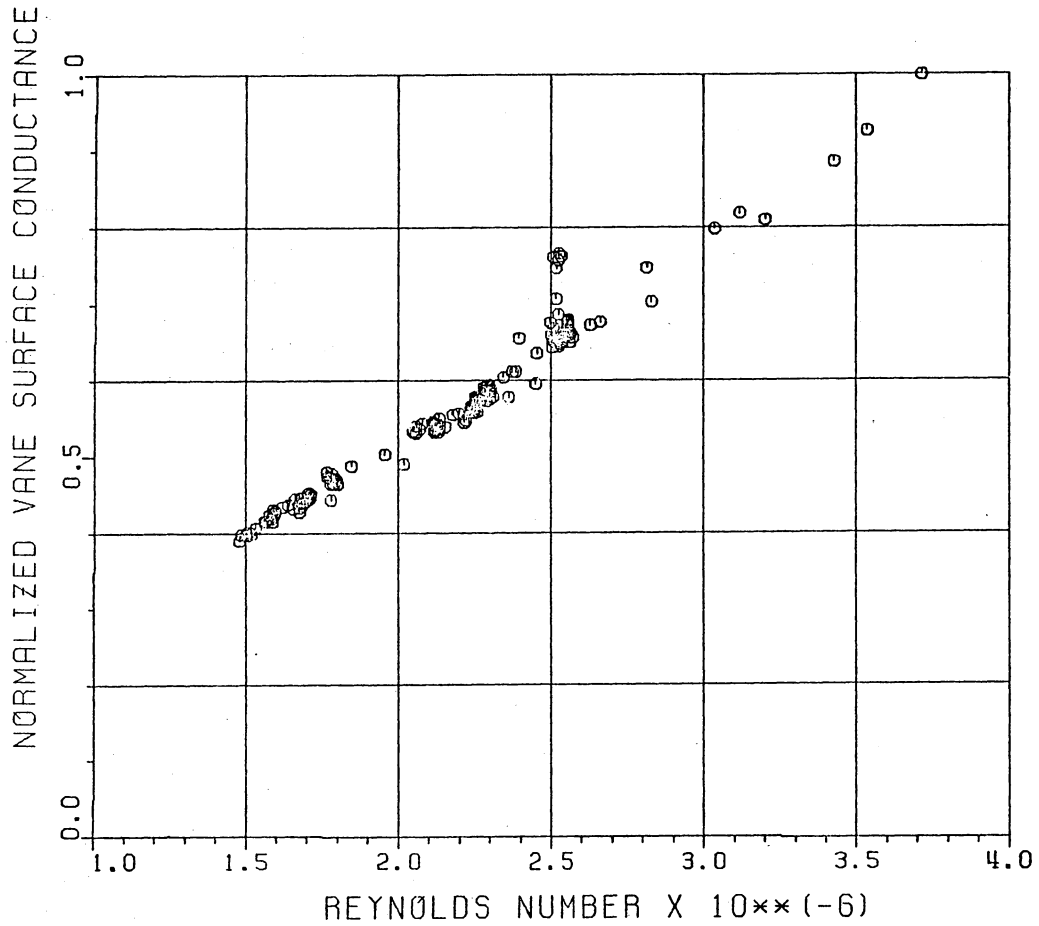

FIGURE 27
VANE 2 PRESSURE FACE SURFACE CONDUCTANCE VARIATION
WITH REYNOLDS NUMBER FOR CLEAN NOZZLE SECTOR

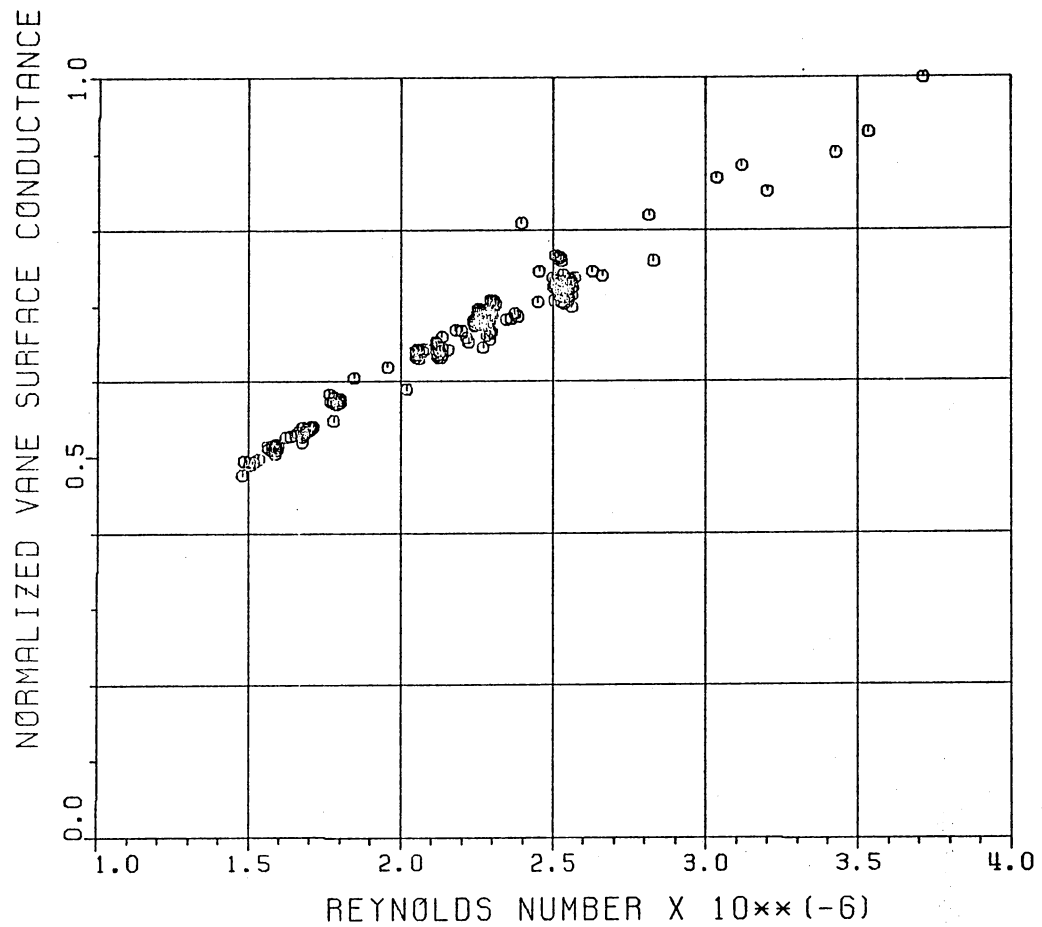

FIGURE 28
VANE 3 SUCTION FACE SURFACE CONDUCTANCE VARIATION
WITH REYNOLDS NUMBER FOR CLEAN NOZZLE SECTOR

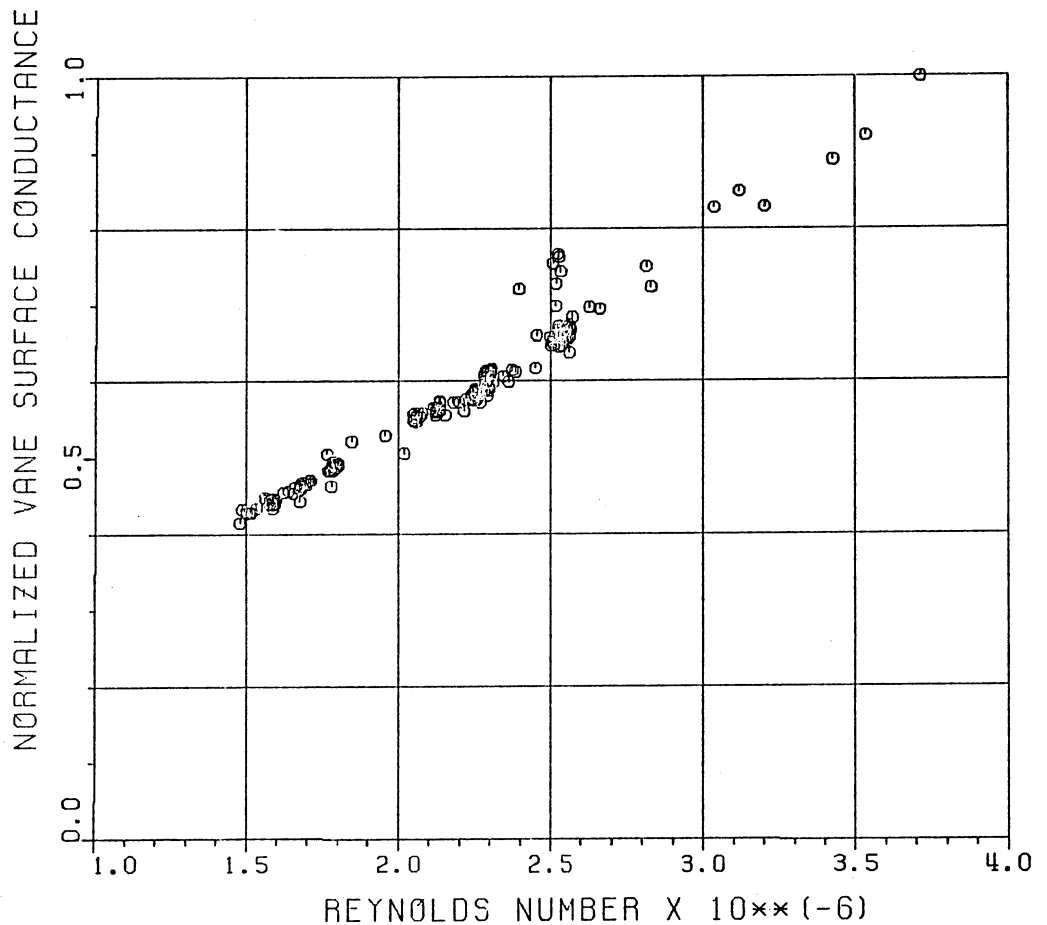

FIGURE 29
VANE 3 PRESSURE FACE SURFACE CONDUCTANCE VARIATION
WITH REYNOLDS NUMBER FOR CLEAN NOZZLE SECTOR

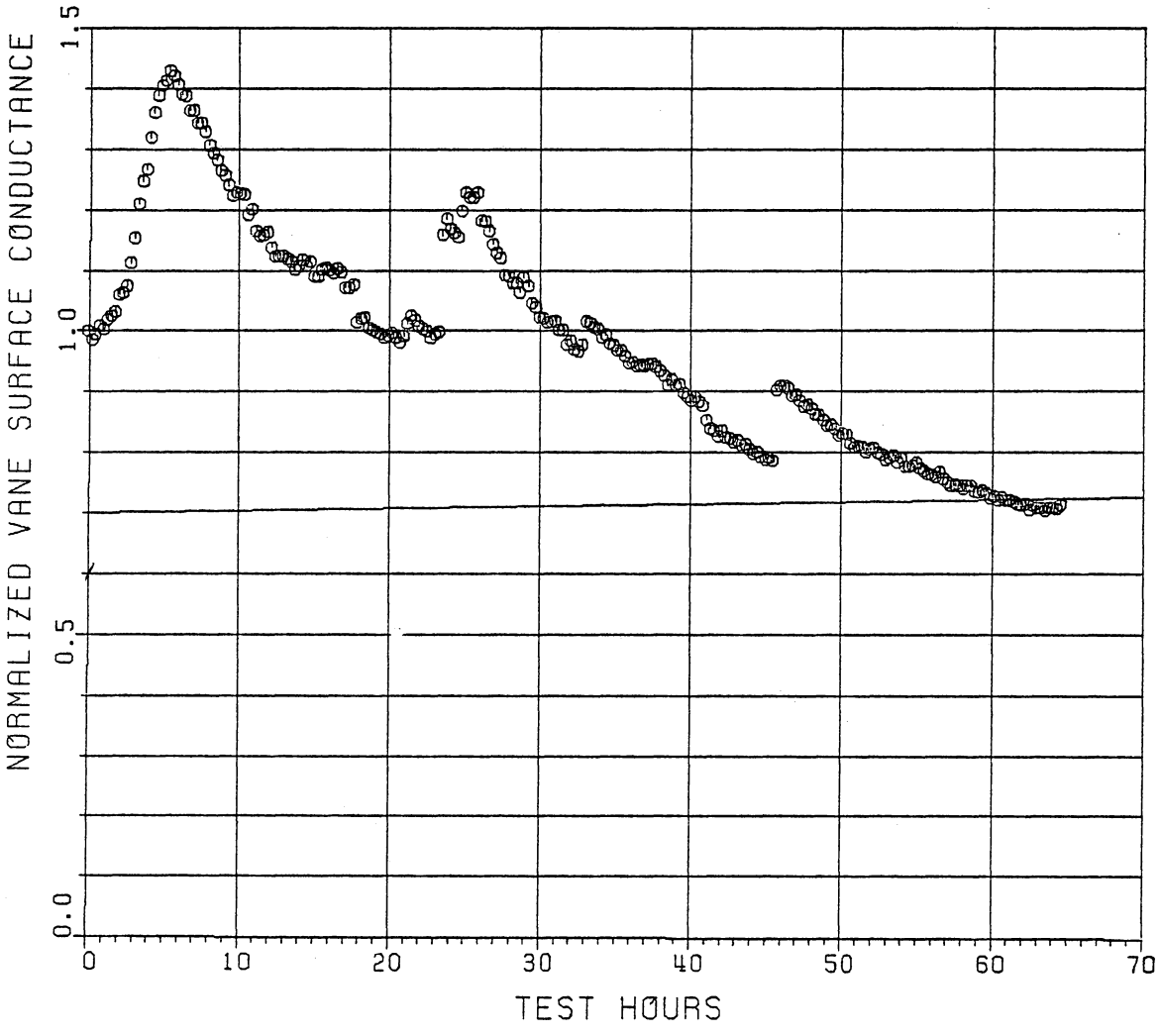

FIGURE 30
VANE 2 SUCTION FACE SURFACE CONDUCTANCE
HISTORY FOR TEST NUMBER 2

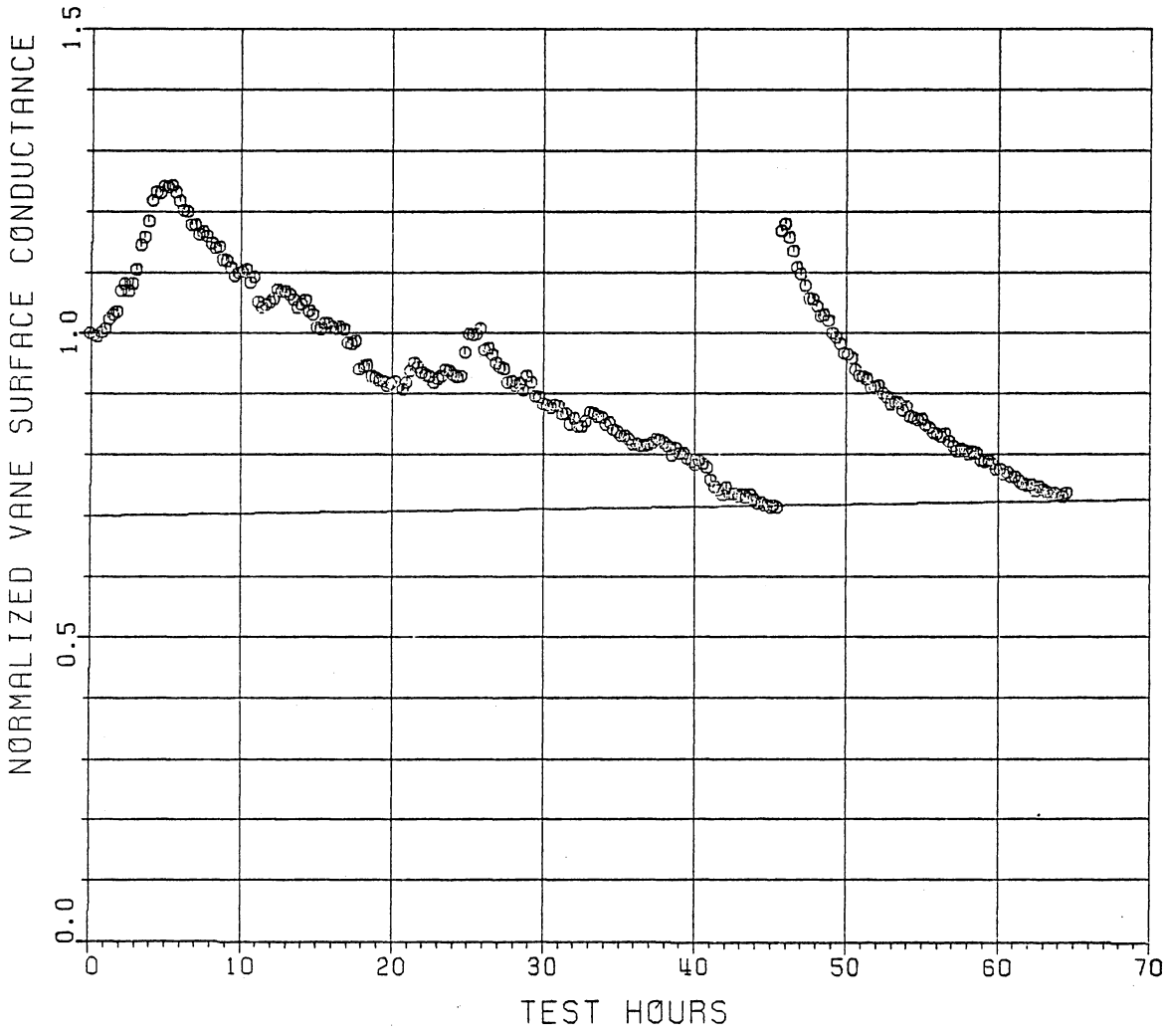

FIGURE 31
VANE 2 PRESSURE FACE SURFACE CONDUCTANCE
HISTORY FOR TEST NUMBER 2

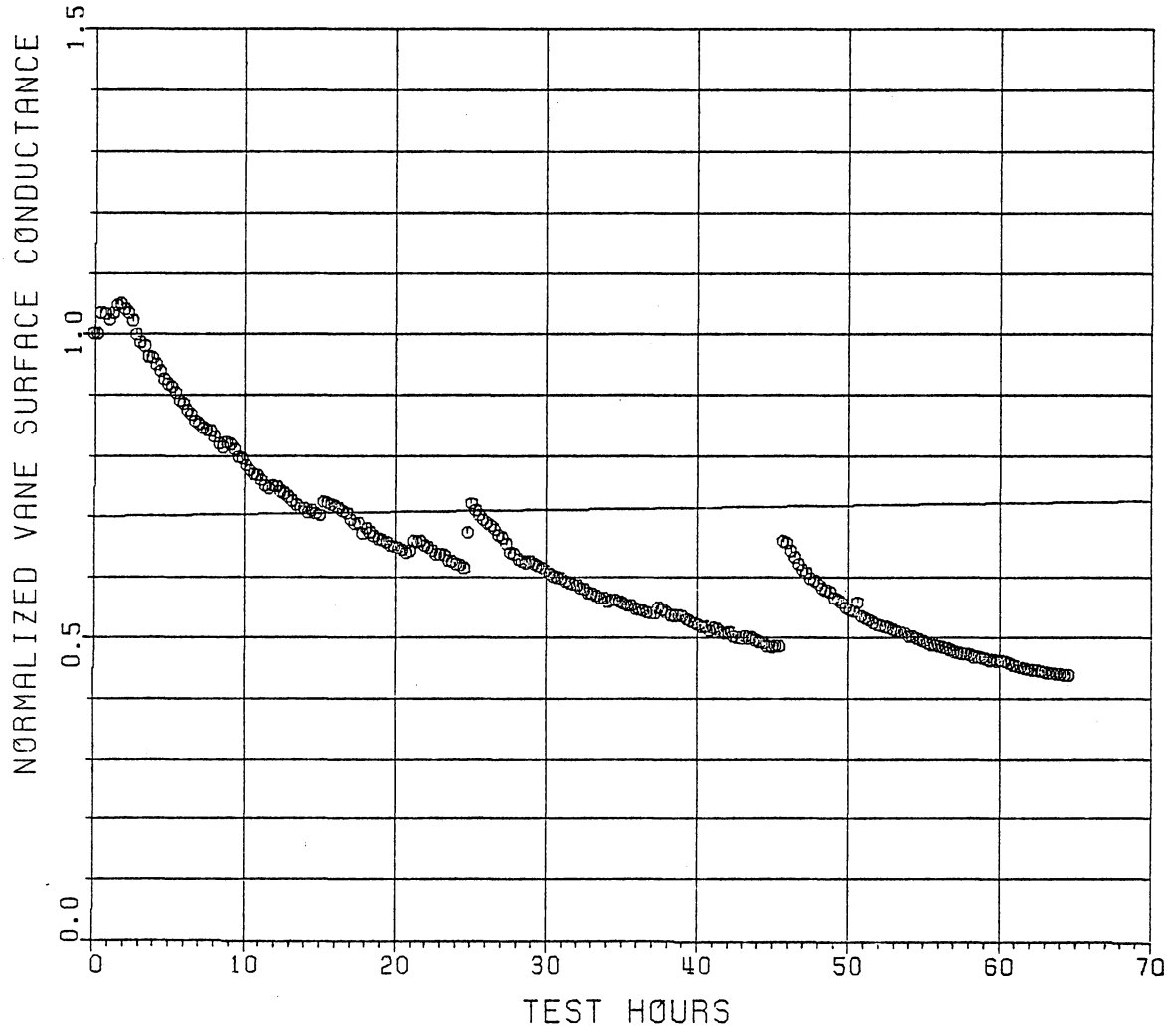

FIGURE 32
VANE 3 SUCTION FACE SURFACE CONDUCTANCE
HISTORY FOR TEST NUMBER 2

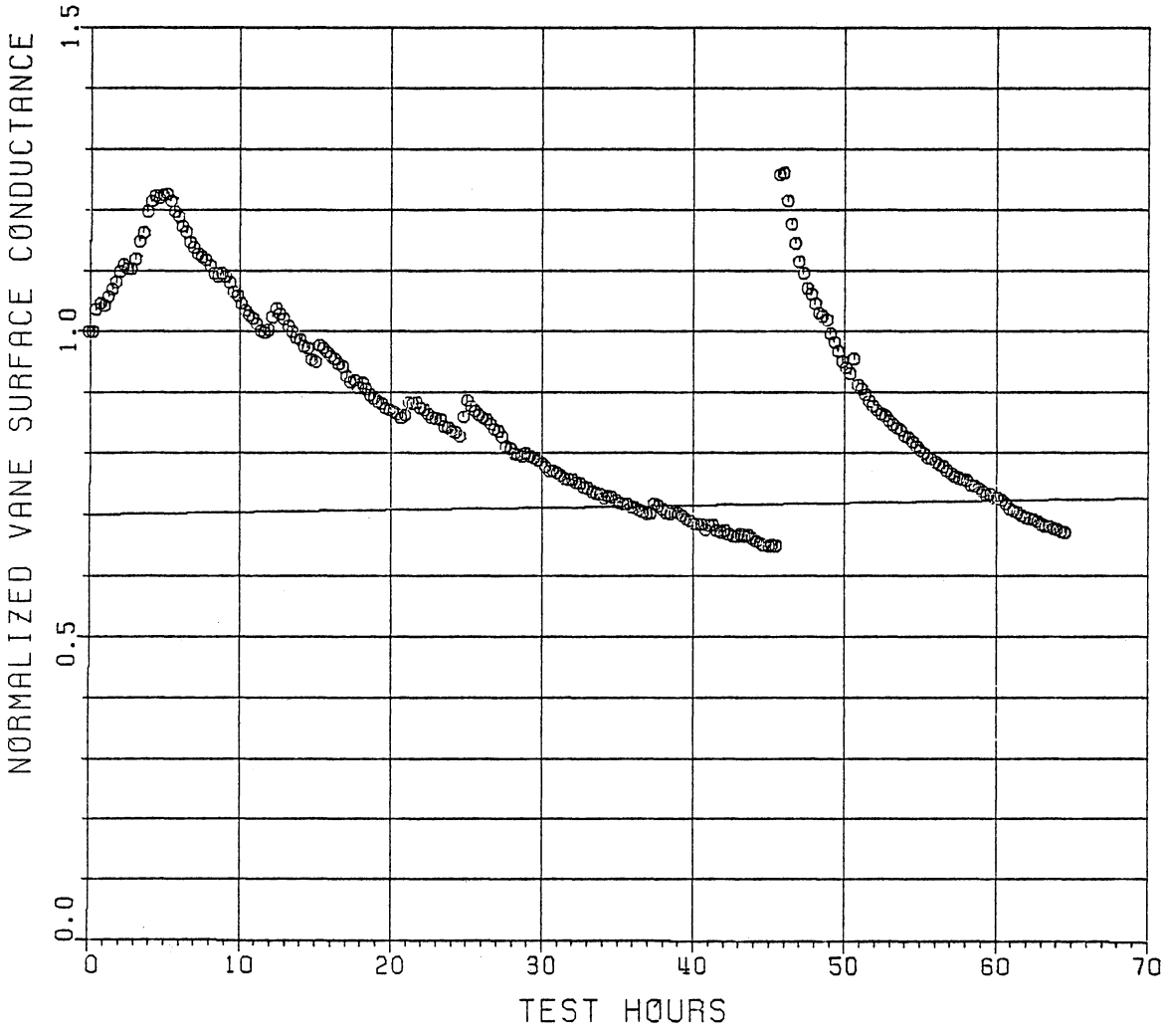

FIGURE 33
VANE 3 PRESSURE FACE SURFACE CONDUCTANCE
HISTORY FOR TEST NUMBER 2

The nozzle heat load history for test number 5 is shown in Fig. 34. Note that, as with test number 2, the heat load follows the same trends as the throat area (see Fig. 14). In this case, however, the nozzle heat loads immediately after ash removal events were actually higher than the values at the beginning of the test with a clean nozzle. As with the data of test number 2, the throat area and heat load data were cross-plotted to evaluate the correlation between the two. This is shown in Fig. 35. Note that, as before, much scatter exists in the data. To separate the "unsteadyness" of the ash removal and reattachment from the "steady" ash deposition data, the periods 0-9.6 hours, 15-35.7 hours, and 41-48.4 hours were plotted separately in Figs. 36-38, respectively. Note that for throat area reductions of up to 5 to 6 per cent a near-linear correlation with heat load is observed. For higher plugging, however, the data appear to be nonlinear and a maximum heat load reduction of approximately 17 to 18 per cent was observed. From a comparison of Figs. 37 and 38 with Fig. 36 it was observed that immediately following ash removal very high heat loads are experienced which then very quickly drop down to values observed prior to the ash loss. Figure 35 also confirms this. Throat area reduction, however, is not recovered quickly (see Fig. 14).

The dimensionless vane temperatures for test number 5 are shown in Figs. 39-42. The full temperature scale for these plots ($0 \leq \Phi \leq 1$) is approximately 1133 K (2040 F) or about 113K (204 F) per division. Note that the temperatures all increase in the initial portion of the test, and then decrease. This same phenomena was observed in test number 2,

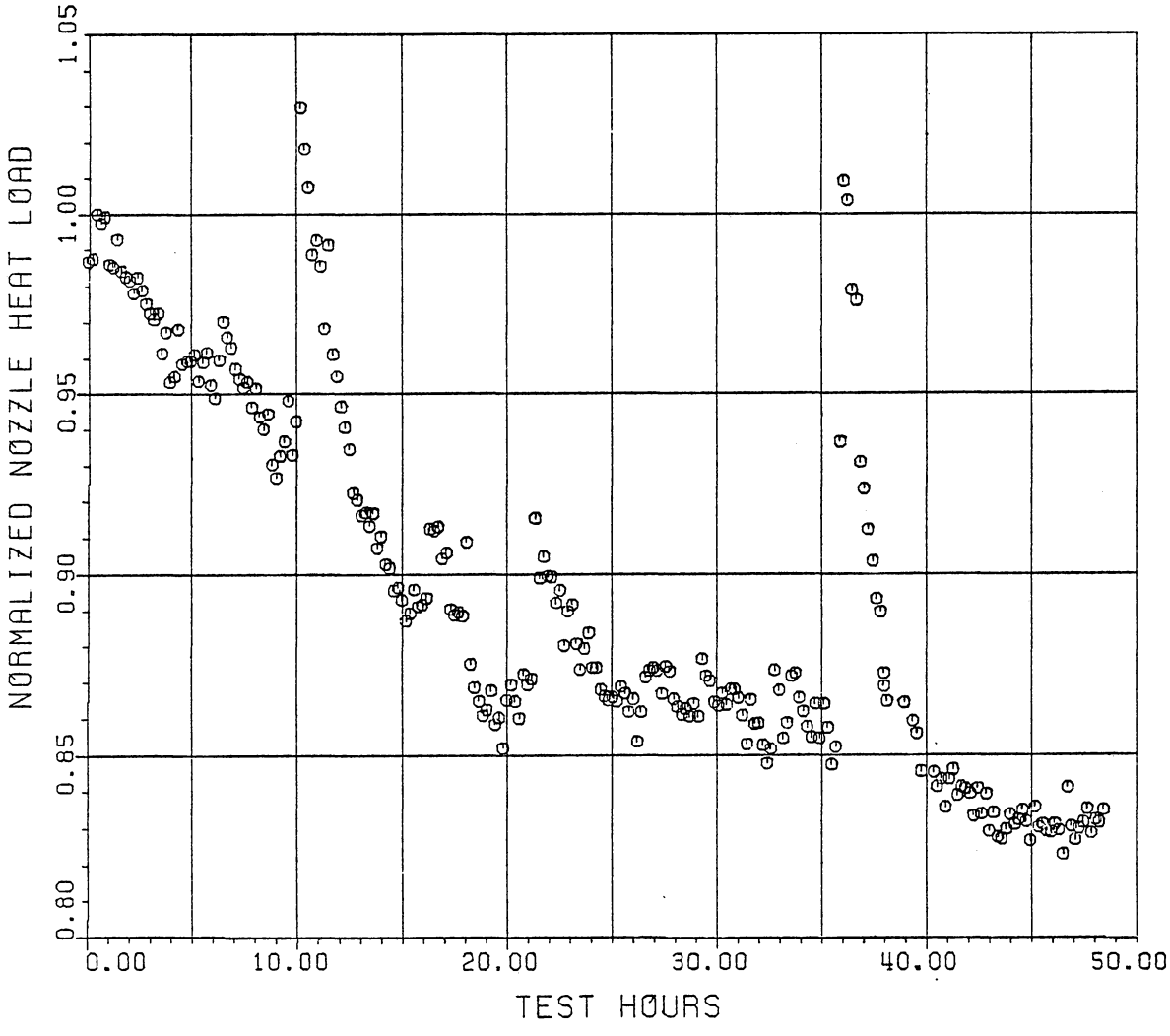

FIGURE 34
NOZZLE HEAT LOAD HISTORY FOR TEST NUMBER 5

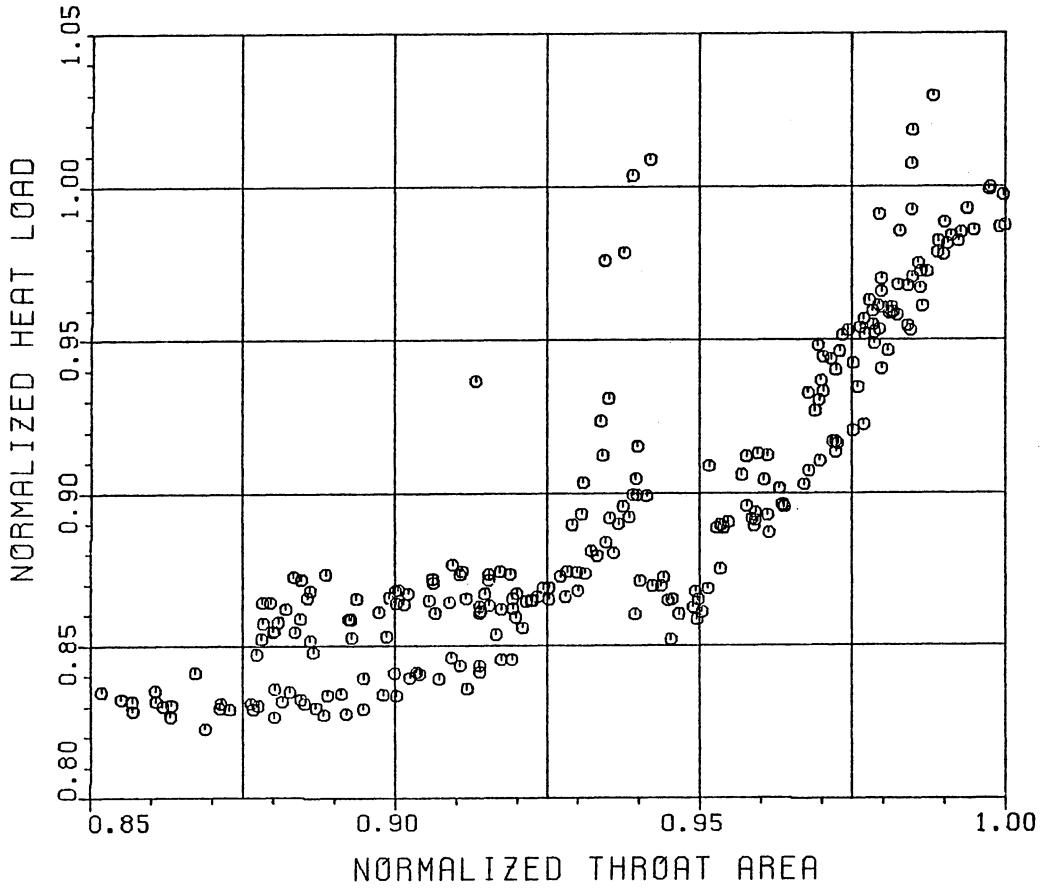

FIGURE 35
NOZZLE HEAT LOAD VARIATION WITH
THROAT AREA FOR TEST NUMBER 5

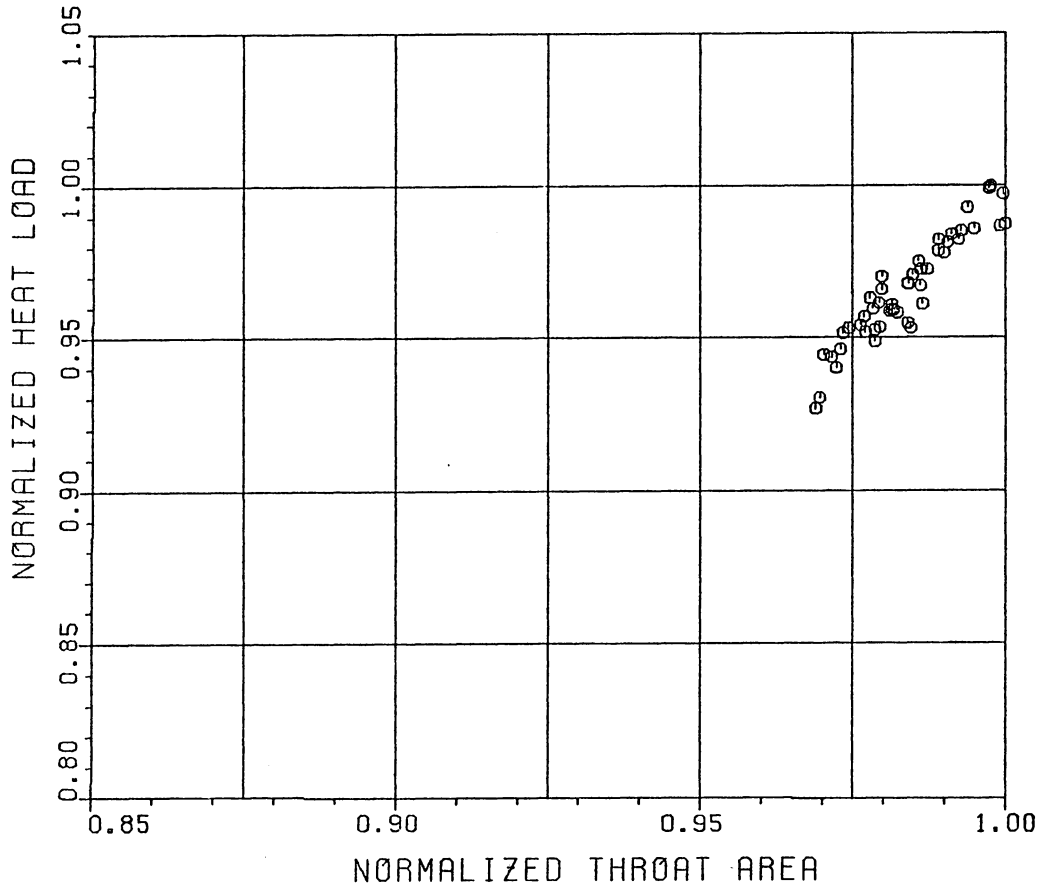

FIGURE 36
NOZZLE HEAT LOAD VARIATION WITH
THROAT AREA FOR TEST NUMBER 5
(0-9.6 HOURS)

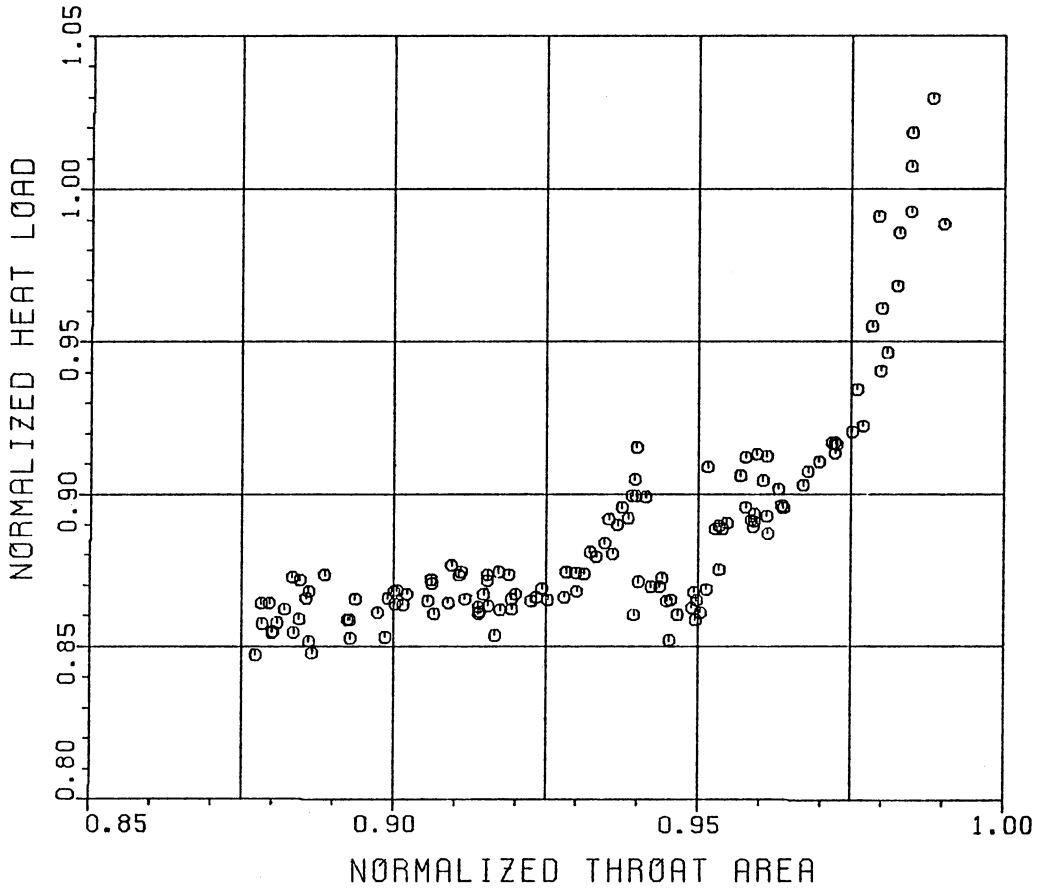

FIGURE 37
NOZZLE HEAT LOAD VARIATION WITH
THROAT AREA FOR TEST NUMBER 5
(15-35.7 HOURS)

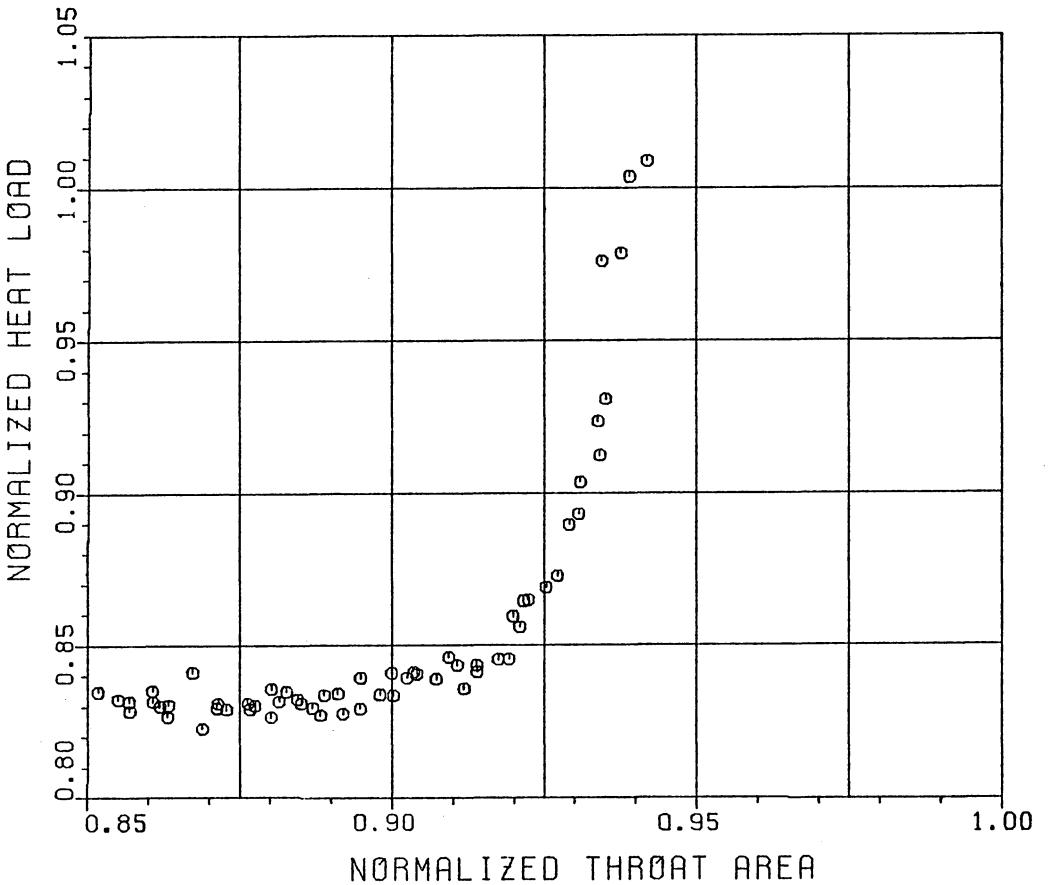

FIGURE 38
NOZZLE HEAT LOAD VARIATION WITH
THROAT AREA FOR TEST NUMBER 5
(41-48.4 HOURS)

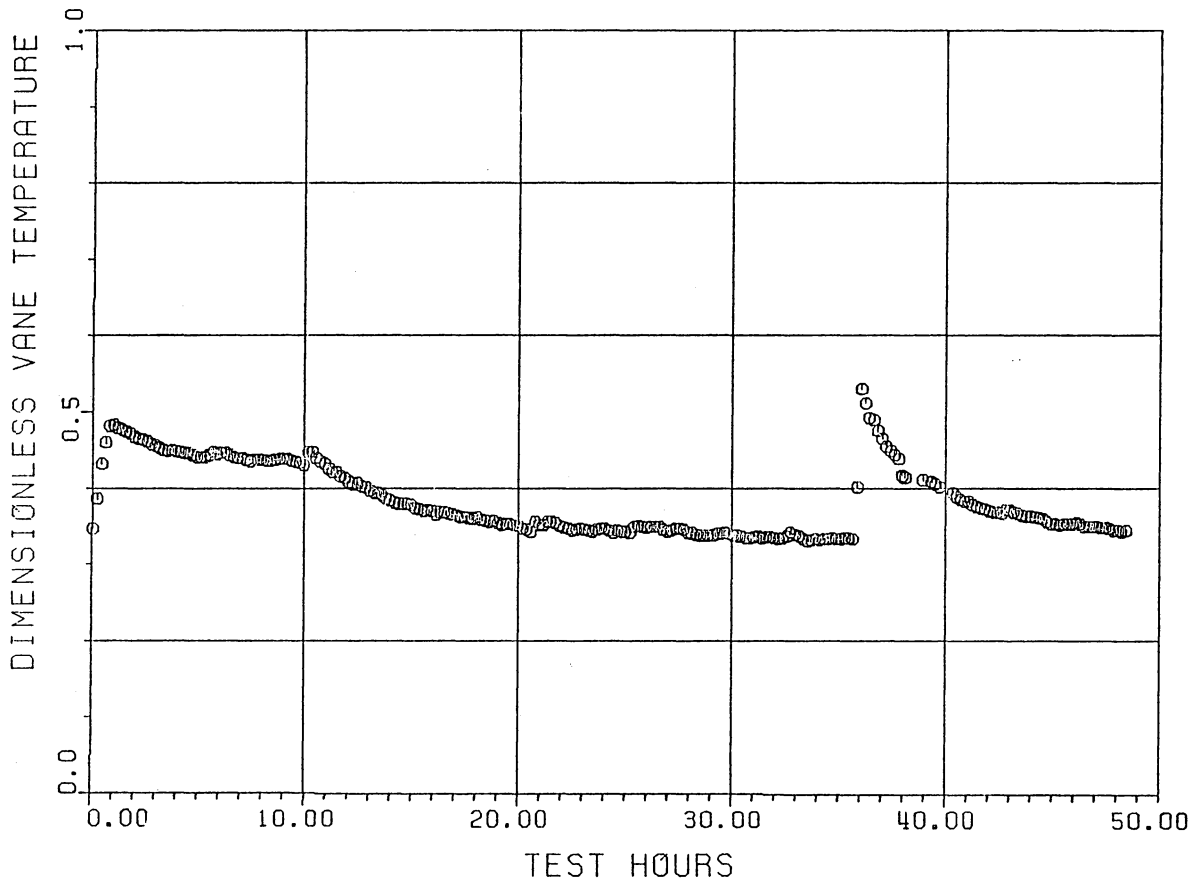

FIGURE 39
VANE 2 SUCTION FACE SURFACE TEMPERATURE
HISTORY FOR TEST NUMBER 5

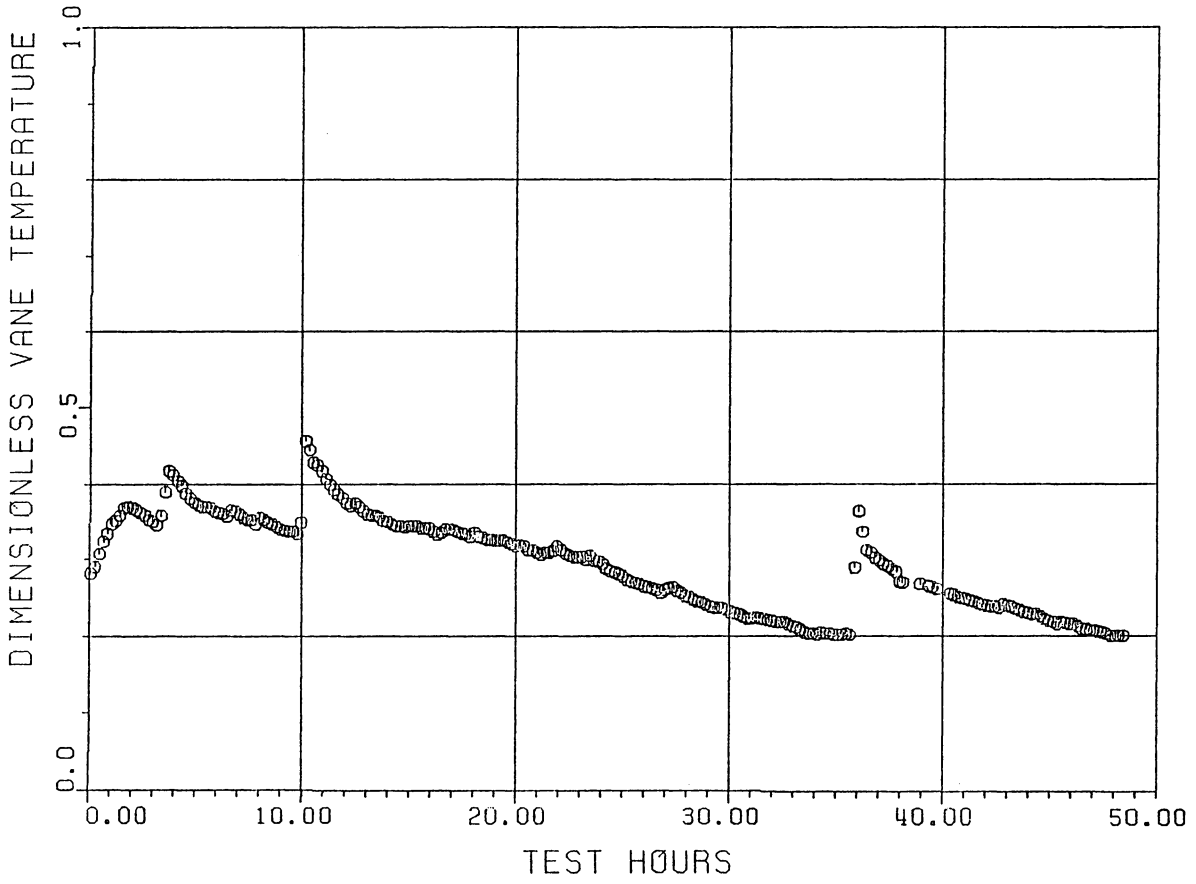

FIGURE 40
VANE 2 PRESSURE FACE SURFACE TEMPERATURE
HISTORY FOR TEST NUMBER 5

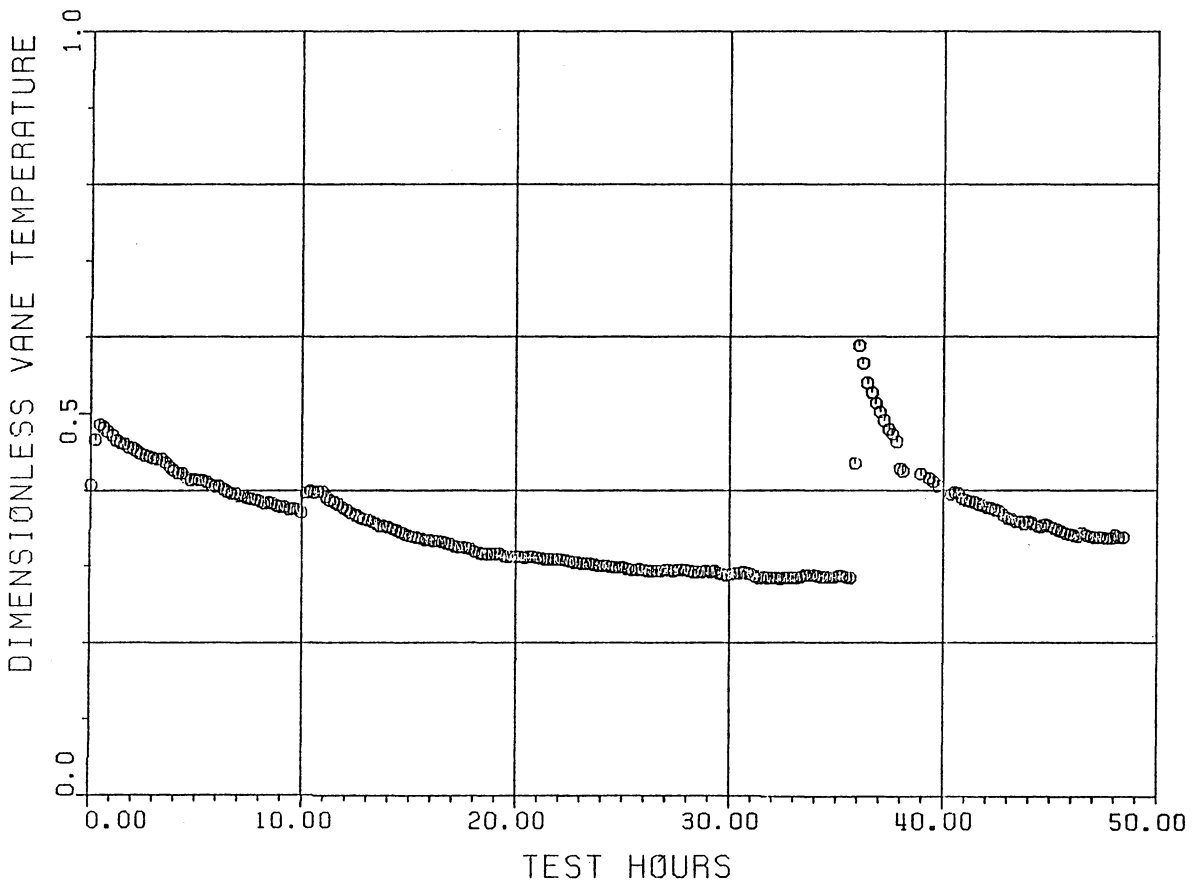

FIGURE 41
VANE 3 SUCTION FACE SURFACE TEMPERATURE
HISTORY FOR TEST NUMBER 5

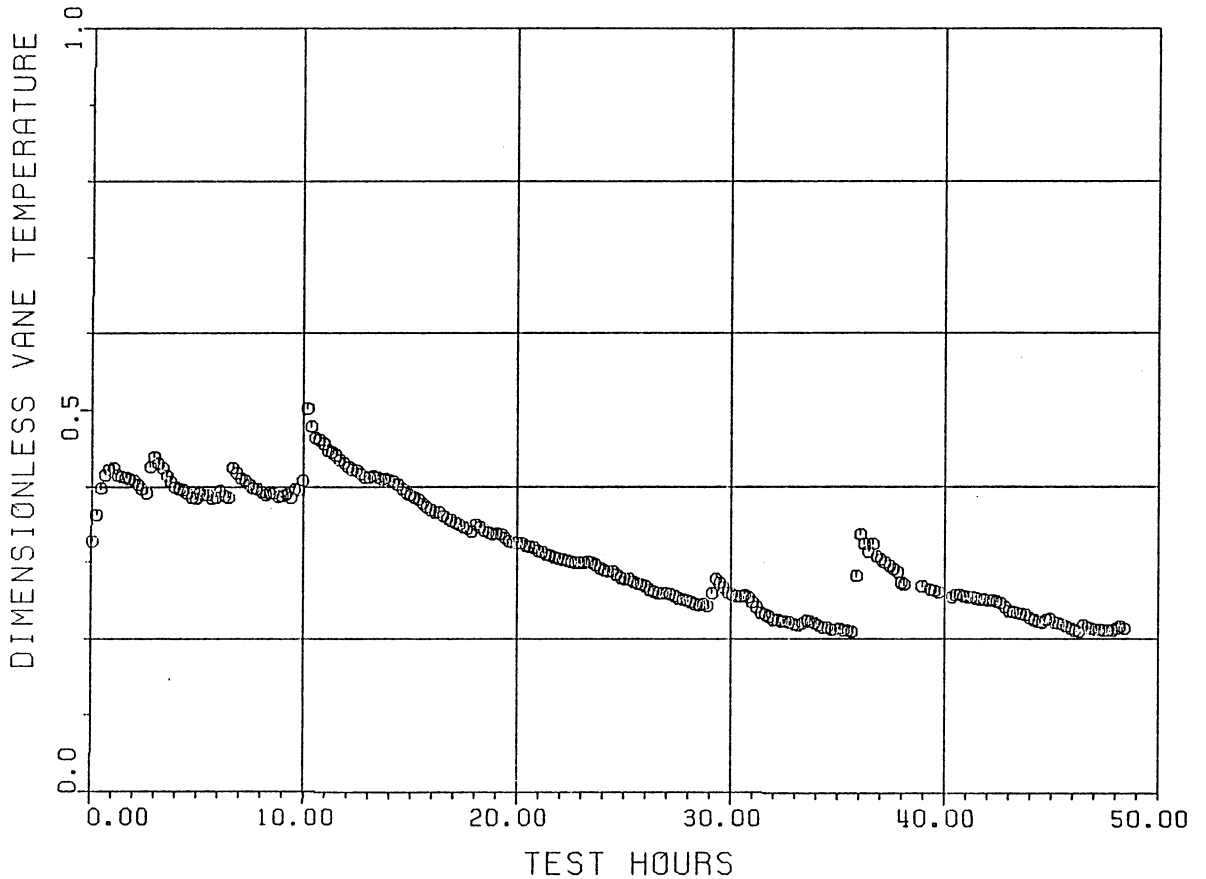

FIGURE 42
VANE 3 PRESSURE FACE SURFACE TEMPERATURE
HISTORY FOR TEST NUMBER 5

although for test 5 the temperatures rose more quickly and reached the peak values sooner. The percentage increase was less for test number 5. The suction face temperatures, shown in Figs. 39 and 41, show very similar trends. Only a very small perturbation was observed at the first ash loss (thermal excursion) at 9.9 hours but a very significant temperature increase occured at the second excursion at 35.9 hours. On the pressure faces, however, significant temperature perturbations were observed at both disturbances.

The variation in airfoil Reynold's number for test number 5 is shown in Fig. 43. The nominal Reynold's number for the test was $3(10^6)$, and the maximum variations experience were -6.9 to +10.3 per cent. The Reynold's number values from this and the following test were slightly lower than for test 2 because the increased gas temperature results in a decrease in density. These Reynold's number values were used to correct the dimensionless heat transfer conductance as before.

The corrected dimenionless heat transfer conductances for test number 5 are shown in Figs. 44-47. The suction face results now clearly show both ash disturbance incidences. Note that the second disturbance, at 35.9 hours, was the more influential of the two. The pressure face results also show large heat transfer increases at each disturbance, with the first being the larger in magnitude. Note also that during the first 9.9 hours there were numerous small ash removal incidences evident in the pressure face data. These incidences were obviously local in nature as the throat area history was not affected (see Fig. 14).

The nozzle heat load history for test number 6 is shown in Fig. 48.

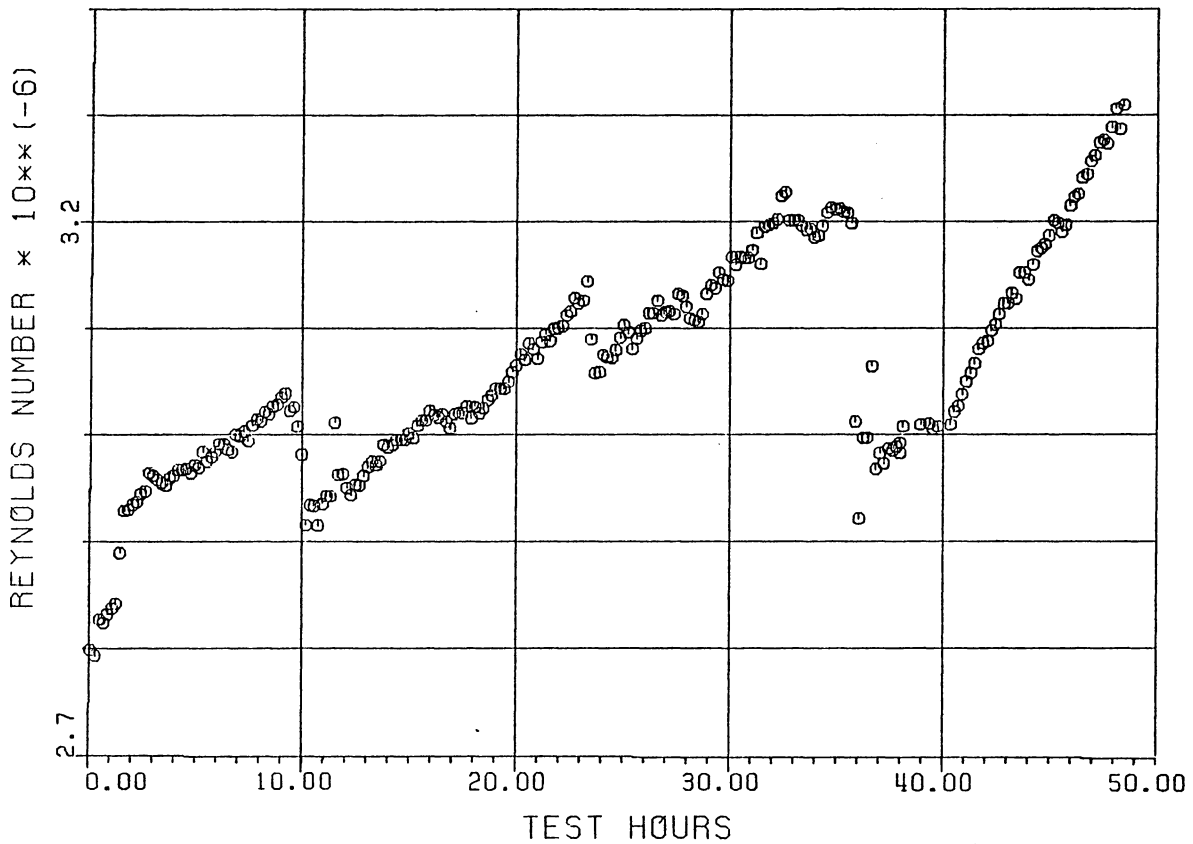

FIGURE 43
REYNOLDS NUMBER HISTORY FOR TEST NUMBER 5

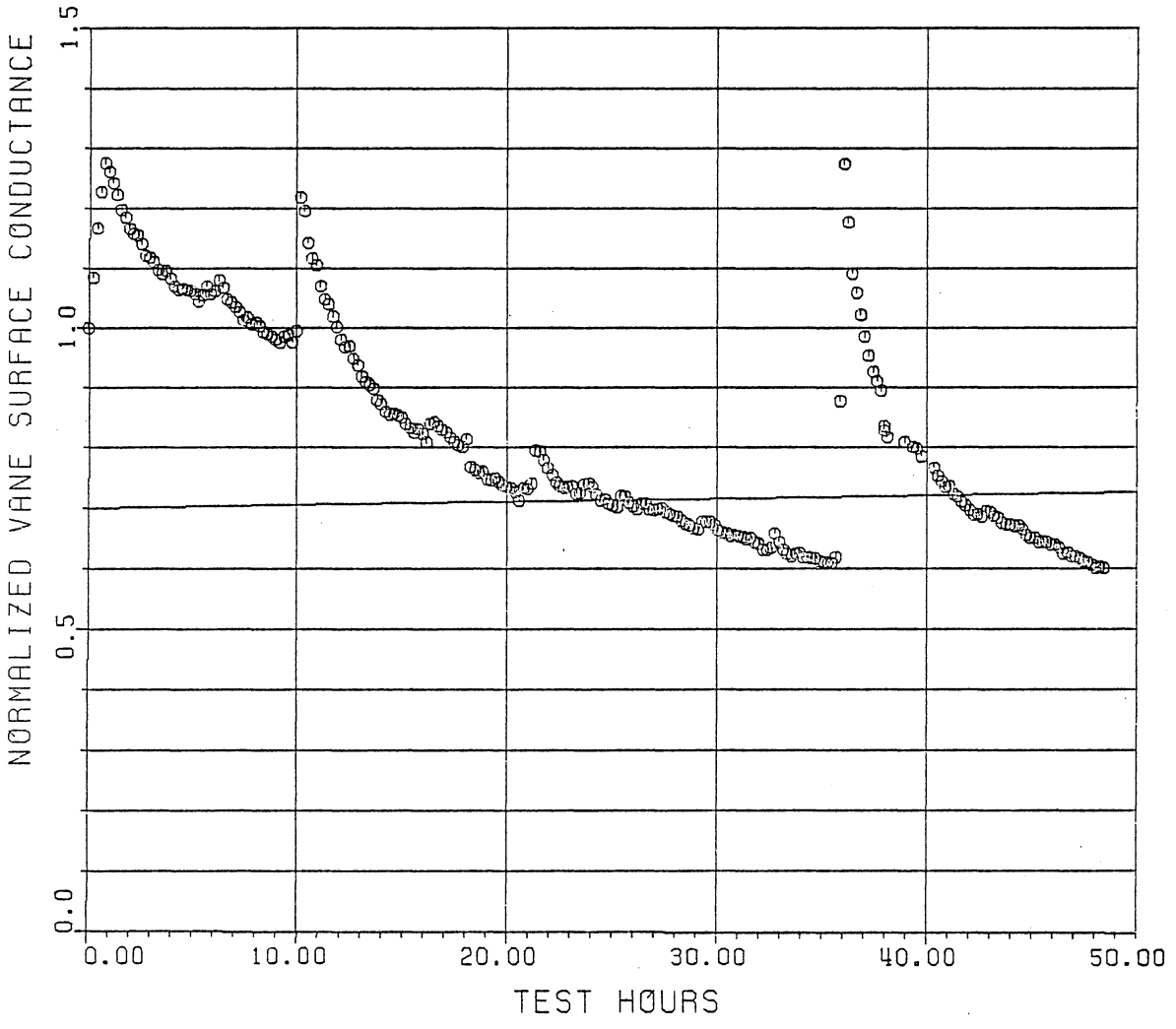

FIGURE 44
VANE 2 SUCTION FACE SURFACE CONDUCTANCE
HISTORY FOR TEST NUMBER 5

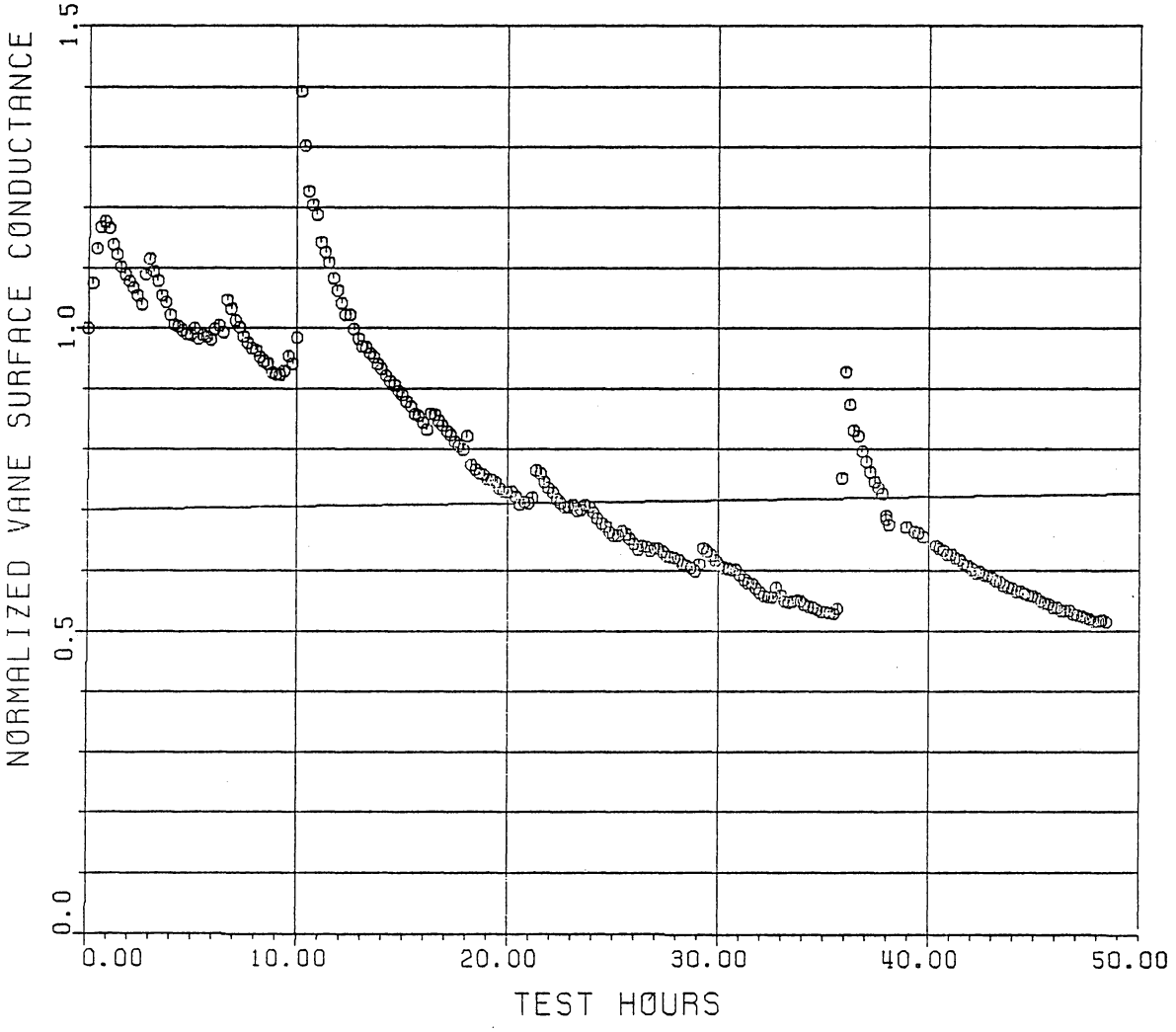

FIGURE 45
VANE 2 PRESSURE FACE SURFACE CONDUCTANCE
HISTORY FOR TEST NUMBER 5

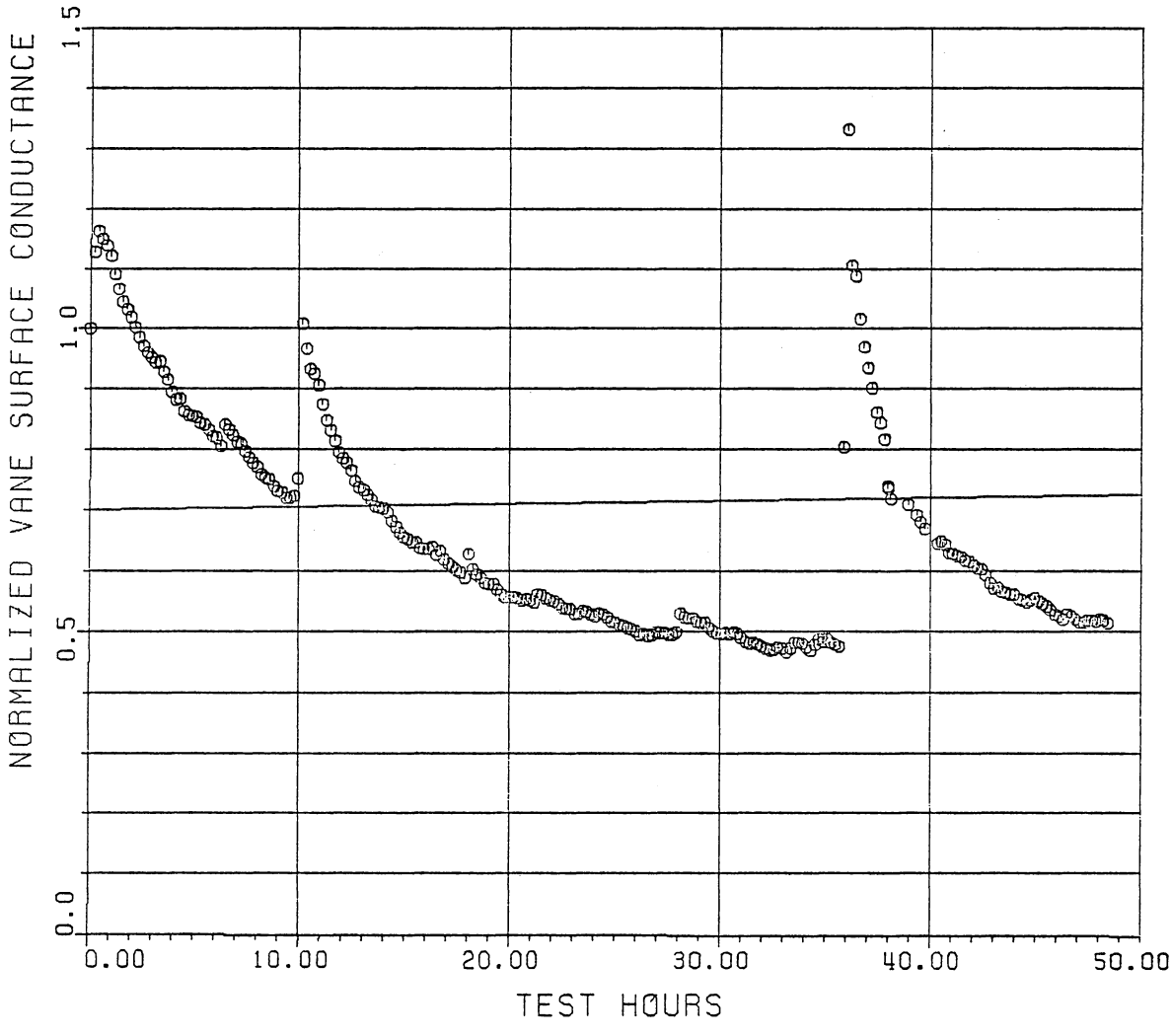

FIGURE 46
VANE 3 SUCTION FACE SURFACE CONDUCTANCE
HISTORY FOR TEST NUMBER 5

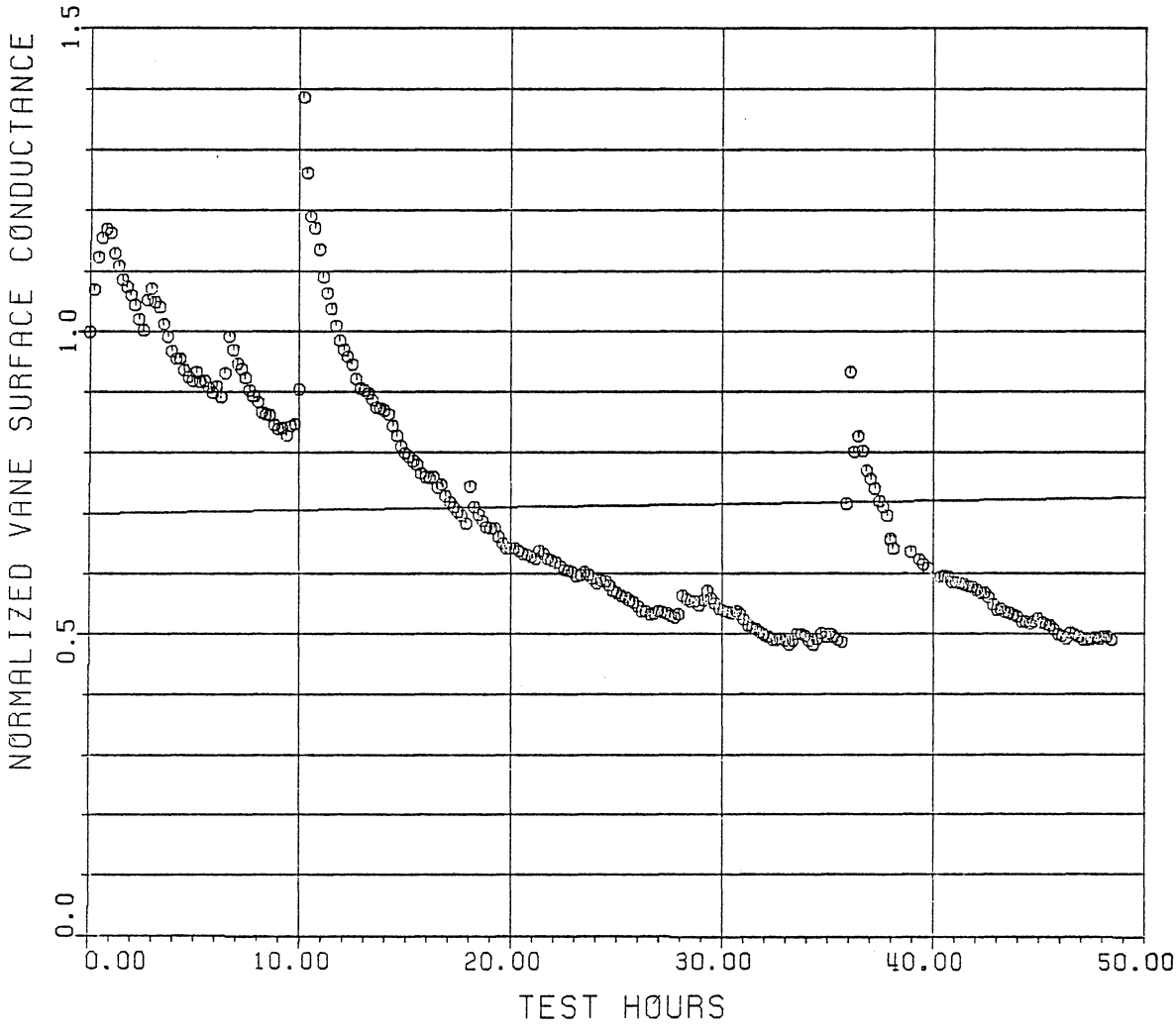

FIGURE 47
VANE 3 PRESSURE FACE SURFACE CONDUCTANCE
HISTORY FOR TEST NUMBER 5

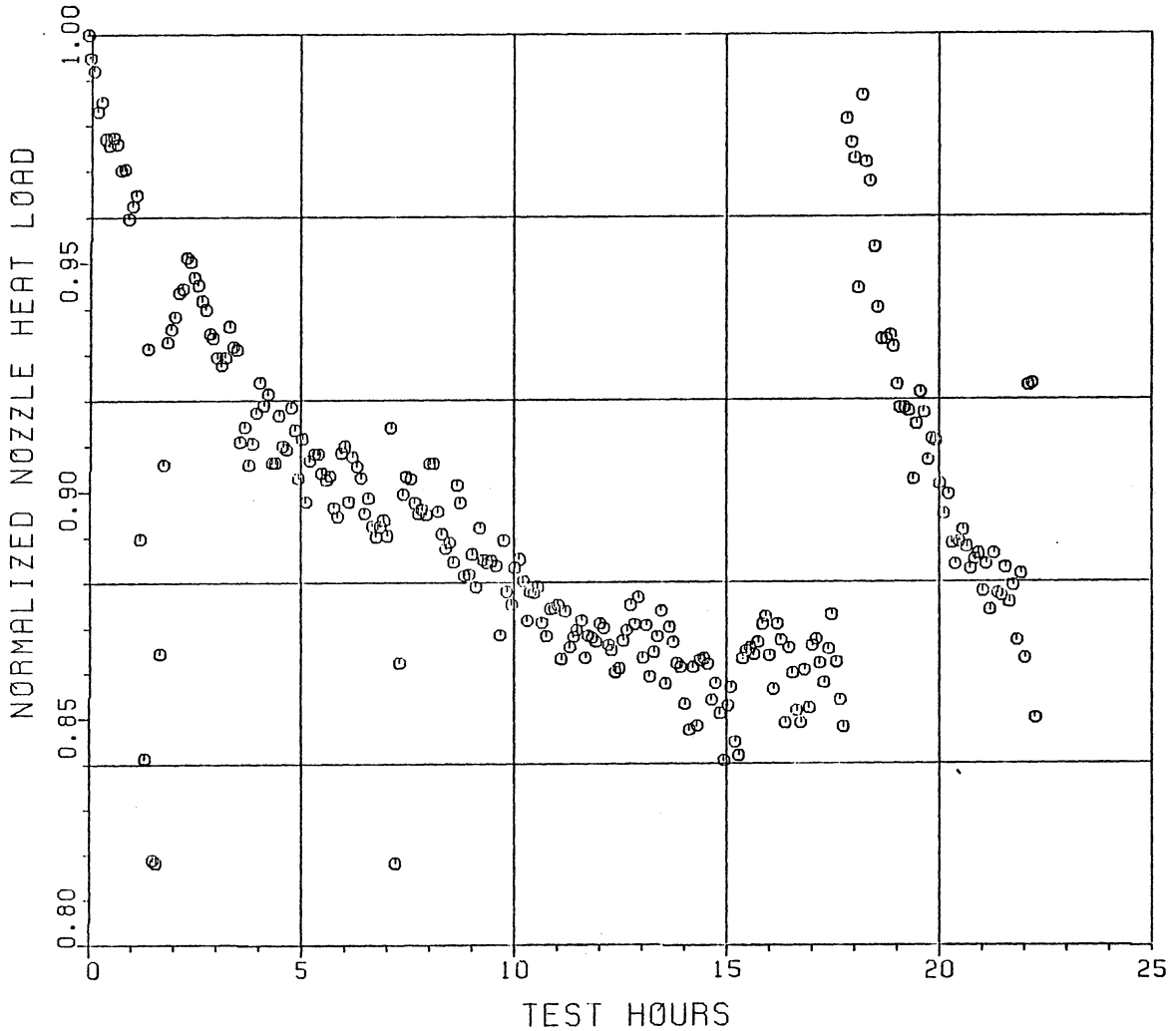

FIGURE 48
NOZZLE HEAT LOAD HISTORY FOR TEST NUMBER 6

As in the previous tests, the general trends of decreased heat transfer with time is noted. The large increase in heat transfer 17.8 hours into the test coincides with the ash removal due to nutshell injection. Two large downward spikes appear in the data at 1.6 and 7.2 hours. These are the result of failures of the gas-fired air preheater, which caused a decrease in the temperature and pressure of the air entering the turbine simulator. The heat load was recovered when the preheater was restarted.

A cross plot of the heat load versus the throat area is shown in Fig. 49. Note that there is substantial scatter in the data, particularly for plugging above 5 per cent. Most of this scatter is due to the transient nature of the sudden ash removal during the nutshell injection and the recovery period that follows. Figure 50 shows the same data except only the first 17.7 hours of data are plotted. Except for the heat load decreases due to the preheater failures, the data are very well behaved. The linearity of the heat load/throat area relationship appears to be preverved only for approximately 2 per cent plugging, after which a maximum decresase in heat load of about 15 per cent is observed.

The dimensionless vane surface metal temperature histories for test number 6 are shown in Figs. 51-54. One surprising observation that is immediately made is that the dimensionless temperature increases at the points where the heat load dropped due to preheater failures. This apparent discrepancy is a result of the manner which the dimensionless temperature is defined, eq. (4.11). In this case, the metal surface

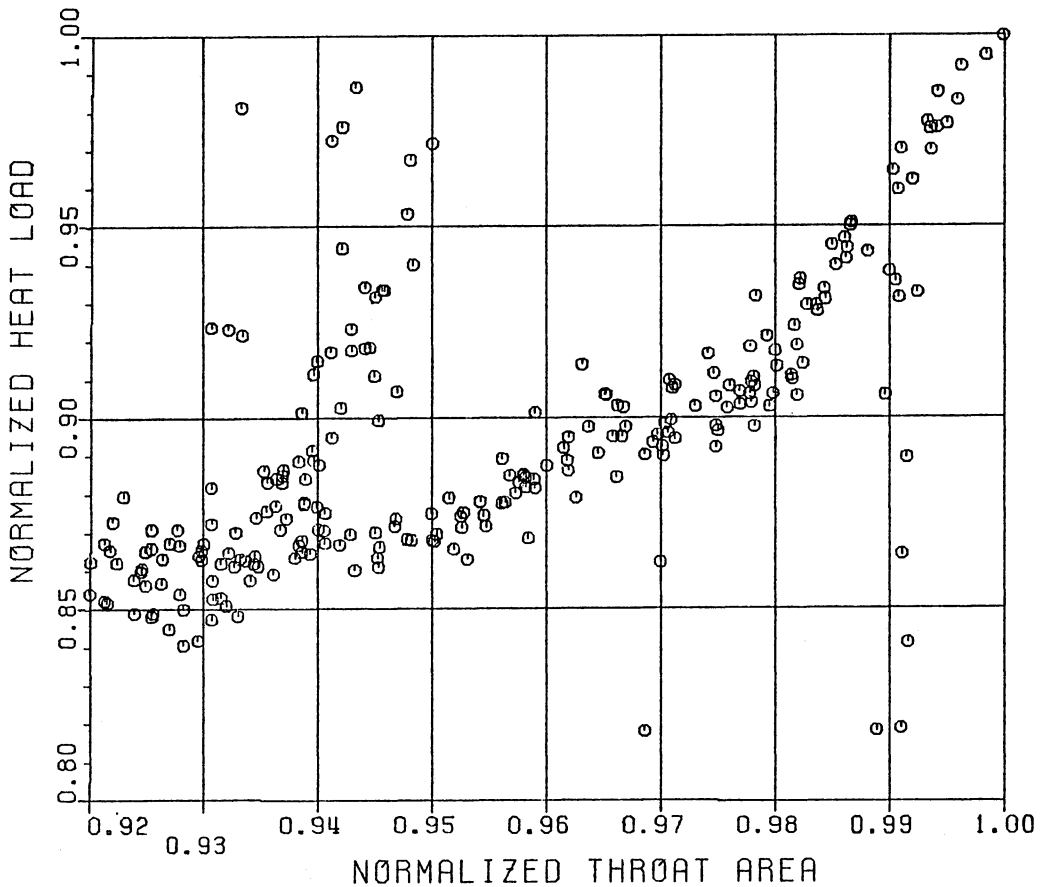

FIGURE 49
NOZZLE HEAT LOAD VARIATION WITH
THROAT AREA FOR TEST NUMBER 6

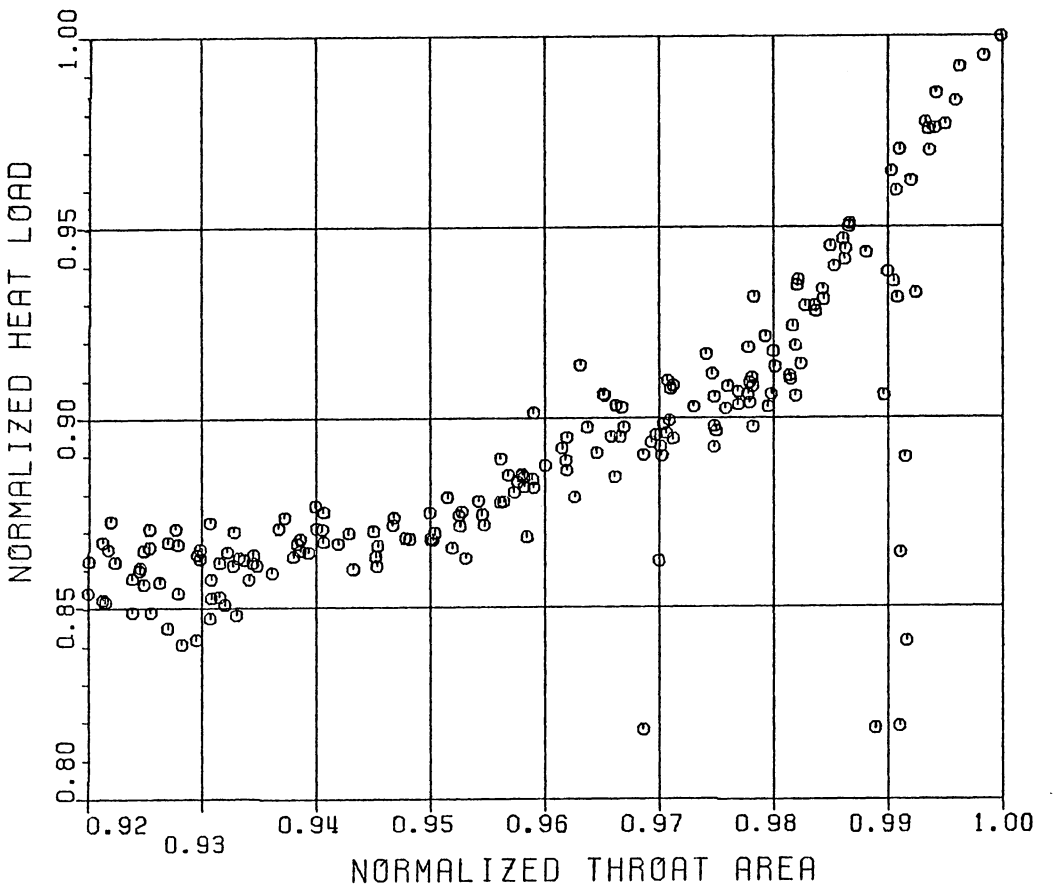

FIGURE 50
NOZZLE HEAT LOAD VARIATION WITH
THROAT AREA FOR TEST NUMBER 6
(0-17.7 HOURS)

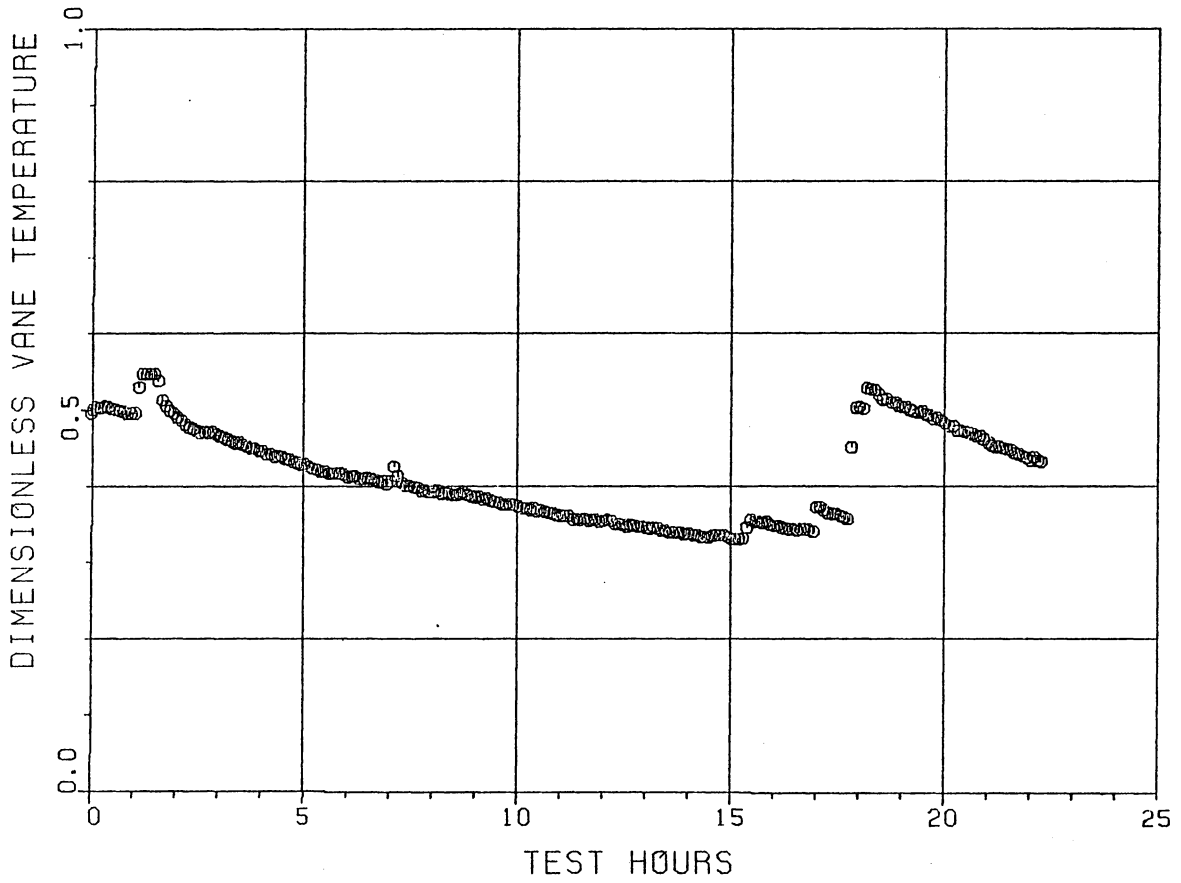

FIGURE 51
VANE 2 SUCTION FACE SURFACE TEMPERATURE
HISTORY FOR TEST NUMBER 6

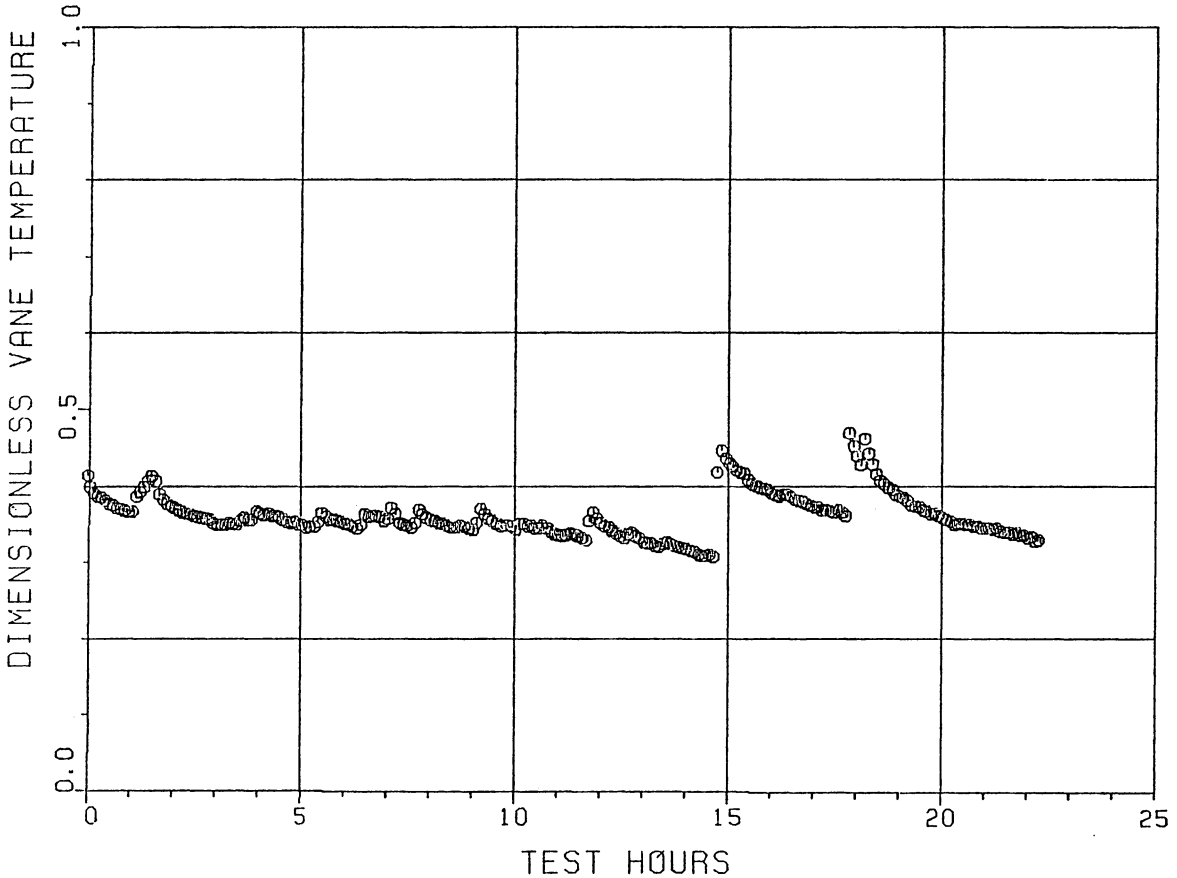

FIGURE 52
VANE 2 PRESSURE FACE SURFACE TEMPERATURE
HISTORY FOR TEST NUMBER 6

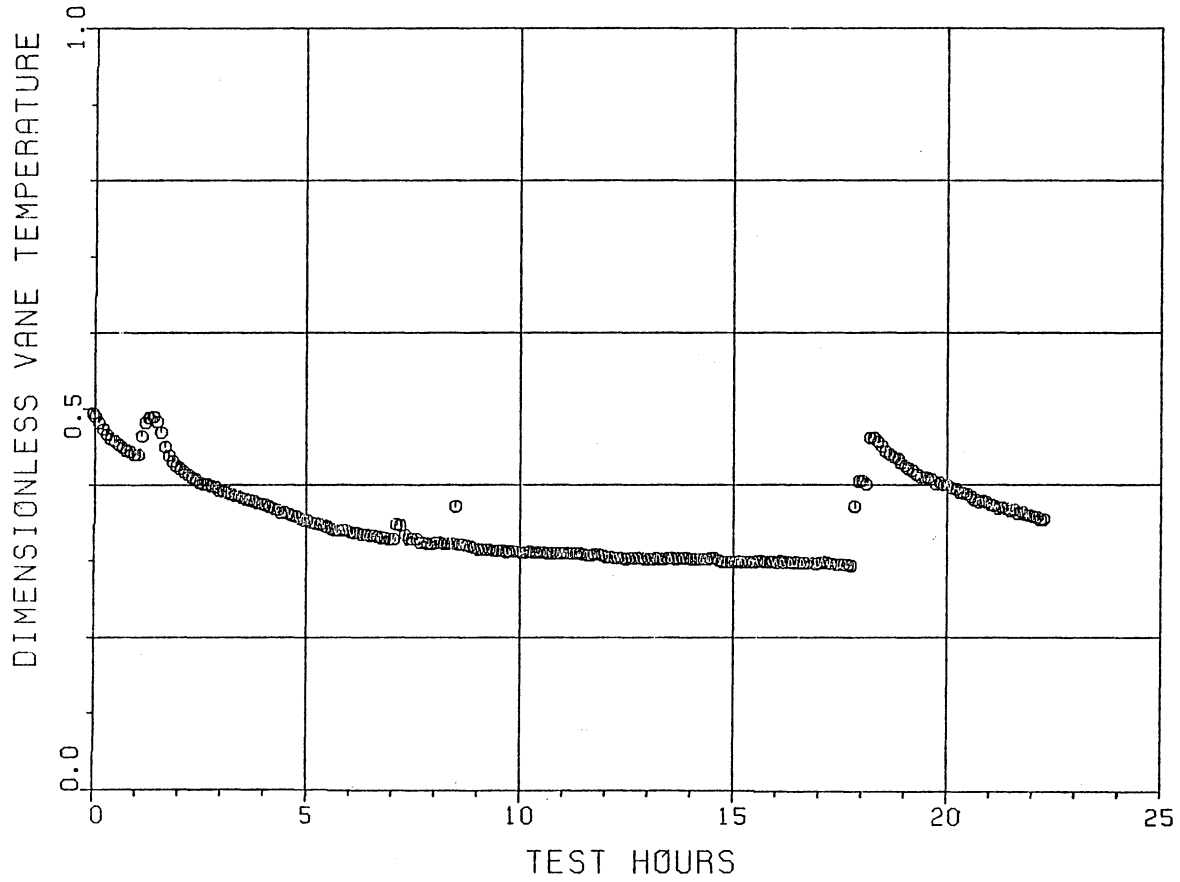

FIGURE 53
VANE 3 SUCTION FACE SURFACE TEMPERATURE
HISTORY FOR TEST NUMBER 6

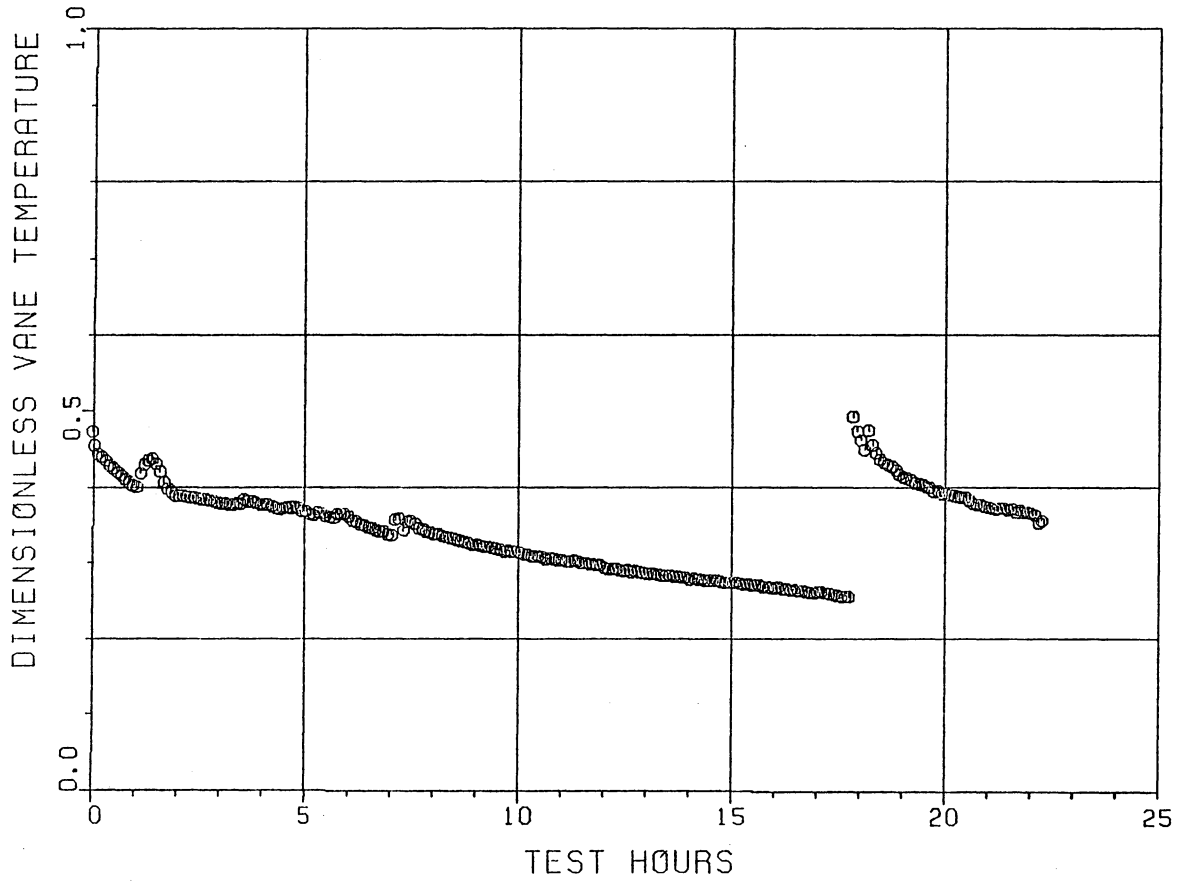

FIGURE 54
VANE 3 PRESSURE FACE SURFACE TEMPERATURE
HISTORY FOR TEST NUMBER 6

temperature actually dropped, but since the gas temperature also decreased, the dimensionless value can and does increase. Note also that a sudden, unexpected increase in the pressure face temperature of vane 2 occurred at a point 14.6 hours into the test. This would apparently indicate that some disturbance of the ash layer occured.

The airfoil Reynold's number history for test number 6 is shown in Fig. 55. Note that the trend is a steady increase which would be expected for a well-controlled test with the combustor pressure steadily increasing. The throat area recovery results in an increased pressure and thus a decreased Reynold's number. Reynold's number increases at 1.6 and 7.2 hours correspond to decreases in pressure and temperature with preheater failure, with the temperature decrease dominating in eq. (4.20).

The corrected dimensionless heat transfer coefficents for test number 6 are shown in Figs. 56-59. This particular set of data offers strong justification for the method used to reduce the data. The heat transfer perturbations resulting from the preheater flameout are almost completely compensated for by the Reynold's number correction. The disturbance in the surface temperature on the pressure face of vane 2 at 14.6 hours is also compensated for. None of these incidences therefore had any effect on the ash deposit.

One phenomenon present in tests 2 and 5 but not in test 6 was the increase in heat transfer in the early stages of the test. This will be discussed in more detail in the next chapter.

Note that there is a pronounced increase in heat transfer on all

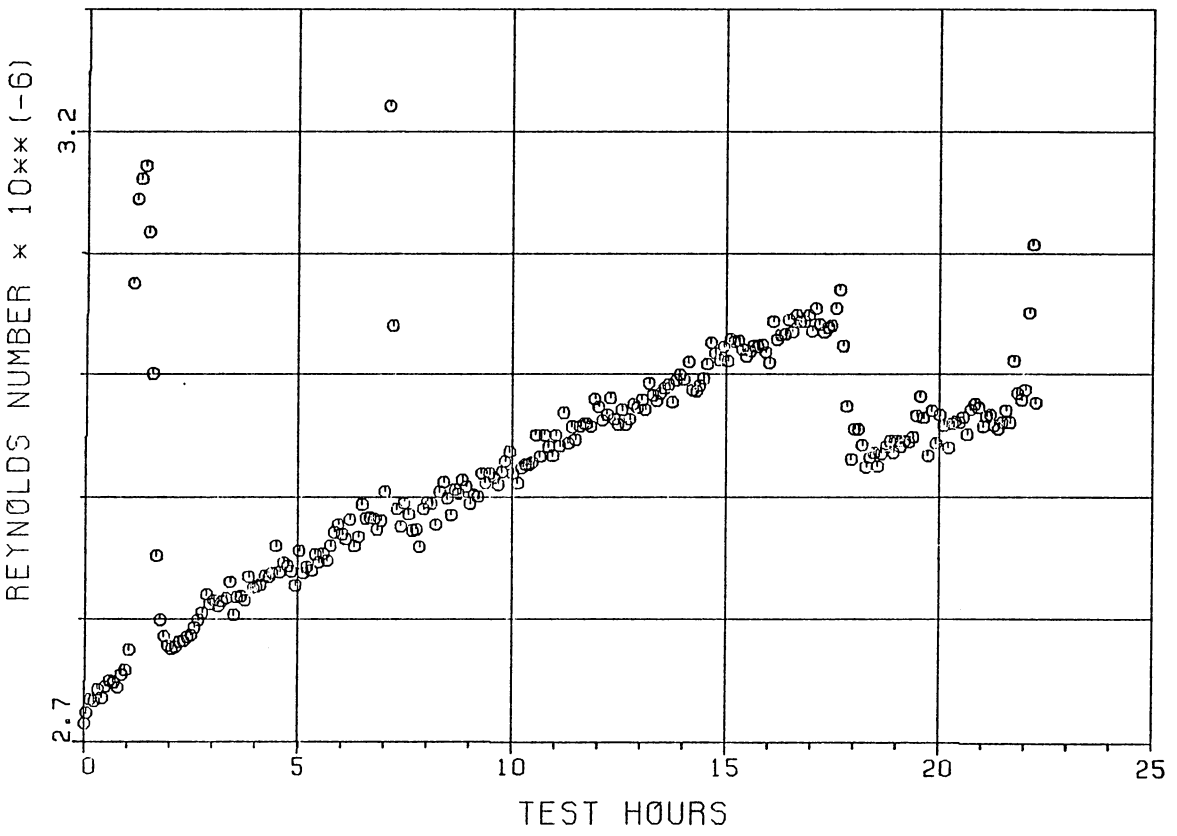

FIGURE 55
REYNOLDS NUMBER HISTORY FOR TEST NUMBER 6

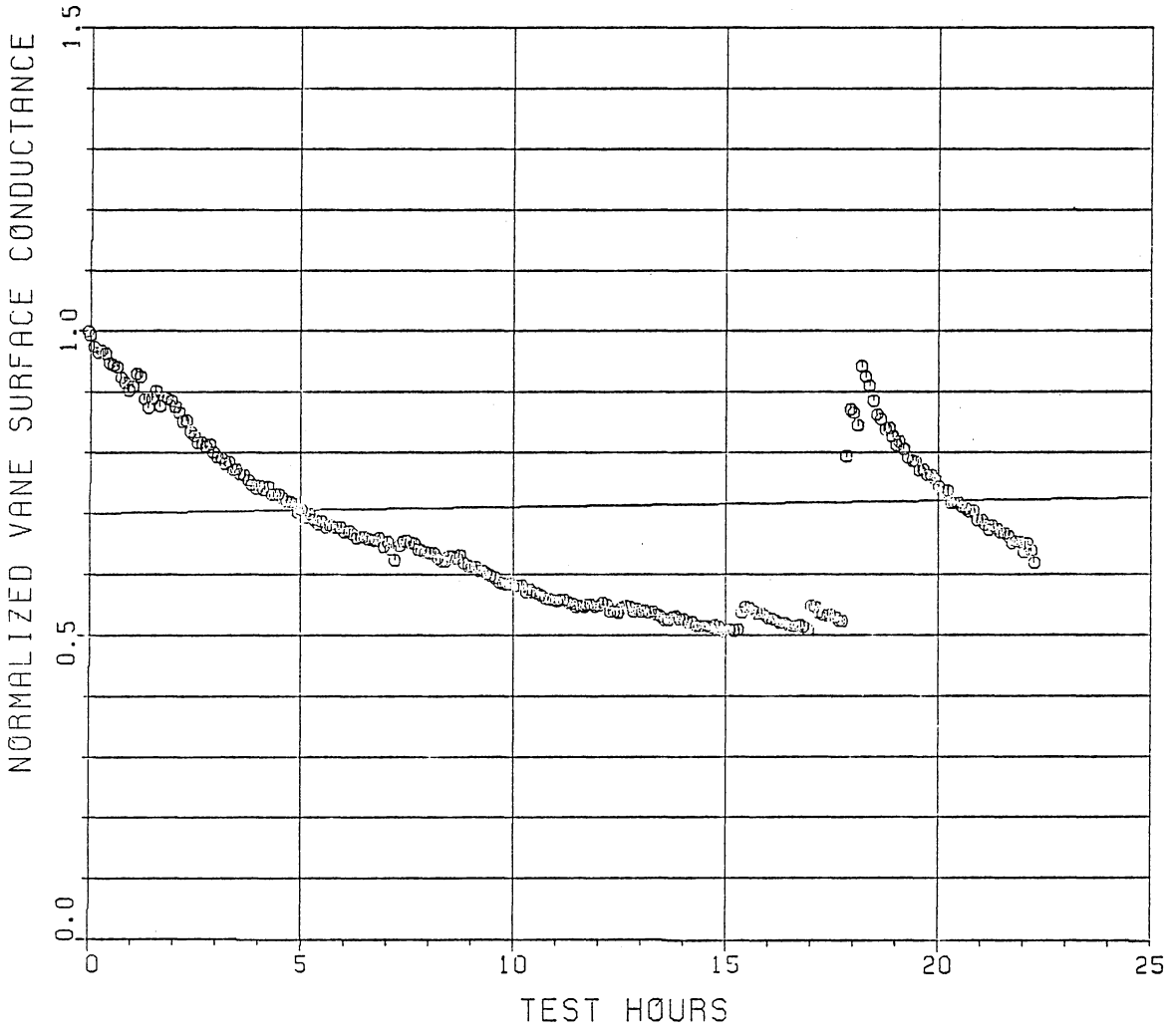

FIGURE 56
VANE 2 SUCTION FACE SURFACE CONDUCTANCE
HISTORY FOR TEST NUMBER 6

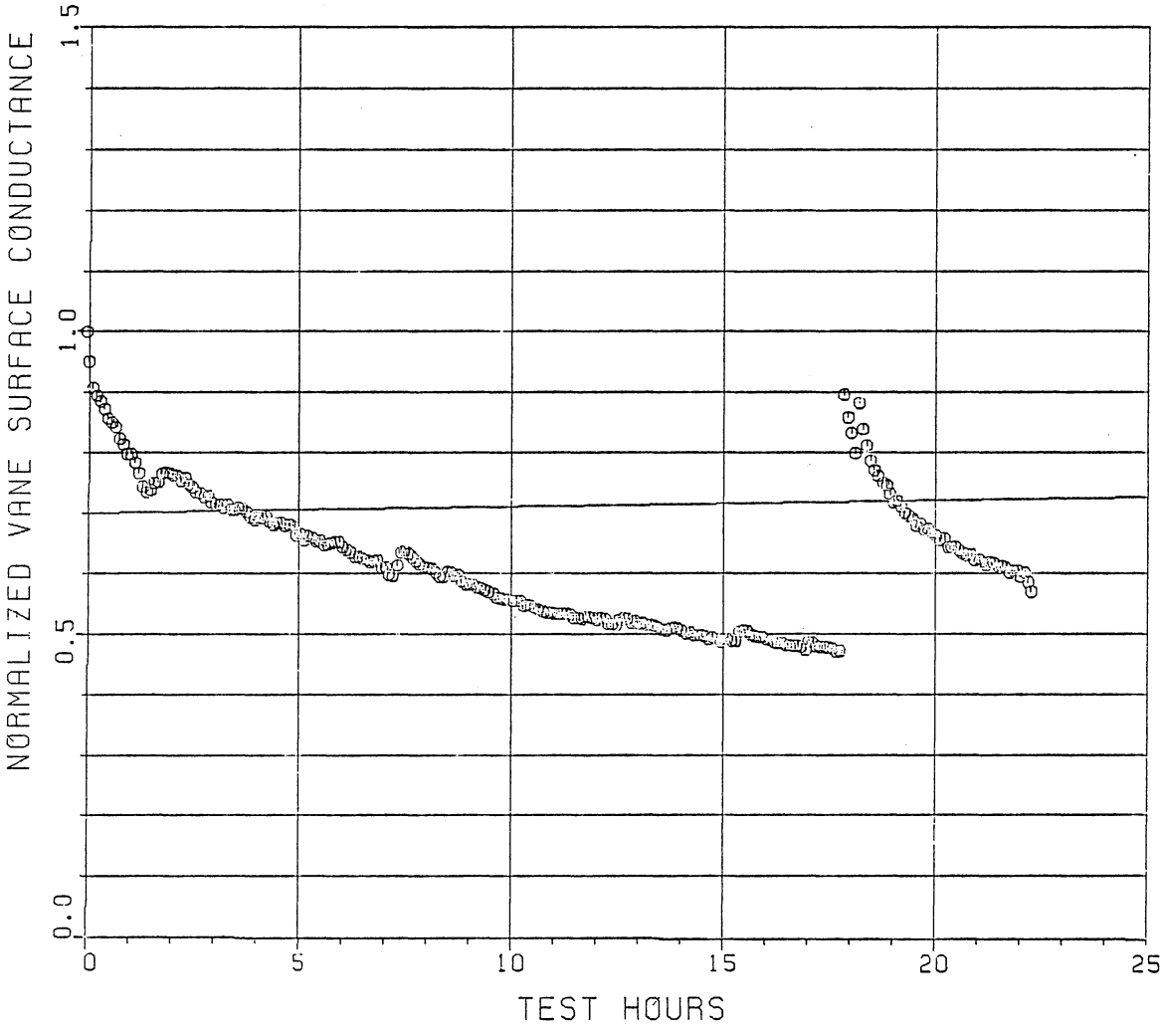

FIGURE 57
VANE 2 PRESSURE FACE SURFACE CONDUCTANCE
HISTORY FOR TEST NUMBER 6

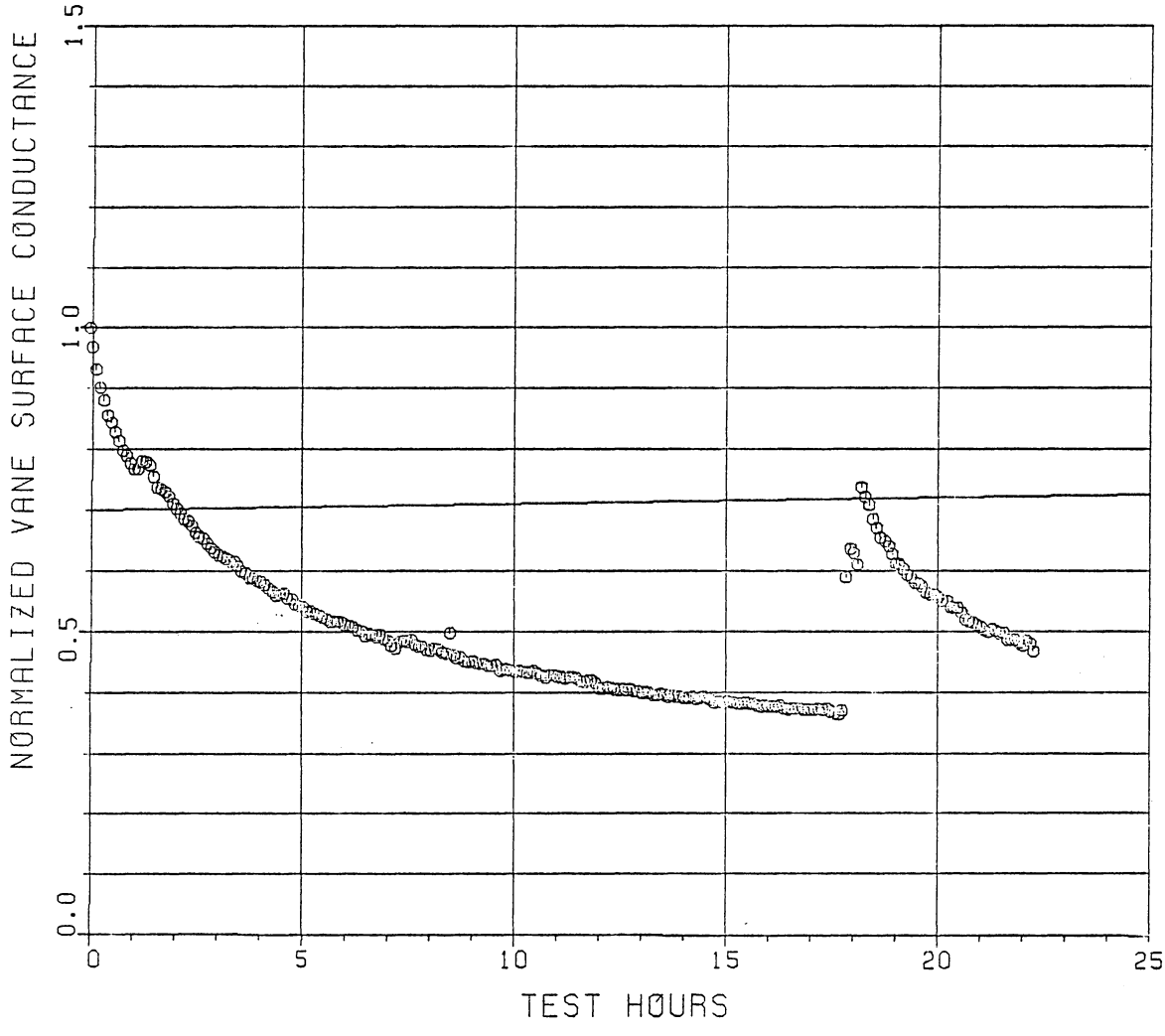

FIGURE 58
VANE 3 SUCTION FACE SURFACE CONDUCTANCE
HISTORY FOR TEST NUMBER 6

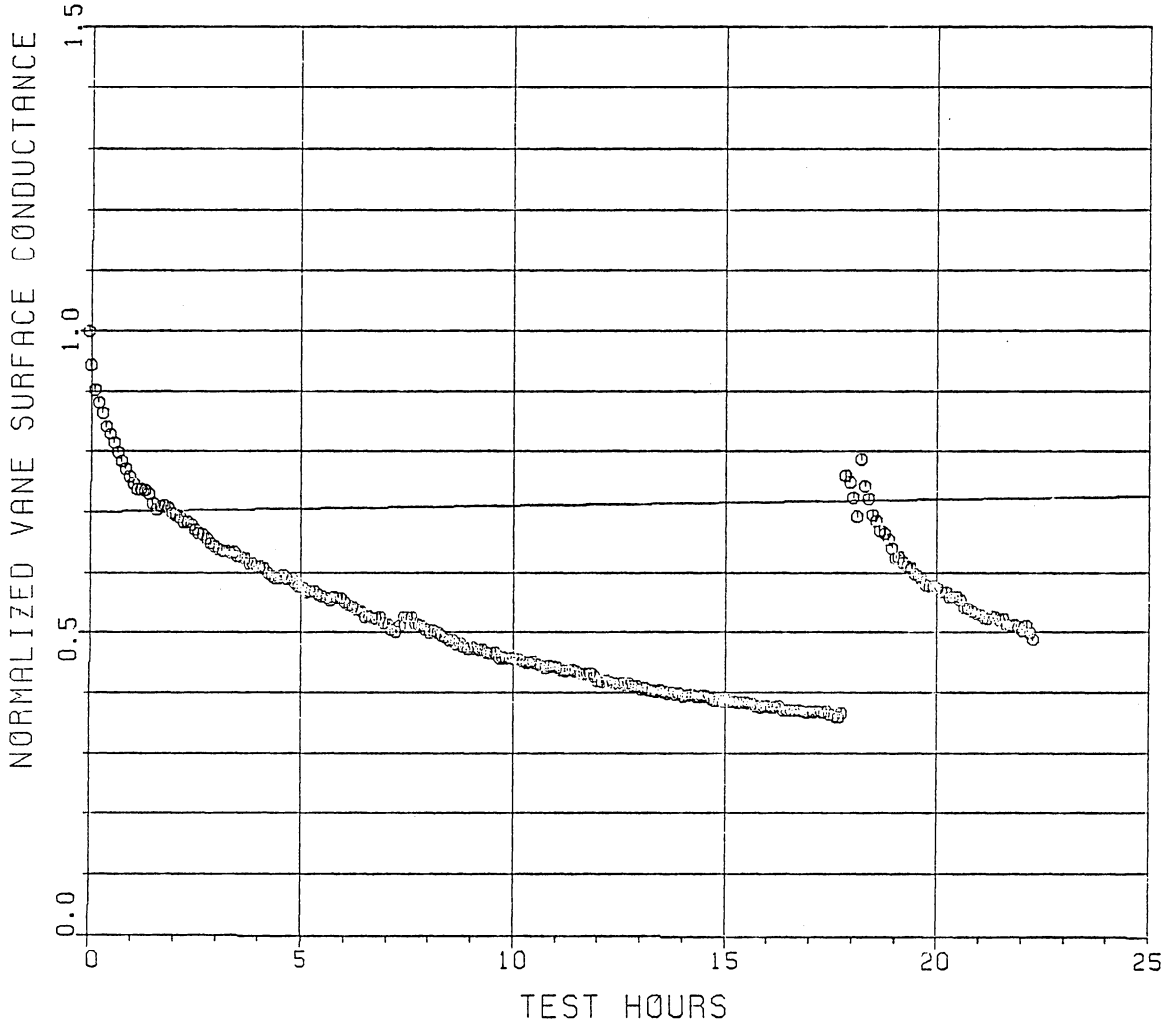

FIGURE 59
VANE 3 PRESSURE FACE SURFACE CONDUCTANCE
HISTORY FOR TEST NUMBER 6

surfaces with the ash removal by nutshell injection. The magnitude of the increase, however, is not as great as had been observed previously in some cases of thermal spalling of the ash deposit with gas temperature excursions. Note also that the two stages of the nutshelling are discernable in the data. The first load of nutshells were injected at 17.7 hours and the second load at 18.1 hours. There was no further increase in heat transfer with the second nutshelling on the pressure faces. On the suction faces however, there was apparently additional ash removal with the second nutshell injection. A closer examination of the throat area history (Fig. 15) reveals that the separate nutshellings are discernable in these data also. Additional throat area recovery was initiated by the second nutshelling.

The nozzle heat load history for test number 7 is shown in Fig. 60. Because of the high number of nozzle cleanings performed there is substantial unsteadyness in the data. Recall that throat area recoveries occured at points 22.5, 26.4, 39,4, 47.7, and 56.3 hours into the test. Increases in the nozzle heat load were noted at these points.

The dimensionless vane surface metal temperatures and the surface heat transfer conductances are not plotted for this test because of the large number of recovery events and the short duration between the events. No attempt was made to correlate the heat load with the throat area.

The airfoil Reynold's number history for test 7 is shown in Fig. 61. The nominal value was 1.5 (10^6), with variations experienced from -9.6 to +3.3 per cent. The Reynold's number values were lower than

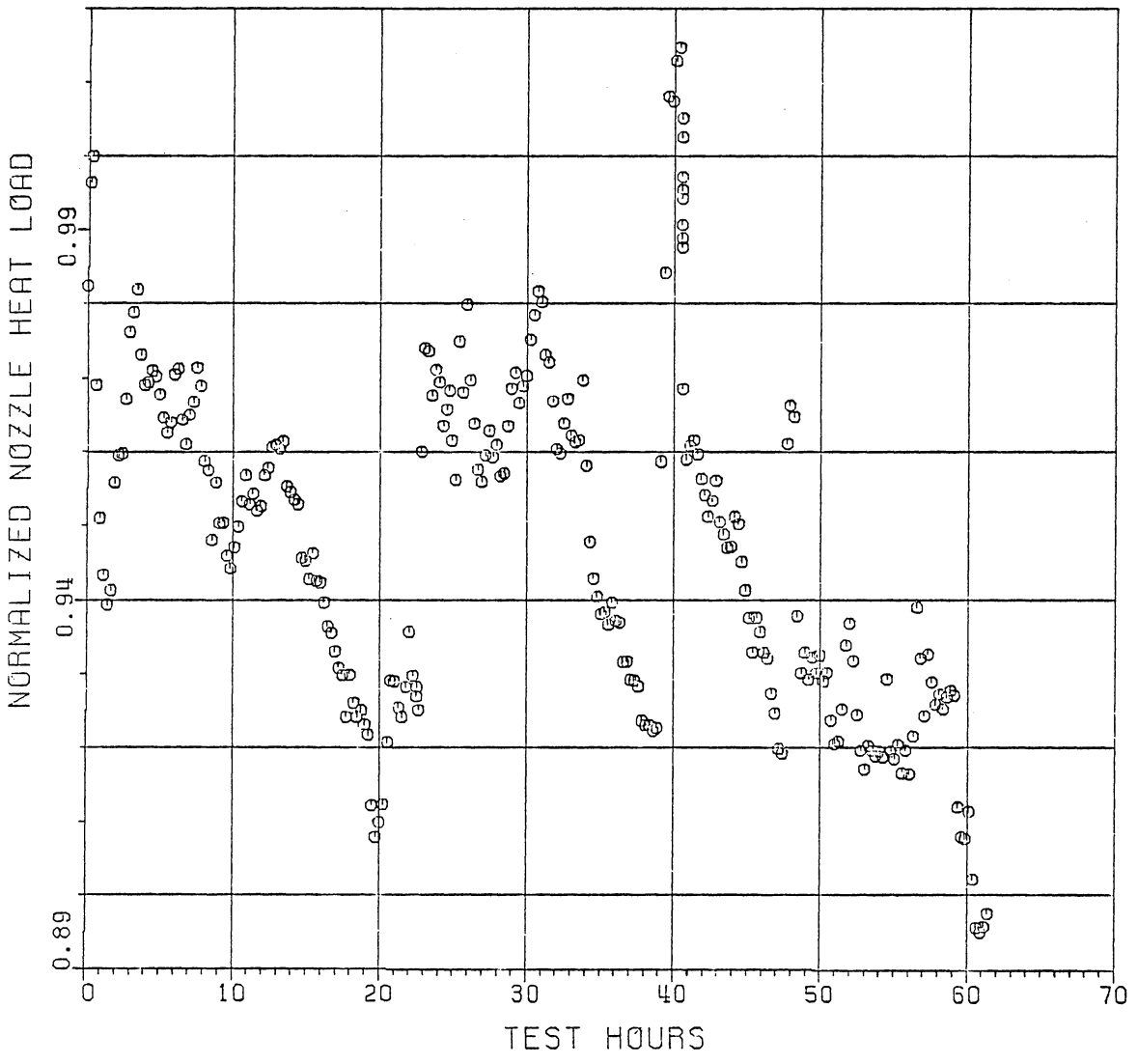

FIGURE 60
NOZZLE HEAT LOAD HISTORY FOR TEST NUMBER 7

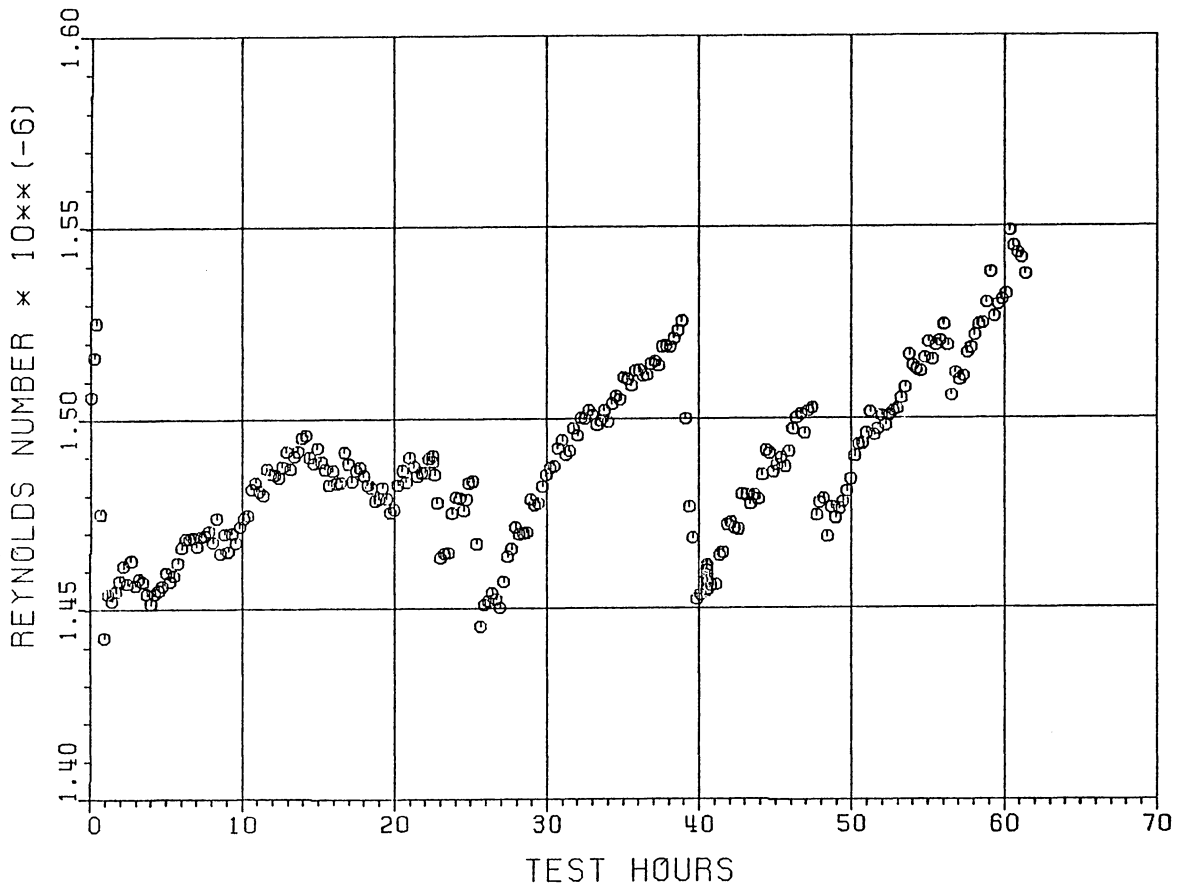

FIGURE 61
REYNOLDS NUMBER HISTORY FOR TEST NUMBER 7

those of tests 5 and 6 because the nozzle inlet pressure was only one-half as much and thus the density was reduced.

6. DISCUSSION OF RESULTS

6.1 Test Conditions

A comparison of the nominal with the actual operating conditions for each test was shown in Table 3. It is very important that deviations from the nominal test conditions be documented and accounted for. It has already been pointed out that the ash deposition rate is a strong function of the gas temperature. Deviations from the nominal firing temperature would thus affect the ash deposition results and make comparisons between tests difficult. The gas pressure also plays an important but not-so-obvious role. The mass flow of combustion gases is directly proportional to the gas pressure. Since the contaminants are added as a constant weight fraction to the fuel and the combustion fuel/air ratio is independent of the gas pressure, the mass flow of contaminants and thus the ash load are also proportaional to the gas pressure. Pressure variations therefore subject the nozzle to variations in ash loading, again making comparisons between tests difficult.

An approximate method for correcting the ash deposition data so that tests could be compared on an equal basis was developed as part of this investigation. This method corrects the ash deposition rate data for both gas pressure and gas temperature variations.

As described above, gas pressure variations result in proportional variations in the ash loading. Data were available from tests numbers 7 and 8 relative to the effect on ash deposit rates of changes in ash loading at constant pressure. These data were incorporated in

developing a linear correction for pressure variations. Gas temperature variations were accounted for by interpolating between the pressure-corrected data from the 6 atmosphere tests. Tests numbers 1 and 3 thus provided two interpolating points for the air-cooled nozzle. Test number 2 and the average from tests 5 and 6 provided the basis for the water-cooled nozzle gas temperature correction. The turbine inlet temperature was chosen as the reference temperature in all cases.

6.2 Ash Deposit Formation

The raw and corrected ash deposition rate data for the complete test program are summarized in Table 5. The pressure and temperature corrections described in the previous section were applied. One surprising observation was that the ash deposit rate did not vary linearly with the ash loading. A halving of the ash loading (100% to 50% of full simulated engine levels) in test number 7 resulted in only a 25 per cent reduction in the ash deposition rate. A similar reduction of the ash loading in test number 8 resulted in a 23 per cent reduction in the deposit rate. These data were used as the basis of a gas pressure correction on all tests. The gas temperature correction also yielded some very interesting results. The sensitivity of the ash deposition rate in the water-cooled nozzle to gas temperature changes was more than twice that of the air-cooled nozzle. Note in Table 5 that tests number 1 and 2 were corrected to the same turbine inlet temperature (1310 K), and tests 3 and 4-8 to a different value (1430 K). With these modifications, the ash deposit data may be more readily interpreted.

TABLE 5

Ash Deposition Rate Data

Test	Type[1]	Uncorrected Deposit Rates, % per 100 hrs[2]	Average Uncorrected Rates, % per 100 hrs	Pressure Corrected Rates, % per 100 hrs	Pressure and Temperature Corrected Rates, % per 100 hrs[3]
1	AC	16.6/17.7	17.2	17.2	16.0
2	WC	11.4/13.6	12.5	12.2	11.9
3	AC	24.3/35.6	30.0	29.1	33.9
5	WC	31.3/42.5/69.9	47.7	47.1	49.9
6	WC	44.5/44.8	44.7	44.7	48.4
7	WC	21.6/28.4//32.7/34.4	25.0//33.6	33.3	32.4
8	AC	39.2//51.0	39.2//51.0	49.6	42.0

[1]Type designation: AC - air-cooled nozzle; WC - water-cooled nozzle.

[2]The single slash (/) separates periods of ash formation broken by throat area recoveries. The double slash (//) separates periods of 50% and 100% additive levels in tests 7 and 8.

[3]Tests 1 and 2 corrected to 1310 K turbine inlet temperature. Tests 3, 5-8 corrected to 1430 K.

Consider first tests 1 and 2, performed at the lower gas temperature level. The rate of ash deposit formation (throat area decrease) for the air-cooled nozzle (test 1) was 16 per cent per 100 hours. The corresponding rate for the water-cooled nozzle (test 2) was approximately 12 per cent per 100 hours, or a reduction of 25 per cent. This was the expected trend, as it was believed that the lower surface temperatures in the water-cooled test would inhibit adhesion of the ash.

The result of test number 3, performed at the higher gas temperature, was again as expected. The ash deposition rate of 34 per cent represented a slightly more than 100 per cent increase in the rate obtained at the lower gas temperature. Trends of this nature had been observed and documented in earlier investigations [13,14].

As would be expected, the ash deposition rates of tests 5 and 6 were higher than the rate observed in test 2, since the gas temperature was increased. What was not expected, however, was that the rates in tests 5 and 6 exceeded the rate of test 3 for the air-cooled nozzle. This surprising development was contrary to the previously-held beliefs regarding ash deposits on cooled surfaces. The sensitivity of the water-cooled nozzle to gas temperature changes was very high. The ash deposit rates in tests 5 and 6 were 300 per cent higher than that in test 2.

The unexpected trends observed in tests 3-5 were influential in the planning of the remainder of the test program. The final two tests of the series, performed at reduced gas pressure, were added with the intention to further investigate ash deposition at higher gas

temperatures. The reduced gas pressure resulted in the substantially lower metal surface temperatures (see Table 3). The ash deposition results were again a surprise. The trends observed in tests 3-5 were reversed so that agreement with tests 1 and 2 was achieved. The ash deposit rate in test 7 (water-cooled) is reduced approximately 34 per cent from the results of tests 5 and 6. In test 8 (air-cooled), however, the observed ash depostion rate was 24 per cent higher than in test number 3. This particular result does not seem possible in the light of the previous data and observed trends.

If one considers tests 5 and 6 as representing one data point, then six ash deposition rates are produced from the test program. The one point which seems out of place is the rate from test number 3. Consider the trends one would observe, for example, if the corrected ash deposition rate in test 3 was 64 per cent per 100 hours rather than 33.9 per cent as documented. The same gas temperature trend would then be observed in both the air-cooled and water-cooled nozzle tests, i.e., an increase in ash deposition rate of 300 per cent with the increase in gas temperature. The same trend would also be observed with the decrease in gas pressure, i.e., a decrease in ash deposition rate of 34 per cent. This near-exact agreement is almost too good to be coincidental. It is thus possible that for some reason the results of test 3 are faulty. This is therefore presented as one possible explanation for the observed discrepancy in the data.

If one assumes that all of the test data are valid, and this is most probable, then some very complicated mechanisms must be acting.

With the air-cooled nozzle being film-cooled, one could speculate that plugging at the nozzle throat is strongly dependent on how the cooling air penetrates the deposit layer. This would explain how ash deposit formation in the air-cooled nozzle could be very inconsistent.

The above are two possible explanations for the erratic data of test number 3. Ideally the test should be redone to verify the ash deposit rate, but this cannot be practically done because of the time and expense.

One point that should be kept in mind when discussing the effect of vane surface temperatures on the ash deposit formation is that as the ash deposits build in thickness a thermal barrier is formed. This would in effect insulate the surface from the gas stream. The new surface, upon which new deposits form, is the ash surface itself. The temperatures of this surface are much higher than the metal surface because of the thermal barrier effect. In the case of the air-cooled nozzle, since the film-cooling air penetrates the ash layer, some film-cooling of the ash layer surface itself would occur. This would of course not occur in the water-cooled nozzle. The implication of this point is that, at least in certain physical locations, the air-cooled nozzle ash surface temperatures could be lower than for the water-cooled nozzle. This phenomenon would tend to complicate a physical understanding of the ash deposit mechanism even further.

To gain any understanding of the mechanism of ash deposit formation, one must consider what the method of adhesion of the ash to the gas path surface is. It is not known exactly what the characteristics

of the ash are in the combustion gases. At the turbine inlet temperatures, the ash should be in solid form, but depending on the residence times some molten material may be present. The particles which deposit appear to be spherical in shape [18]. At the temperatures of the metal surfaces, the ash matter would most certainly be solid in phase. Just how this matter adheres to the surface is a subject of much debate. One test, performed at General Electric*, seems to indicate that condensing vapor phases containing sodium and vanadium form a "glue" which causes adhesion of the ash particles to surfaces and to each other. At higher temperatures, however, above the dew point of the vapor species, other mechanisms may be prevalent. One possibility is simple "sintering", or direct impact of molten or semi-molten particles into the high-temperature ash surface. This mechanism may be active in the latter stages of high temperature tests. Consider, for example, test number 5, where glue-forming sodium was inadvertantly omitted from the fuel additives in the latter part of the test, with no apparent effect on the ash deposition rate.

A more detailed examination of the mechanisms of ash deposit formation is outside the scope of this investigation.

6.3 Ash Deposit Removal

The ash deposit removal characteristics are of equal importance to

---

*This test was discussed by Mr. H. Von E. Doering at the panel discussion," Deposition Effects in Gas Turbines," session 72 at the ASME Gas Turbine Conference and Product Show, Houston, TX, March 8-12, 1981.

the deposition rates in the operation of a combustion turbine engine burning a residual fuel oil. A high ash deposition rate would not be a serious obstacle if the deposits could be readily removed on-line without shutting down the engine.

Methods of removing ash deposit from the turbine on-line may be divided into two categories. The first category involves ash removal by direct mechanical action. This would include the abrasive cleaning techniques investigated in tests 6-8. The second category involves ash removal by indirect means and would include the thermal excursions of tests 2-5 and the atomizing air pressure fluctuation of test number 7. Ash removal by indirect means would imply some change in the operating condition of the turbine engine. The resulting thermal transient would affect a spalling of the ash deposit.

The principle off-line method used for cleaning of ash deposits is the water wash/soak/refire sequence discussed earlier. This method has been very successful in the field in removing ash deposits during shutdowns. On-line methods are of course preferred, particularly for high load factor operation.

A summary of all the throat area recovery events which occurred during the test program is given in Table 6. The numbers in parenthesis which appear with each recovery magnitude indicate the per cent decrease in nozzle throat area which had occurred up to that point in the test.

The direct action cleaning by nutshell injection was marginally effective (39% recovery at 8% plugged) in test number 6. In practice an actual engine would more than likely be cleaned before reaching this

TABLE 6

Summary of Throat Area Recovery Events[1]

Test	Type[2]	On-Line: Nutshell Injection	On-Line: Thermal Excursion Type I	On-Line: Thermal Excursion Type II	On-Line: Atomizing Air Pressure Fluctuation	Off-Line: Wash Sequence
1	AC	——	——	——	——	90(8)
2	WC	——	43(5)	——	——	100(5.5)
3	AC	——	——	23(18)	——	90(20)
5	WC	——	68(3)	55(12)	——	100(14)
6	WC	39(8)	——	——	——	——
7	WC	95(3) 58(3)	——	——	37(3)	——
8	AC	60(4) 72(8)	——	——	——	——

[1]Throat area recoveries are given as percentage of lost area to that point recovered. The numbers in parentheses are the percentage throat area lost at the point of the recovery.

[2]Type designation: AC - air-cooled nozzle; WC - water-cooled nozzle.

magnitude of throat area reduction. What effect cleaning at a lower ash accumulation would have on throat area recovery is not clear. No nutshell injection was attempted in test number 3, although in retrospect the omission was not wise. Past data, however, indicate that unsatisfactory results would have been obtained [13,14]. Higher recoveries were obtained in the 3-atmosphere tests (7 and 8), seemingly implying that the ash formed at the lower surface temperatures is more readily removed. The cleanability of the air-cooled nozzle in test 8 is at least equal to that of the water-cooled nozzle in test number 7. Note also in test number 8 that better recovery was obtained when the nozzle was cleaned at the higher ash accumulation level.

Indirect cleaning by thermal excursions is not at present considered to be a viable method for intentionally cleaning turbine nozzles because of the potential for thermal damage. With the thermal insulating value of an established ash deposit, however, the damage potential may be reduced to the point that thermal cleaning is an alternative. The throat area recoveries obtained were comparable in magnitude to the direct cleaning methods, although direct comparisons are not possible because different tests were involved. The type I excurson (increased fuel flow) appeared to be more effective than the type II (reduced air flow). The type I excursion would, however, result in more severe thermal distress to the nozzle because of the higher pressure. Of course, this very reason is most probably why the ash removal is more effective.

The single attempt at indirect cleaning by variation of atomizing

air pressure resulted in a 37 per cent recovery (at 3% plugged). This was not as effective as nutshell cleaning earlier in the same test (number 7), but it is possible that better results could be obtained with some experimentation.

One of the prime questions regarding application of on-line cleaning techniques is at what point should be the nozzle be cleaned. At present the turbine is allowed to operate for as long as possible before cleaning is attempted. It is certainly possible that more effective operation could be obtained by nutshell injection at some earlier point in the operating sequence.

Off-line cleaning by the conventional water-wash sequence was attempted in the first four full-length tests (all at 6 atmospheres). Ash removal was 100 per cent effective in the water-cooled nozzle, but only approximately 90 per cent in the air-cooled nozzle. Visual inspection revealed that some ash deposit remained on the air-cooled nozzle. It is thus possible that subsequent operation and cleaning could result in a continual buildup of ash deposits each cycle. Eventually this would necessitate disassembly of the turbine to remove the deposits. In practice, however, the residual deposits do not build up continuously.

6.4 Heat Transfer

The heat transfer data, as mentioned previously, only pertained to the water-cooled nozzle tests (2,5-7). The data taken and the method of data reduction were very useful in gaining insight beyond that possible

using ash deposition or throat area data alone.

The data of primary interest are the local vane surface conductances. Recall these quantities are only approximate in an absolute sense because the heat load for the entire vane was used in the calculation. In a relative sense, however, a very useful indicator of surface effects is provided.

Consider first the suction face conductances from test number 2 (see Figs. 30 and 32). Vane number 2 (see Fig. 4 for location reference) serves as an excellent example of the several phenomena which can be observed readily from this type of data. In the initial few hours of a test, the vane surface conductance rises markedly. In this case, the value increased 43 per cent above the nominal conductance. This phenomenon occurs because in the initial part of the test, as the ash deposit first begins to form, the roughening of the gas path surface rsults in significantly enhanced convective heat transfer. This effect completely dominates over the insulating effect of the thin, new deposit, and resistance to heat transfer decreases. As the deposit thickness increases, the thermal barrier effect gradually takes over and the conductance begins to decrease (resistance increases). In this case the maximum conductance was reached after approximately 5.5 hours of operation. From this point on the conductance decreases until some disturbance of the ash in the vicinity of the thermocouple causes some removal of ash and an increase in conductance. Such events occurred points 24.8 and 45.4 hours into the test. As pointed out in the previous chapter, the latter disturbance was the result of the thermal

excursion and was accompanied by an increase in the nozzle throat area. The former disturbance was not observed to effect the throat area and thus was a localized disturbance. The conductance data from the suction face of vane 3 are very similar to vane 2, except that the enhancement at the beginning of the test is almost nonexistent. This would seem to imply that a very smooth deposit is formed in this area. It is worth noting at this point that physical observations of the ash deposits formed on the turbine nozzle revealed that the suction face deposits were indeed smoother-surfaced than the pressure face deposits. This is a phenomena that one might expect after considering how the ash particles arrive at the vane surfaces. The pressure face deposits arrive by inertial mechanisms, i.e., direct impaction. On the suction face, however, the ash is transported to the surface by diffusion mechanisms and by secondary flows. Both would deliver ash particles at much lower velocities and therefore yield a smoother deposit.

The pressure face conductances from test number 2 (see Figs. 31 and 33) show many of the same characteristics noted earlier for the suction surfaces. In this case the peak conductances also occurred approximately 5.5 hours into the test and reached a maximum increase of between 23 and 26 per cent above the nominal values for the clean nozzle sector. The small ash disturbance at the 24.8 hour point also appears in the pressure face conductances. There is some question as to whether or not this apparent disturbance in the pressure face deposit actually occurred. Recall that there was no change in the pressure face temperatures at this point (see Figs. 22 and 24). This particular incident is an

example of the principle weakness of the corrected dimenionless surface conductance. It is entirely possible, and indeed highly probable, that the ash disturbance that occurred at the 24.8 hour point was confined locally to the suction faces of the two vanes in question. In the case of such a localized disturbance, in which a gross redistribution of the heat flow between the coolant and hot gas stream occurs, the data from the affected area could significantly alter the conductance from another, unaffected area. This is apparently what has occurred in this case. One very important observation that can be made regarding this event is that an ash layer disturbance confined to the suction surfaces of the turbine nozzle vanes has no apparent affect on the nozzle throat area.

The pressure face conductances show a dramatic increase at the 45.4 hour point corresponding to the ash removal caused by the thermal excursion. Note that the conductance levels increase beyond the value for a clean nozzle on both faces, indicating a significant ash removal and/or surface roughening effect. A very rapid decrease in conductance occurs, however, immediately following the excursion, which tends to bring the data back to the original trend. This phenomenon does not occur with the throat area data, however, which is why the throat area versus heat load relation changes after an excursion (see Fig. 20). One possible explanation for this phenomenon is that following an excursion the cavities formed in the ash layer very quickly are filled with porous, low density ash with low thermal conductivity. This results in an increased insulating effect which rapidly drops the surface

conductance. The throat area, however, is not dependent on the ash density but on the surface profile, and is thus not responsive to the internal sturctural characteristics of the ash layer.

Consider now the heat transfer results of test number 5. In test number 2 recall that the heat load varied more or less linearly with the throat area (see Fig. 20). If these data are compared with data from test 5 contained in Figs. 36-38, some interesting points come up. The data over the first 9.6 hours of test number 5, shown in Fig. 36, seem to show a more or less linear behavior. After the first thermal excursion, over the period from 15 to 35.7 hours, a uniform decrease of heat load with throat area is observed up to a point where the nozzle area has decreased 5 to 6 per cent, but beyond that point very little reduction in heat load occurs. The heat load reduction appears to be approaching a maximum value of approxmately 15 per cent. A similar behavior is observed in the third period (see Fig. 38) of 41 to 48.4 hours following the second thermal excursion, with a maximum heat load reduction of approximately 17 per cent.

A plausible explanation for the behavior described above can be formed after considering the two major differences between test numbers 2 and 5. The first is the gas temperature, which was 1311 K (average turbine inlet) for test 2 and 1421 K for test 5. The second is the extent of ash accumulation in the tests. The maximum throat area reduction in test number 2 was 5.7 per cent; the corresponding value in test 5 was 14.4 per cent. It would thus seem reasonable to expect that the outer layers of the deposit in the latter test would have been at a

significantly higher temperature than in the former test. This hotter ash would have had a higher thermal conductivity than the ash in the lower layers, both because of the temperature and because it would have been more densely packed (most likely semi-molten). As the ash deposit layer thicknened, then, the throat area continued to decrease, but the heat load began to reach a more or less constant value. After the second excursion, the limiting heat load decreased slightly because the resulting cavities were filled with loosely-packed, low-conductivity deposit.

The vane surface and conductance data from test number 5 show the same trends as observed in test 2, with a few minor exceptions. The conductance enhancement in the initial few hours of the test was not as large in magnitude in test 5, and the maximum values were reached earlier in the test. This phenomena could be attributable to the reduction in Reynold's number in test number 5, which would result in somewhat lower surface heat transfer coefficients. Gross disturbances are observed at points 9.9 and 35.9 hours into the test, corresponding to the two thermal excursions. Each excursion appears to have resulted in disturbances to both the suction and pressure surface ash deposits. The first event, a type I thermal excursion, seemed to have had a more pronounced effect on the pressure face deposits than those on the suction face. This agrees with observations from test number 2. The second event, a type II thermal excursion, appears to have been more effective in disturbing the suction face deposit. Noting from table 6 that the first excursion resulted in a greater throat area recovery than

the second, an additional data point is obtained supporting the theory that the pressure face deposits dominate the throat area reduction.

In test number 6 a similar behavior of the heat load reduction with throat area was observed as in test 5. The data from the first 17.7 hours of testing, prior to the nutshell injection, is shown in Fig. 50. Note that a maximum reduction in heat load of approximately 15 per cent is attained.

There is a very significant difference in the conductance data from test 6 and that from tests 2 and 5. There is no increase whatsover in the surface conductance in the early stages of the test. The reason for this is that test number 6 was begun immediately following the water wash and refire sequence of test 5. The nozzle surface was thus void of ash but was not completely clean from a mechanical and chemical standpoint. The surfaces were thus already in a roughened state and the surface heat transfer coefficients were high initially.

The ash removal resulting from the nutshell injection appears to have been effective on both the suction and pressure faces. Removal of the pressure face deposit is by direct inertial impaction causing fracture of the ash structure. Suction face deposit removal is either by impaction from rebounding ash and/or nutshell particles or by a "domino effect" peeling back of the deposit layer initiating at the leading edge.

The heat transfer data taken during deposition tests with the

water-cooled turbine nozzle are thus seen to yield significant additional insight into the ash deposit formation and removal phenomena.

7. ENGINE SIMULATION MODEL

7.1 Introduction

The experiments described and discussed in the previous four chapters involved the use of a laboratory-scale turbine simulator device. The objective of these types of tests is the assess in some manner the performance of full-scale combustion turbine engines using similar fuels to those used in the simulator tests. This assessment involves consideration of the geometry and thermodynamics of the combustion turbine engine.

The majority of gas turbines fired with residual fuel oil are used for electric utility power generation [3]. In this application, the engine speed remains constant (3600 rpm in the U.S., 3000 rpm in most other countries), and the engine operating point is controlled by varying the fuel flow and hence the turbine inlet temperature. The most common means of controlling the fuel flow is by measurement of the turbine exhaust temperature and adjusting the fuel flow to hold a predetermined temperature. Assuming that no changes in the operating characteristics of the engine components occur, a constant electrical power output will be delivered. At part-load conditions, a lower turbine exhaust temperature is used. The engine heat rate will in general be higher at part-load conditions, since the engine components would be operating at off-design.

When treated residual fuels are used in a gas turbine engine

operating at constant exhaust temperature, two major effects are observed. First of all, the engine power output decreases, indicating a change in either the operating characteristics of the engine components or in the engine operating point, or both. Secondly, the specific fuel consumption increases, indicating an increase in the engine heat rate. This could result from either a decrease in one or more engine component efficiences, or a shift to an off-design operating point, or both.

7.2 Model Formulation

In order to analytically investigate the operation of a gas turbine engine fired with treated residual fuel, one must model two phenomena as closely as possible. First of all, the effect of the fuel burned on the engine components must somehow be quantified. The particular components involved are the combustion system, the turbine, and the exhaust diffuser. The second aspect that one must model is the off-design performance of all of the individual engine components. Some means of component "matching" must be incorporated into the model so that the engine operating point can be determined.

Consider, for example, a large single-shaft, simple-cycle, heavy-duty gas turbine engine as shown in schematic form in Fig. 62. The numbering scheme used for thermodynamic state points in the present model is shown in the schematic. Note that in this model the turbine first-stage nozzle is considered separately from the rest of the turbine. Also, the compressor inlet and the turbine exhaust diffuser are

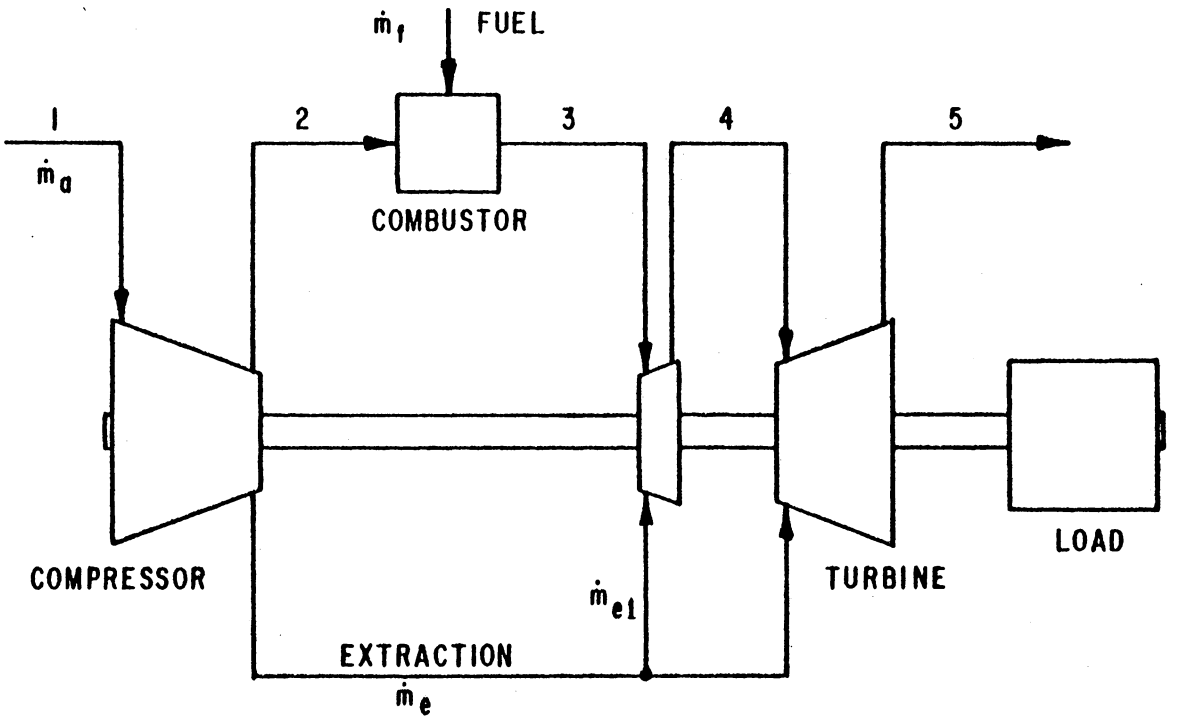

FIGURE 62

AIR-COOLED COMBUSTION TURBINE ENGINE SCHEMATIC

considered to be part of the compressor and turbine, respectively. The compressor isentropic efficiency would thus describe losses in the compressor inlet system as well as the compressor itself. Similarly, the turbine efficiency includes exhaust diffuser losses.

Typical performance characteristics for a compressor and a turbine are shown in Figs. 63 and 64, respectively. Component characteristics given in this manner are sometimes referred to as operating performance "maps". Notice that the general trend for a compressor operating at constant speed is for the pressure ratio to decrease as mass flow decreases. The compressor isentropic efficiency is also a function of the mass flow, with the maximum value at a given speed occurring at the mass flow corresponding to the minimum average gas incidence through the blade rows. The flow characteristic for a turbine is similar to what one would expect for flow through a fixed nozzle passage. The mass flow is increased by increasing the pressure ratio, and decreased by in creasing the turbine inlet stagnation temperature. The maximum turbine mass flow is limited by choking in the blade passages; if choking occurs in stationary passages (nozzles), then the choking mass flow is independent of engine speed. The turbine isentropic efficiency is not as strongly affected by off-design conditions as the compressor efficiency, although shock losses can become important at large pressure ratios.

Given the operating characteristics or performance "maps" for the compressor and turbine along with some other data relating to fluid pressure and mechanical losses in other components, the engine operating point can be determined for a fixed engine speed and turbine exhaust

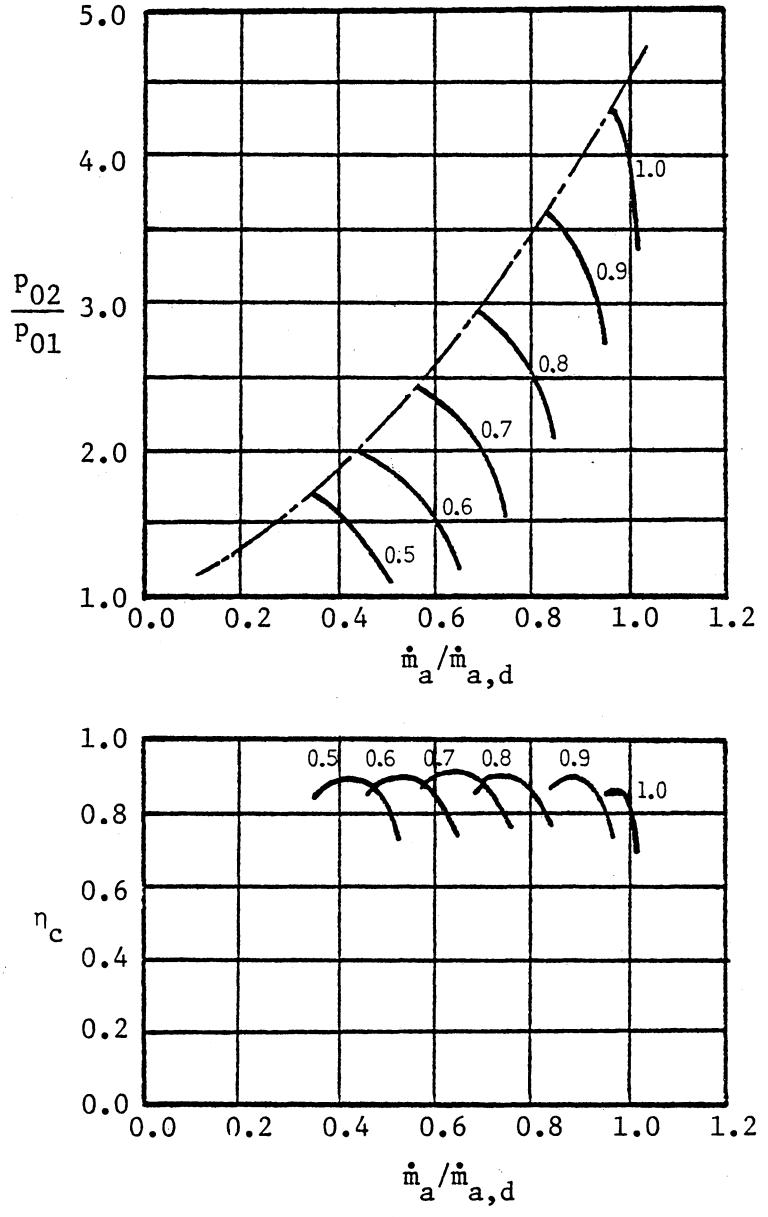

FIGURE 63

Typical Axial-Flow Compressor Characteristics

(Note: Labels on curves indicate speed as a fraction of the design dimensionless speed, $N/\sqrt{T_{01}}$.)

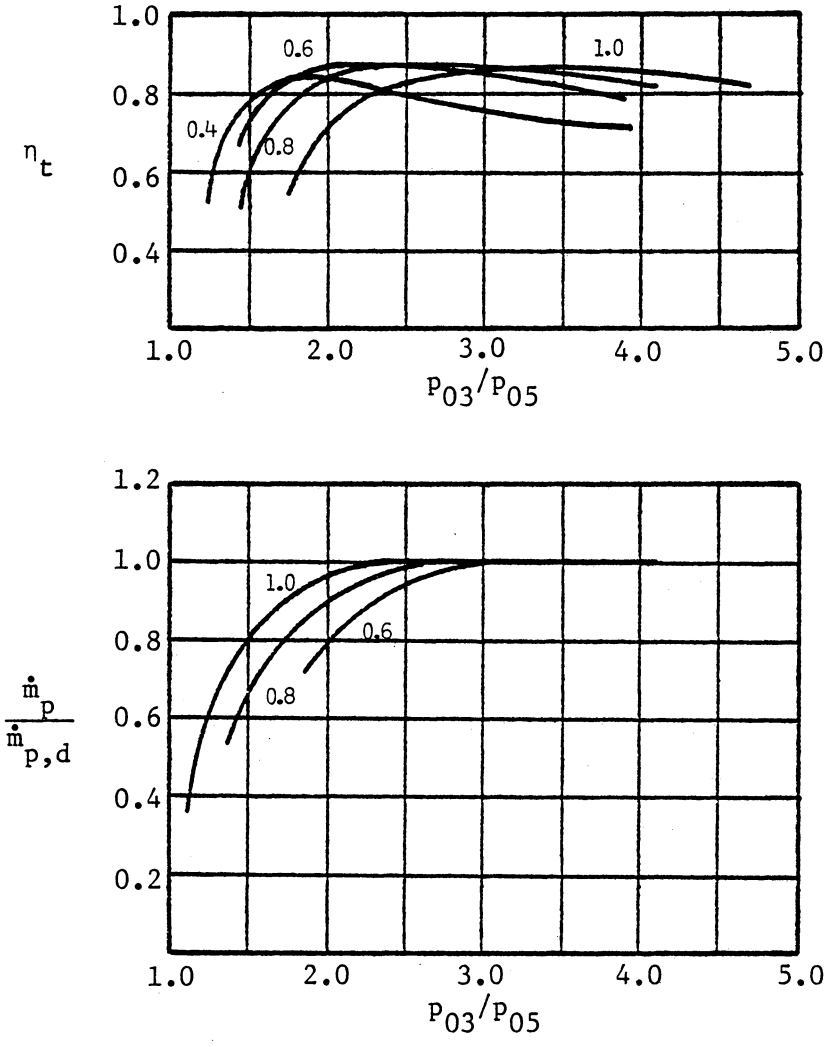

FIGURE 64

Typical Axial-Flow Turbine Characteristics

(Note: Labels on curves indicate speed as a fraction of the design dimensionless speed, $N/\sqrt{T_{03}}$.)

temperature. The procedure involves satisfying mass flow and pressure ratio compatibility between the compressor and turbine. A flow chart outlining the matching procedure is given in Fig. 65. The equations used in the cycle analysis are summarized in the Appendix.

Since it is desired to evaluate the effect of firing with treated residual fuel on the gas turbine engine operation, one must model the effect of the fuel on the individual engine components. In the present model, there are six available parameters which can be used to model this effect. The combustion system efficiency and stagnation pressure loss can be varied to account for the effect of the fuel combustion characteristics and ash deposition in the combustor liner and hot gas transition piece, respectively. The turbine flow characteristic can be modified to account for the restriction in the mass flow through the turbine passages. This restriction is the result of both the physical thickening of ash deposits on the turbine airfoil and endwall surfaces, and increased boundary layer dispacement thicknesses on the gas path surfaces. In the model, both phenomena are assumed to produce the same effect on the turbine flow characteristic: the curve is simply displaced to the left. Thus, for a given pressure ratio and turbine inlet stagnation conditions, a lower mass flow will be delivered. The fourth parameter which can be varied to simulate the effect of firing treated residual fuel is the turbine efficiency, which decreases during operation due to ash deposits. This decrease results from both airfoil profile losses and possibly also from an increase in secondary flow activity. The airfoil profile losses account for losses due to

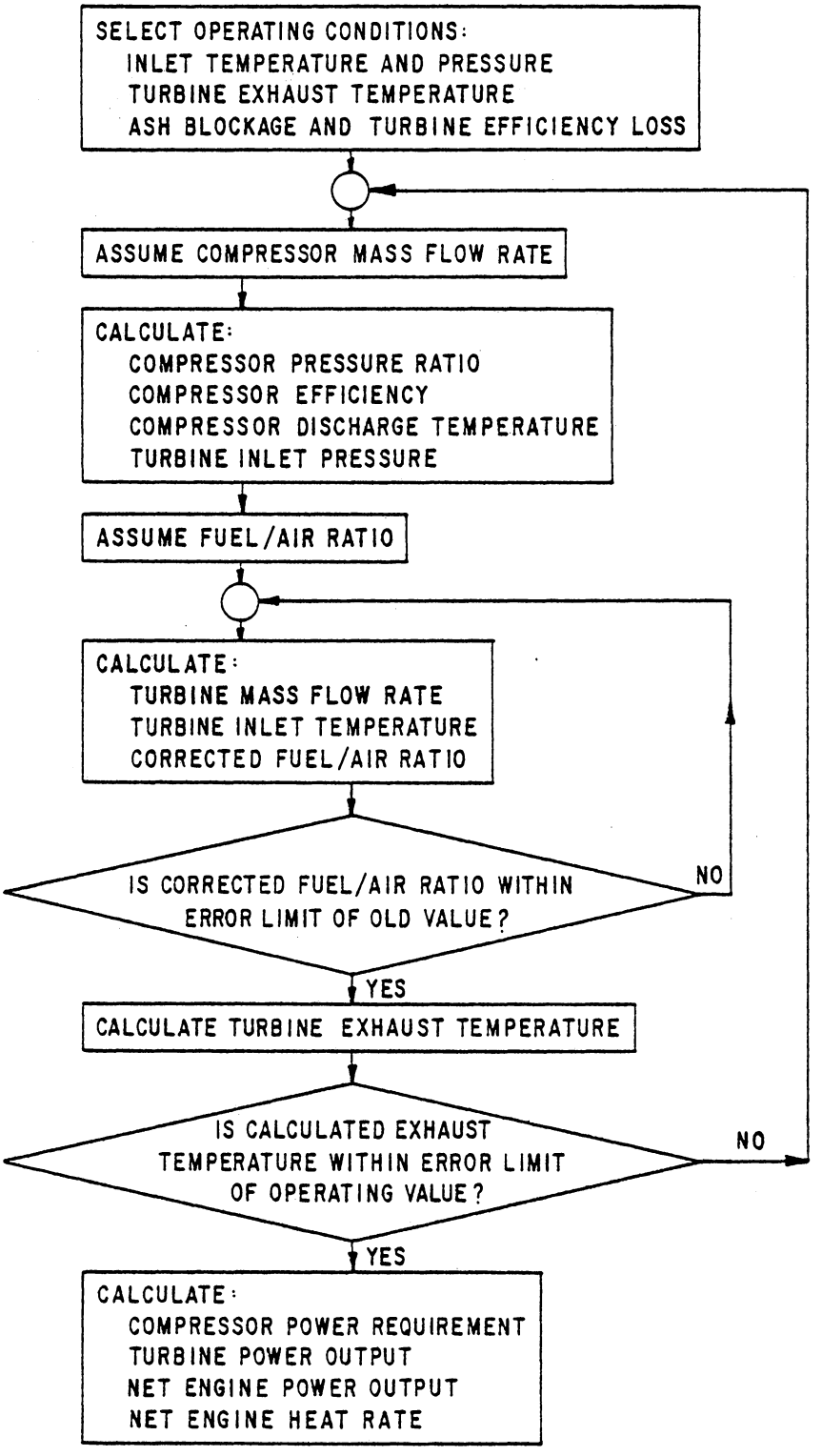

FIGURE 65
FLOW CHART OF COMBUSTION TURBINE ENGINE ANALYSIS PROCEDURE

boundary-layer growth on the pressure and suction surfaces of the turbine vanes, including the effects of flow separation and the resulting wake losses at the trailing edge. Obviously, with the effective thickness of the airfoils increasing because of ash deposits, one would expect these losses to increase. The increased secondary flow activity would result from thicker endwall boundary layer entering the blade rows [27]. The final two operating parameters which could be affected by ash deposits are percentages of compressor discharge air extracted for turbine cooling. If any plugging of airfoil film cooling holes occurs, these percentages would be reduced. In the turbine simulator test results presented earlier, there was no observable indication of any film hole plugging in the air-cooled turbine nozzle. Based on this observation, the mass percentages of extraction air were assumed to be constant in the engine simulation model.

7.3 Model Application

With the model thus developed for predicting gas turbine performance at off-design conditions with means for accounting for the effects of ash-bearing fuel, a numerical investigation was undertaken. The full-sized engine that was modeled was the General Electric Company model MS7001B simple-cycle single-shaft packaged power unit. The design point performance specifications for this unit are given in Table 7. Data are from Reference 32. In order to completely quantify all the design point parameters needed for the model, certain numerical

TABLE 7

General Electric MS7001B Performance Specifications

Inlet Temperature	15 C (59 F)
Inlet Pressure	1 atm
Shaft Speed	3600 rpm
Air Mass Flow	245 kg/s (541 lb/s)
Compressor Pressure Ratio	9.4
Firing Temperature	1010 C (1850 F)
Exhaust Temperature	510 C (950 F)
General Output	60,000 kW
Heat Rate	11,740 kJ/kW hr (11,130 Btu/kW hr)

assumptions had to be made. These are listed in Table 8, along with results of a complete cycle analysis performed at the design point.

The off-design characteristics of the compressor and turbine had to be estimated. A parabolic variation of pressure ratio and efficiency versus mass flow was used for the compressor. The maximum compressor efficiency was chosen to be at the design point. The maximum pressure ratio was chosen to be 8.2 per cent above the design value and to occur at a mass flow rate 7.0 per cent below the design flow. For the turbine, an "ellipse law" pressure characteristic [33] was used. This resulted in a turbine mass flow rate of 99.4 per cent of the choking mass flow. The turbine efficiency was assumed to be independent of mass flow rate. The characteristic performance "maps" for the compressor and turbine are shown in Figs. 66 and 67, respectively, along with the equations used to describe the curves.

A numerical study was undertaken to investigate the effect of variations in turbine flow blockage and turbine efficiency on the engine performance. The combustion efficiency and combustor stagnation pressure loss were taken to be constant. Turbine flow blockage (throat area decrease) was simulated by introducing a turbine blockage factor (TBF), which simply resulted in a shift in the turbine flow characteristic to the left. A reduction in turbine isentropic efficiency was simultaneously introduced. The engine simulation model then located the new operating point for the engine and calculated the appropriate performance parameters (see Fig. 65).

Accurate simulation of an actual gas turbine engine is dependent on

TABLE 8

MS7001B Design Point Cycle Analysis

-Assumptions and Results

Assumptions	
Compressor Isentropic Efficiency	0.867
Combustor Pressure Drop	0.04 P_{02}
Turbine Inlet Temperature	1043 C (1910 F)
Fuel Lower Heating Value	42,600 kJ/kg (18320 Btu/lb)
Combustion Efficiency	0.99
Results	
Fuel/Air Ratio	0.0189
Compressor Discharge Temperature	309 C (588 F)
Total Turbine Cooling Air Flow	0.094 $\dot{m}_{air}$
First Stage Nozzle Cooling Air Flow	0.047 $\dot{m}_{air}$
Rotor and Generator Loss	2560 kW
Turbine Isentropic Efficiency	0.974

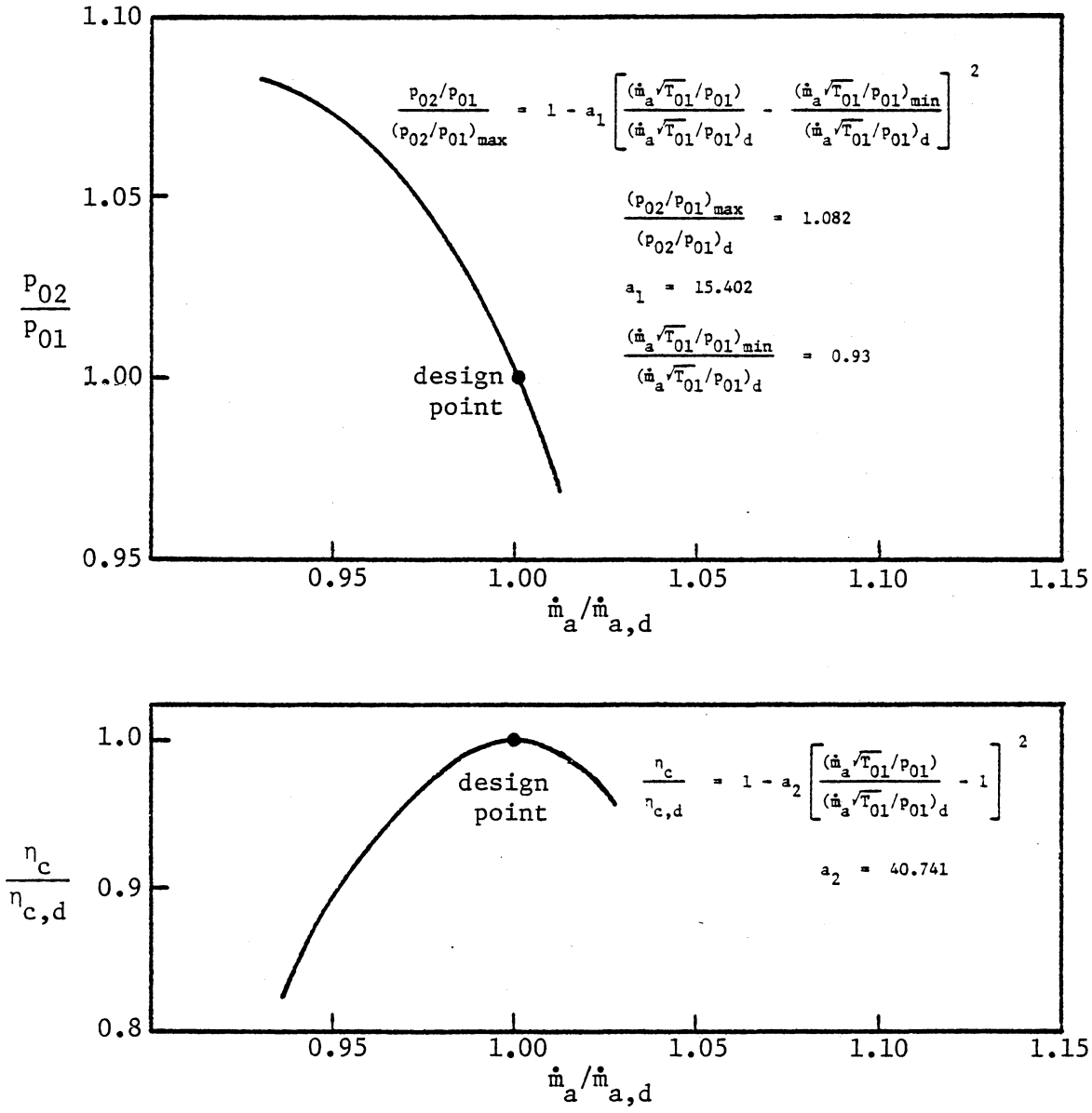

FIGURE 66

Assumed MS7001B Compressor Performance Characteristics at 3600 RPM

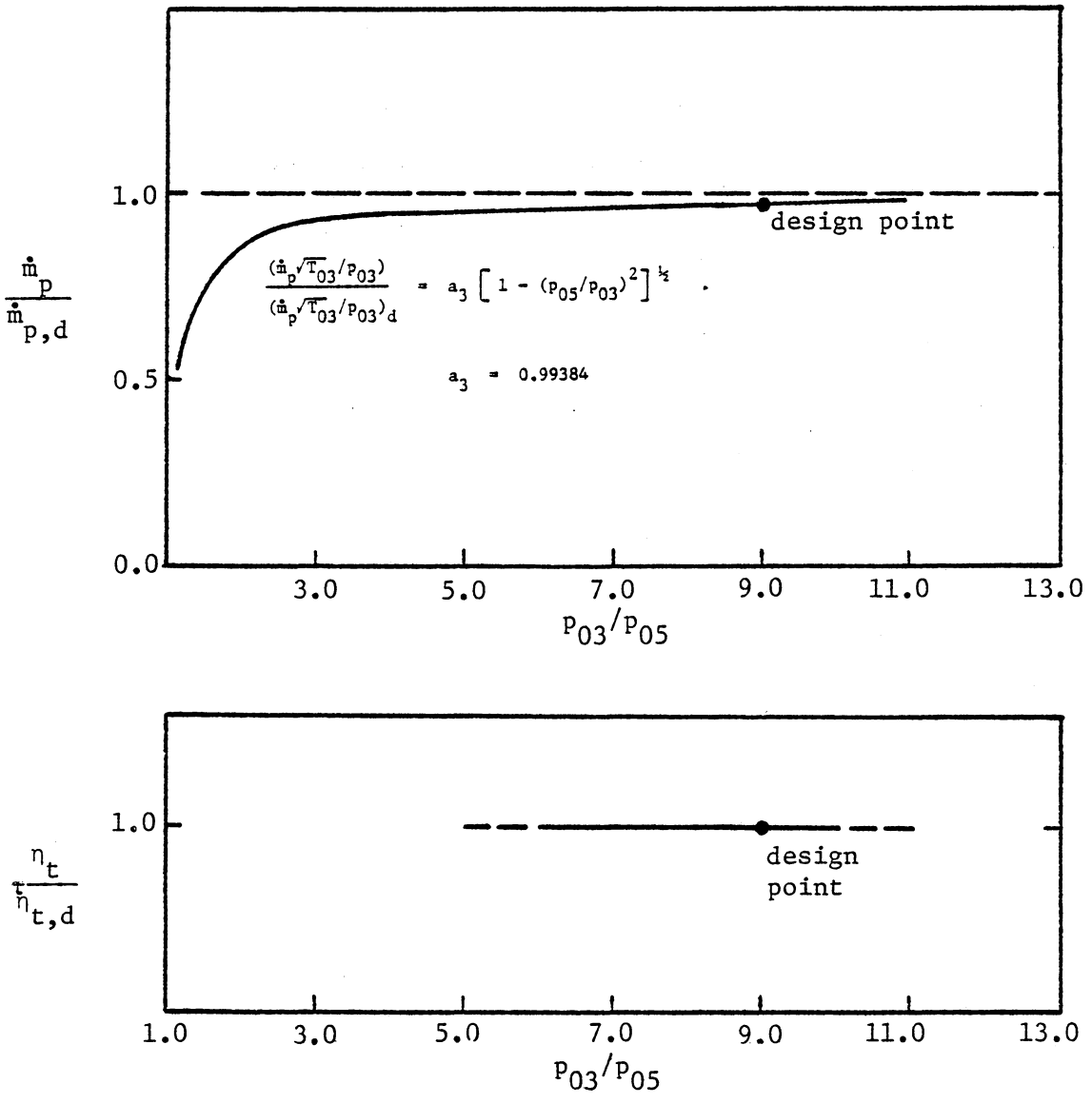

FIGURE 67

Assumed MS7001B Turbine Performance Characteristics at 3600 RPM

knowledge of the variation in turbine flow blockage and turbine efficiency. The turbine flow blockage can be determined for various turbine firing conditions from the results of turbine simulator experiments, such as those described earlier. For scaling to full-size dimensions, the ratio of nozzle throat widths between the simulator and engine turbine nozzles is used. These dimensions are given in Table 9. The turbine efficiency variation, however, cannot be determined from simulator experiments. Data from field operation are required.

There are two MS7001B gas turbine engines in field operation from which reliable data are available at the present time [3]*. The first of these is one of six regenerative units located at the Florida Power and Light Corporation's DeBary site. These units are operated at 1283 K (1850 F) firing temperature (first stage turbine rotor inlet), using residual fuel oil with relatively low contaminant levels. These units are used for peaking power only, and are started each morning and shutdown each evening. Ash deposits are generally quite light because of the fuel contaminant levels and the short operating periods. As of 1979 approximately 15,000 hours of operation on residual fuel oil had been accumulated.

The second machine for which data are available is a single regenerative engine operated by the Alcoa Company at Paramaribo, Surinam. This engine was operated at a 1228 K (1750 F) firing temperature on a

---

*Mr. H. von E. Doering of the General Electric Company is gratefully acknowledged for sharing his insights and observations regarding MS7001B field experience.

TABLE 9

Selected Turbine Nozzle Throat Widths

Unit	Throat Width mm	Throat Width in.
MS7001B	27.33	1.076
MS7001E	34.32	1.351
MS3002 (11000 hp)[1]	19.8	0.780
Monolithic Water-Cooled Sector	20.6	0.810

relatively poor grade residual oil. The application is base load (continuous) industrial power generation. As of 1979 approximately 11,000 hours of operation on residual fuel oil had been accumulated.

The data that are of principal interest from the field experience are the turbine blockage (ash deposition) rate and the rate of decrease of engine power. The turbine blockage is evaluated by measuring the compressor discharge pressure and temperature and the fuel flow rate. The air mass flow is then determined using the known compressor characteristics, and the turbine inlet temperature calculated from air and fuel flow rates, the combustor inlet temperature, and the fuel properties. The turbine mass flow capacity can then be calculated and compared to that for the clean turbine.

Knowing how the turbine power decreases with the turbine blockage, the engine simulation model can be used to determine the variation in turbine efficiency that must be occurring. For the DeBary and Surinam machines, the ratio of turbine power loss to mass flow capacity loss (efffective throat area decrease) was approximately 2.5. Using the engine simulation model with the MS7001B rated performance specifications, it was found that the turbine efficiency decreases at a rate equal to approximately 70% of the throat area decrease (ash deposition rate). Figure 68 shows the results of the engine simulation model, with the turbine efficiency decrease varying linearly with the mass flow capacity decrease. Notice that the abscissa of this plot is the per cent decrease in mass flow capacity (effective throat area), which could be replaced by operational time if the turbine plugging rate is known.

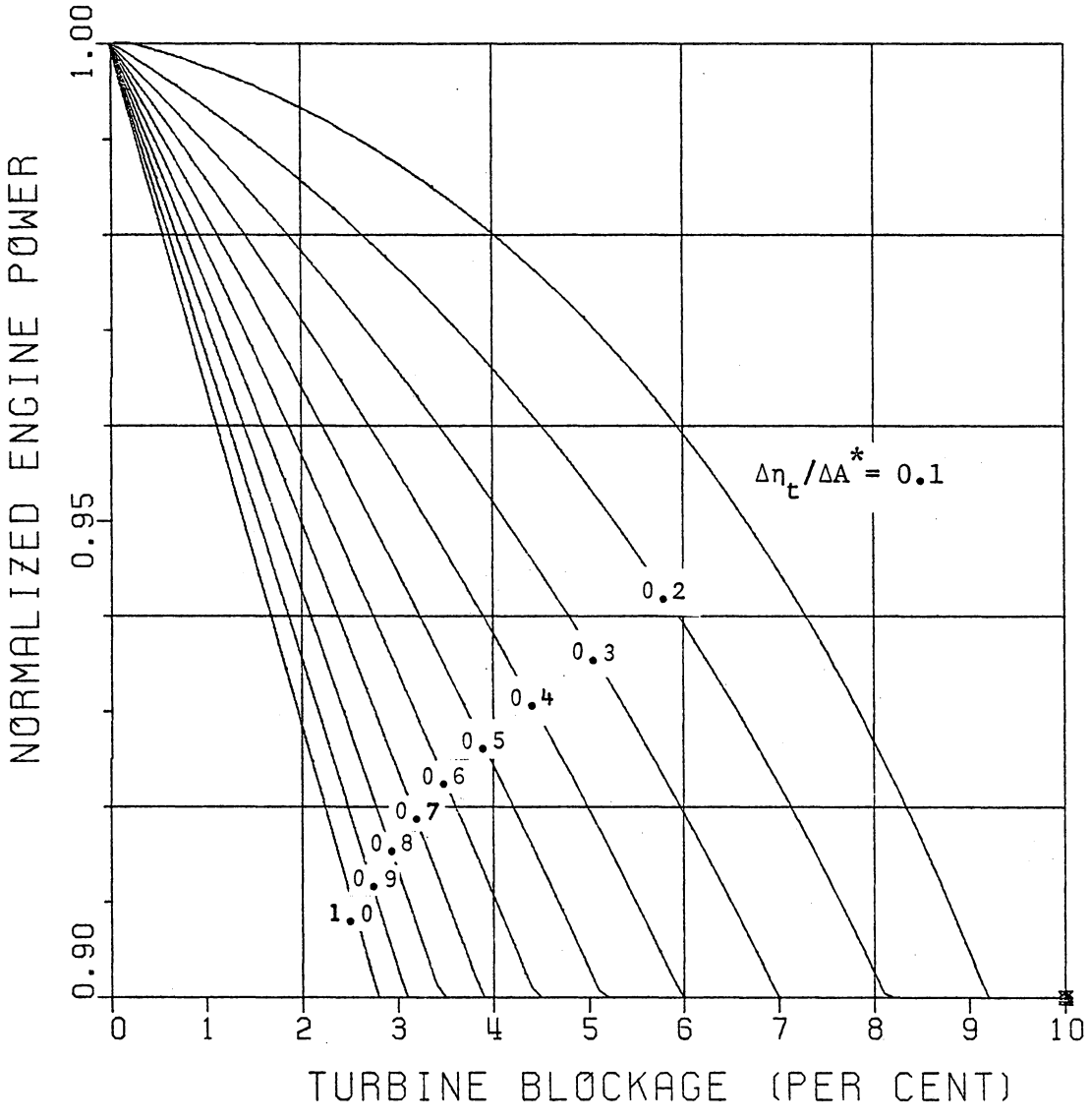

FIGURE 68
ENGINE SIMULATION MODEL
AIR-COOLED TURBINE RESULTS

With the functional variation of turbine efficiency with blockage now determined, it is possible to extend the application of the engine simulation model to other firing conditions and to other geometrically similar turbines. One such extension which is very much of current interest is to the water-cooled gas turbine engine. If the turbine is geometrically similar to the MS7001B, then it is reasonable to assume that the variation in turbine efficiency with blockage would be the same as the cases investigated earlier. Some changes need to be made in the engine simulation model, however, as the water-cooled turbine differs thermodynamically from its air-cooled counterpart.

Figure 69 shows a schematic diagram of a simple-cycle, single-shaft heavy duty gas turbine engine with a water-cooled first stage turbine nozzle. Notice that the only difference between this engine and the engine of Fig. 62 is that heat is rejected to a coolant (water) in the first-stage turbine nozzle in a closed circuit, i.e., this energy is removed from the cycle. There is thus less air extracted for turbine cooling and a greater percentage of the compressed air passes through the combustor. These differences were accounted for in a modified engine simulation model. The additional data required to implement the modification were the amount of heat transfer from the combustion products in the first-stage turbine nozzle, and the variation in the heat transfer affected by the ash deposition. These data were obtained from the results of turbine simulator test number 2.

The heat transfer measured in the turbine simulator nozzle under full-fired conditions at the beginning of test number 2 was approximately

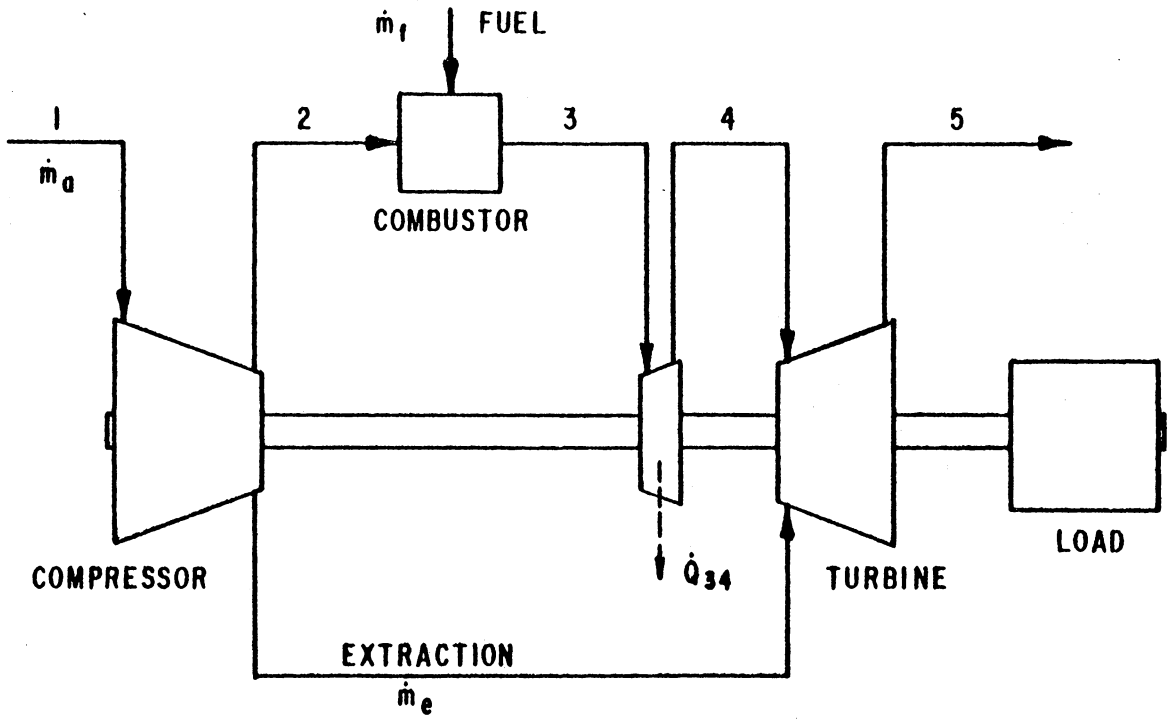

FIGURE 69

WATER-COOLED COMBUSTION TURBINE ENGINE SCHEMATIC

35 kJ/kg of gas flow. The Reynolds number for this condition (3.5 x 10^6) is approximately one-half that of an MS7001B first stage nozzle. Scaling geometrically for the heat transfer in the MS7001B nozzle obtains a value of approximately 20 kJ/kg of gas flow. This value was used in the modified engine simulation model.

The effect of the ash deposition on the heat transfer in a water-cooled turbine nozzle was studied in detail in test number 2, and reported in previous references [17,18]. The heat transfer decreases as the ash forms due to the insulating thermal barrier presented by the ash layer. In test 2 it was observed that heat transfer decreases at a linear rate when plotted against the effective nozzle throat area. The data for the first 40 hours of the test is reproduced in Fig. 70, along with a solid line which results from a least-squares analysis of the data. The slope of this line is approximately 2.6, thus the heat transfer decreases at a rate 2.6 times the decrease in throat area. This relation was used in the modified engine simulation model.

The results of the modified engine simulation model, shown in Fig. 71, indicated that for the same variation in turbine efficiency used previously, the rate of decrease in power output would be smaller - approximately 2.2 times the ash deposition rate rather than 2.5 as before. For equal time rates of ash deposition, therefore, one would expect that the water-cooled turbine would be available for 12 per cent longer before a given power loss occurred. In actual operation, however, the ash deposit rates for a water-cooled turbine and an air-cooled turbine are different, and this fact should be incorporated into the model

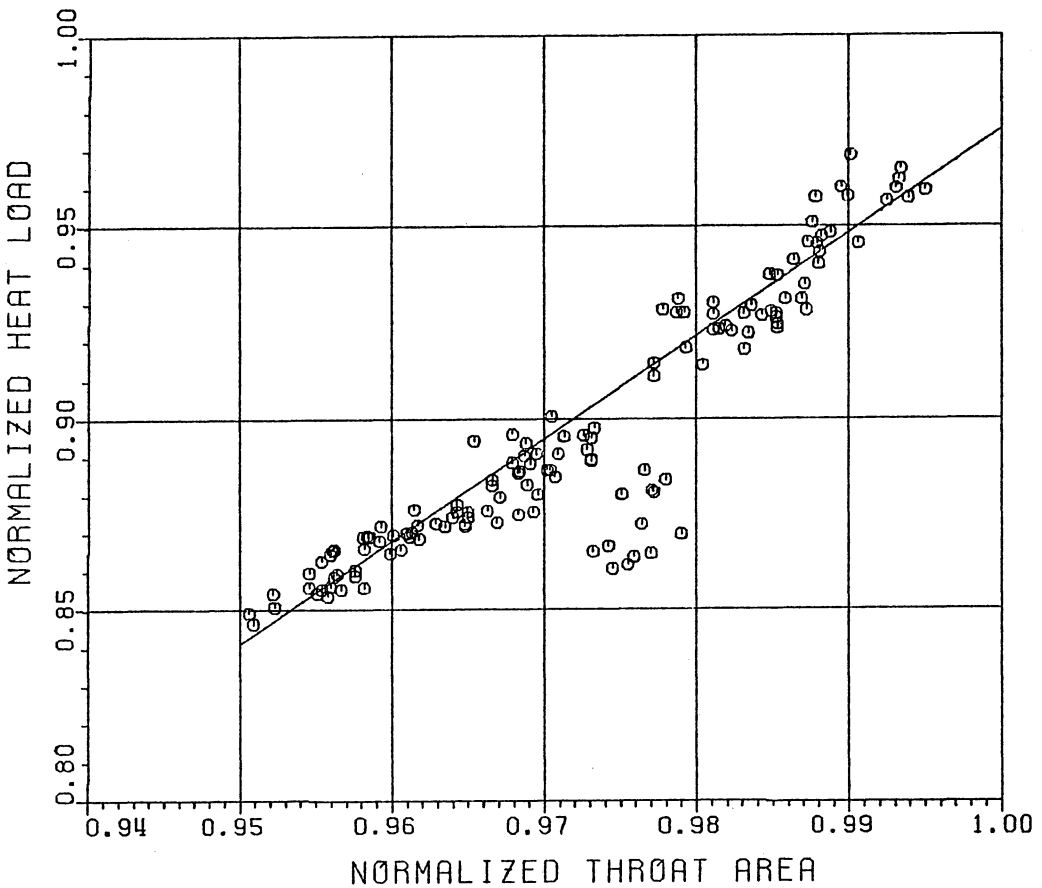

FIGURE 70
NOZZLE HEAT LOAD VARIATION WITH
THROAT AREA CORRELATION

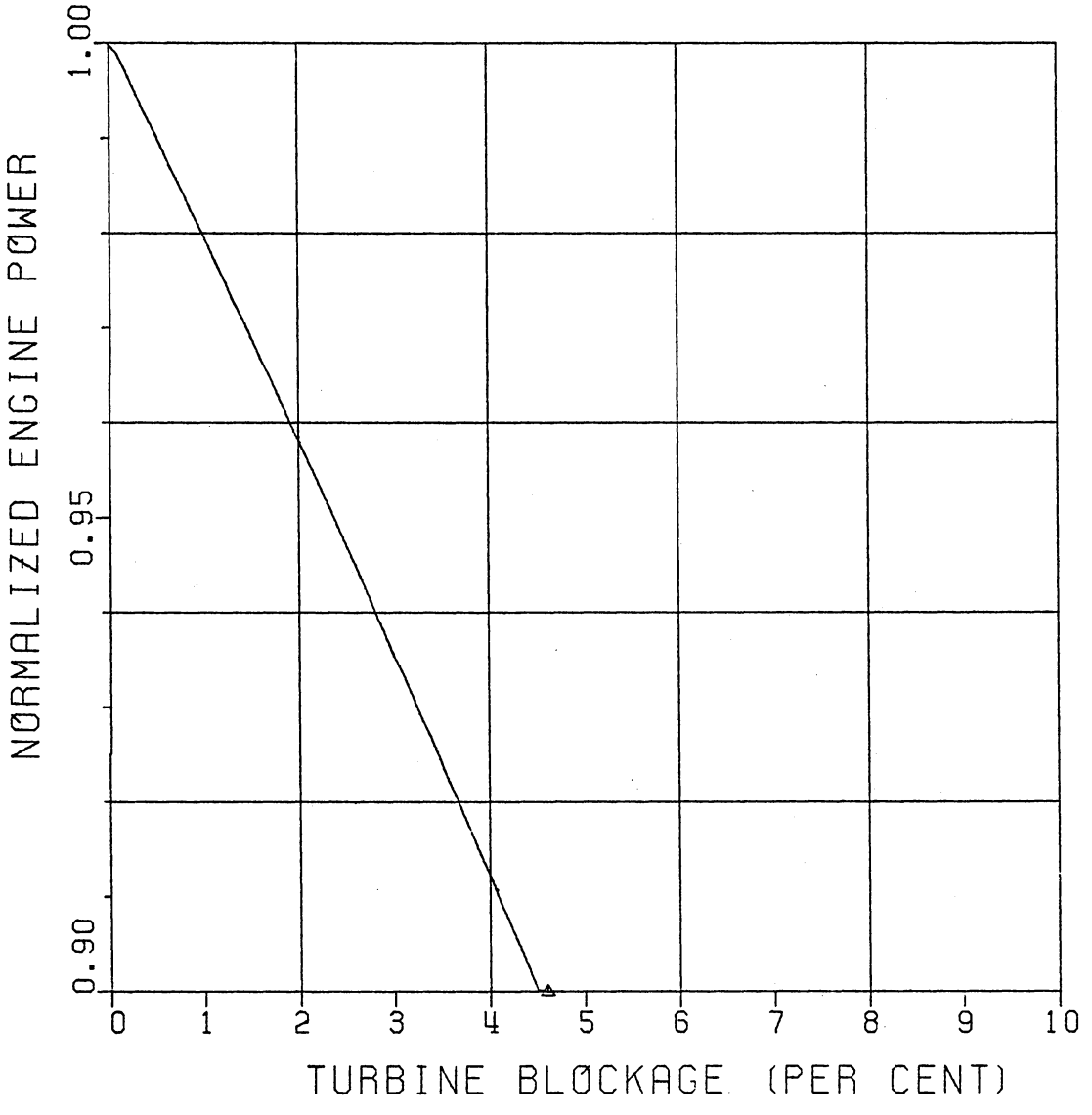

FIGURE 71
ENGINE SIMULATION MODEL
WATER-COOLED TURBINE RESULTS

before a one-to-one comparison can be made.

As previously mentioned, scaling the turbine simulator ash plugging data to a full-sized engine is accomplished by multiplying by the ratio of the turbine nozzle throat widths. The actual engine (MS7001B) has a larger nozzle throat than the turbine simulator cascade and would thus suffer a smaller throat blockage for the same amount of ash deposit. The scaling factor used in the present case is 0.780/1.076 = 0.725 (see Table 9) for the air-cooled case and 0.810/1.076 = 0.753 for the water-cooled case.

As an example, consider the ash deposition rates obtained in turbine simulator tests 1 and 2 (see Table 5). The firing temperature for this test was the same as for an MS7001B. The ash deposition rates were 16 and 12 per cent per 100 hours, respectively, for the air- and water-cooled turbine nozzles. Using the scaling factors from the above and retaining two significant digits yields corrected rates for a full-scale engine of 12 and 9.0 per cent per 100 hours. Incorporating these rates to create a time scale for the engine simulation models, the variation in engine output power with time can be predicted. For the two cases and under consideration, the results are as shown in Fig. 72. The rate of power decrease for the engine with an air-cooled turbine is approximately 27 per cent per 100 hours, and for the engine with a water-cooled first stage turbine nozzle approximately 19 per cent per 100 hours. Assuming power decrease to be the criterion for engine shutdown to affect cleaning of deposits, the water-cooled turbine is thus seen to increase engine time availability by approximately 45 per

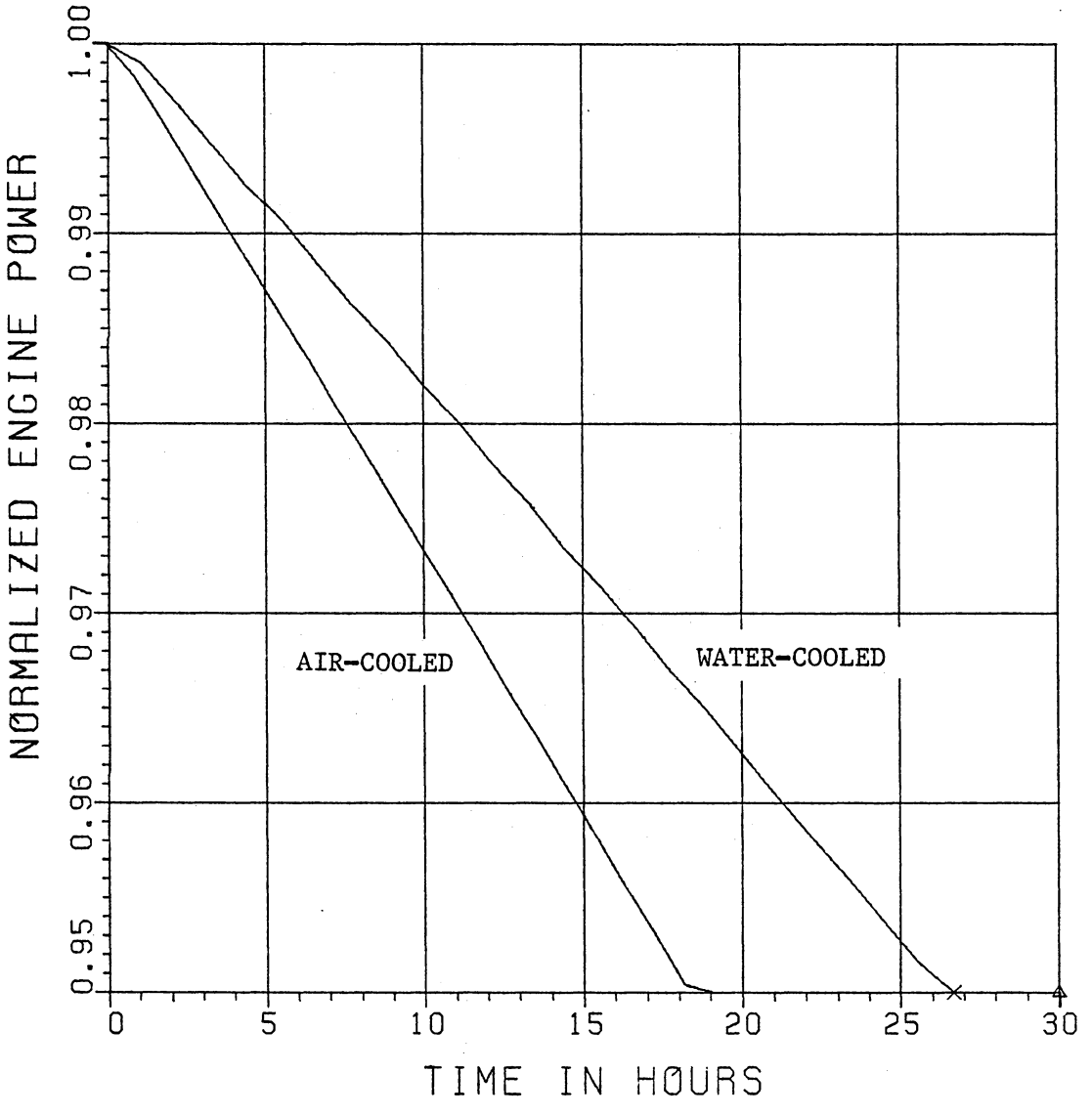

FIGURE 72
ENGINE SIMULATION MODEL
REAL-TIME SIMULATION OF AIR-
AND WATER-COOLED ENGINES

cent.

Other parameters besides the power output can be calculated in the engine simulation model. Three parameters which are of particular interest are the compressor pressure ratio, the turbine inlet temperature, and the specific fuel consumption. The compressor pressure ratio is important since as the turbine plugs with ash deposits, the resulting restriction in mass flow causes the compressor discharge pressure to rise. Substantial pressure increases can result in serious reduction in the compressor surge margin. The compressor pressure ratio in the air-cooled tests was observed to increase at a rate equal to approximately 57 to 58 per cent of the ash deposition rate. For example, if the air-cooled turbine engine is allowed to operate until the power output decreases by 10 per cent, the resulting decrease in mass flow restriction would be 4 per cent and the compressor discharge pressure would increase approximately 2.3 per cent. In the simulation of the water-cooled turbine engine the compressor pressure ratio was observed to increase at a rate of approximately 59 to 60 per cent of the ash deposition rate. For a 10 per cent power reduction with resulting 5.3 per cent mass flow restriction, the compressor discharge pressure increases approximately 3.1 to 3.2 per cent. In both the air- and water-cooled cases, the pressure ratio increases observed are not of the magnitude that would result in a problem with compressor surge. In addition, the gas turbine engine would in practice not be allowed to operate for this long a period.

The turbine inlet temperature is a very important variable since

under no circumstance should it be allowed to increase. In the engine simulation of both the air- and water-cooled turbine engines, the turbine inlet temperature was observed to decrease at a rate equal to approximately 34 per cent of the ash deposit rate. This translates to about a 4.5 K temperature decrease for each 1.0 per cent reduction in the effective throat area or mass flow capacity.

The specific fuel consumption is an important parameter, particularly for base load applications. In the air-cooled engine simulation, the specific fuel consumption was calculated to increase at a rate 1.5 to 1.7 times the ash deposition rate. A 10 per cent power decrease would thus effect an increase in specific fuel consumption of approximately 6 to 6.8 per cent. In the water-cooled engine simulation the specific fuel consumption was calculated to increase at a rate 1.1 to 1.3 times the ash deposition rate. A 10 per cent power decrease because of ash deposits would result in an increase in specific fuel consumption of approximately 5.2 to 6.1 percent.

8. CONCLUSIONS AND RECOMMENDATIONS

The experimental program which formed the basis for the present investigation consisted of eight ash deposition tests performed in a turbine simulator. Only seven of the tests yielded useful data relating to ash deposit formation and removal. The principle data of interest from the experiments were the ash deposit rates and the effectiveness of the ash removal events. Useful data related to gas path heat transfer were also obtained in the tests involving the water-cooled nozzle sector.

Six useful data points characterizing the ash deposition rate data were obtained. From these data, several conclusions may be drawn. The effect of increasing the gas temperature with other parameters held constant is to increase the ash deposition rate dramatically. This observation is consistent with previous investigations into the ash deposition phenomenon. The effect of decreasing the surface temperature appears, in most cases, to have resulted in decreased ash deposition rates. The only exception was the very low rate observed in test number 3. Based on these conclusions, it is recommended that in further testing an attempt be made to verify or refute the data of test number 3.

Another area which needs to be investigated further is the effect of proportionally consistant variations (i.e., relative levels are constant) in the fuel contaminant levels. The results of tests number 7 and 8 revealed that doubling the contaminant levels does not double the

ash deposition rate. This discovery could have an effect on the manner in which previous investigators interpreted test data.

It is not likely that combustion turbine engine manufacturers will make the significant committment of time and resources necessary to redesign and manufacture engines specifically for use with ash-bearing fuels. It is thus the task of research and development personnel to determine the optimum conditions under which these fuels can be burned in existing engines. Up to now, most of the data acquired in support of this effort has related to variations in the fuel composition and operating temperature and pressure of the turbine. Very little, if any, attention has been given to the combustion system and how modifications there might effect ash formation. Fuel nozzle design and fuel atomization are two areas which certainly effect ash formation and should be studied in detail. An investigation into this area is strongly recommended.

The importance of ash deposit removal characteristics has already been described. Although the data in this program are by no means complete, it appears that water-cooling does lead to enhanced cleanability of ash deposits. One of the criticisms one could make of the present on-line cleaning data, however, is that there is a lack of commonality in the tests. No direct cleaning was attempted in test number 3, and many of the recovery events documented occurred under such vastly different conditions that comparisons between them are difficult to make.

There is evidence to support the theory that the majority of the

throat area reduction observed in a turbine nozzle is due to the deposit on the pressure face of the vanes. This observation should be recognized as a significant new discovery which could not have been made without the aid of the heat transfer measurements.

From the measurements taken before, during, and after events of throat area recovery, it was observed that direct cleaning techniques affect both the pressure and suction surfaces of the vanes. The thermal excursions, however, were preferential in their effects: a Type I excursion (increased fuel flow) disturbed principally the pressure face deposits while the Type II excursion (decreased air flow) resulted in disturbances felt primarily on the suction surfaces.

It is strongly felt that the Type I thermal excursion should be examined as a candidate for on-line ash removal in combustion turbine engines. It is recommended that further turbine simulator testing be performed, and that studies regarding thermal damage resulting from excursions be undertaken.

The engine simulation model was developed and implemented as part of this investigation to aid in the interpretation of the data taken in turbine simulator tests and from field experience. This model provides a simple means of interpreting the effect of ash deposits on turbine efficiency, and subsequent extension of the results to other applications (e.g., water-cooled turbine engines). One of the conclusions drawn from application of the model is that the engine with a water-cooled turbine will suffer less performance degradation (power loss) when operating on ash-bearing fuels than its air-cooled counterpart at similar conditions.

It should be noted that the engine simulation model as presented is only approximate. Much improvement and refinement may be possible if better off-design performance data for the compressor and turbine become available. A larger base of data for field operation would also be very welcome. As these data become available, it is recommended that they be incorporated into the model.

The final item which rates some comment regards the programmatic objective. From the conclusions discussed above it appears, although the evidence is by no means complete, that water-cooling of the turbine gas path will lead to increased availability of the engine, both because of reduced performance degradation rates and enhanced ash deposit cleanability.

REFERENCES

1. Foster, A. D., Doering, H. von E., and Hickey, J. W., "Fuel Flexibility in GE Gas Turbines," Gas Turbine Reference Library publication no. GER-2222L, the General Electric Company (1977).

2. Buckland, B. O., Kindl, F. H., and Lukas, H., "Worldwide Survey of Current Experience Burning Residual and Crude Oils in Gas Turbines," AF-1243, Technical Planning Study (TPS) 78-833, prepared by Encotech, Inc. for EPRI (Dec. 1979).

3. Hefner, W. V. and Lordi, F. D., "Progress in Heavy Fuels," Gas Turbine Reference Library publication no. GER-3110A, the General Electric Company (1979).

4. Tabakoff, W., Kotwal, R., and Hamed, A., "Erosion Study in Turbomachinery Affected by Coal Ash Particles," presented at the ASME Gas Turbine Conference, London, England, April, 1978; paper no. 78-GT-136.

5. Fraas, A. P., "Survey of Turbine Bucket Erosion, Deposits, and Corrosion," presented at the ASME Gas Turbine Conference, Houston, TX, March, 1975; paper no. 75-GT-123.

6. White, A. O., "20 Years Experience Burning Heavy Fuels in Heavy Duty Gas Turbines," presented at the ASME Gas Turbine Conference, Zurich, Switzerland, April 1974; paper no. 74-GT-22.

7. Frieder, A. J., Felix, P. C., and Hess, H. J., "Experiences with Gas Turbines Burning Non-Refined Fuel Oils and Related Theoretical Investigations," presented at the ASME Gas Turbine Conference, Zurich, Switzerland, April 1974; paper no. 74-GT-12.

8. Halstead, W. D., "Calculations on the Effects of Pressure and Temperature on Gas Turbine Deposition," in Deposition and Corrosion in Gas Turbines, A. B. Hart and A. J. B. Cutler (eds.), John Wiley and Sons (1973), pp. 22-33.

9. Spengler, C. J., Lee, S. Y., and Young, W. E., "The Pressurized Passage, a Laboratory Rig for Gas Turbine Simulation," in Deposition and Corrosion in Gas Turbines, A. B. Hart and A. J. B. Cutler (eds.), John Wiley and Sons (1973), pp. 294-330.

10. Lay, K. W., "Ash in Gas Turbines Burning Magnesium-Treated Residual Fuel," Transactions, ASME, Journal of Engineering for Power, vol. 95 no. 2 April 1974, pp. 134-137.

11. Pavri, R. E., and Hill, J. M., "Thermodynamics of Heavy Fuels Operation in Gas Turbine," presented at the ASME Gas Turbine

Conference and Product Show, New Orleans, LA, March, 1980; paper no. 80-GT-171.

12. Lee, S. Y. and Spengler, C. J., "Characterization of Corrosion and Deposits in the Laboratory Gas Turbine Simulator Burning Heavy Fuels with Additives," in Ash Deposits and Corrosion Due to Impurities in Combustion Gases, R. W. Bryers (ed.), Hemisphere Publishing Corp. (1977), pp. 285-308.

13. Urbas, T. A. and Tomlinson, L. H., "Part I: Formation and Removal of Residual Fuel Ash Deposits in Gas Turbines Formed at Firing Temperatures Below 982 C (1800 F)," in Ash Deposits and Corrosion Due to Impurities in Combustion Gases, R. W. Bryers (ed.), Hemisphere Publishing Corp. (1977), pp. 309-320.

14. Urbas, T. A. and Tomlinson, L. H., "Part II: Formation and Removal of Residual Fuel Ash Deposits in Gas Turbines Formed at Firing Temperatures Above 982 C (1800 F)," in Ash Deposits and Corrosion Due to Impurities in Combustion Gases, R. W. Bryers (ed.), Hemisphere Publishing Corp. (1977), pp. 321-333.

15. Horner, M. W., Caruvana, A., Cohn, A., and Smith, D. P., "Near Term Application of Water-Cooling," presented at the ASME Gas Turbine Conference, New Orleans, LA, Mar 1980; paper no. 80-GT-159.

16. Nealy, D. A., Timmerman, W. H., and Cohn, A., "Investigation of the Influence of Contaminated Fuel on Turbine Vane Surface Deposition," presented at the AIAA/SAE/ASME 16th Joint Propulsion Conference, Hartford, CT, June, 1980; paper no. AIAA-80-1113.

17. Blanton, J. C. and Durgin, G. A., "The Effect of Heavy Liquid Fuels Ash Deposition on Heat Transfer in a Water-Cooled Gas Turbine Nozzle Sector," presented at the Joint ASME/AIChE National Heat Transfer Conference, Orlando, FL, July, 1980; paper no. 80-HT-15.

18. Blanton, J. C., Durgin, G. A., and Palko, J. E., "Heavy Fuels Ash Deposit Formation and Removal in Water-Cooled High Temperature Gas Turbines," (to be published, 1982).

19. Horner, M. W., Day, W. H., Smith, D. R., and Cohn, A., "Development of a Water-Cooled Gas Turbine," presented at the ASME Gas Turbine Conference, London, England, Apr, 1978; paper no. 78-GT-72.

20. Vermes, G., "Thermophoresis-Enhanced Deposition Rates in Combustion Turbine Blade Passages," presented at the ASME Winter Annual Meeting, San Francisco, CA, Dec, 1978; paper no. 78-WA/GT-1.

21. Junge, R. M., "The MS7001E Heavy-Duty Gas Turbine," Gas Turbine Reference Library publication GER-3116, the General Electric Company (1979).

22. Deadmore, D. L., and Lowell, C. E., "Airfoil Cooling Hole Plugging by Combustion Gas Impurities of the Type Found in Coal-Derived Fuels," NASA Lewis Research Center, Feb, 1979; NASA TM-79076.

23. Kydd, P. H., and Day, W. H., "An Ultra High Temperature Turbine for Maximum Performance and Fuels Flexibility," presented at the ASME Gas Turbine Conference, Houston, TX, March, 1975; paper no. 75-GT-81.

24. Wolf, J. C., Moskowitz, S., and Manning, G. B., "Development of a High Temperature Turbine for Operation on Coal-Derived Fuel," presented at the ASME Gas Turbine Conference, New Orleans, LA, Mar, 1980; paper no. 80-GT-188.

25. Raj, R., and Moskowitz, S. L., "Transpiration Air Protected Turbine Blades - An Effective Concept to Achieve High Temperature and Erosion Resistance for Gas Turbines Operating in an Aggressive Environment," presented at the ASME Gas Turbine Conference, London, England, April, 1978; paper 78-GT-100.

26. Suo, M., "Turbine Cooling," in The Aerothermodynamics of Aircraft Gas Turbine Engines, Gordon C. Oates (ed.), AFAPL-TE-78-52, Wright Patterson Air Force Base (July, 1978), chap. 19.

27. Taylor, J. R., "Heat Transfer Phenomena in Gas Turbines," presented at the ASME Gas Turbine Conference, New Orleans, LA, March, 1980; paper no. 80-GT-172.

28. Hill, P. G., and Peterson, C. R., Mechanics and Thermodynamics of Propulsion, Addison-Wesley (1965), chap. 3.

29. Holman, J. P., Experimental Methods for Engineers, McGraw Hill (1971), chap. 3.

30. Holman, J. P., Heat Transfer, 4th ed., McGraw Hill (1976), chap. 5.

31. Barnes, J. F., and Edwards, J. P., "Cooled Gas Turbine Blades," in Combustion and Heat Transfer in Gas Turbine Systems, E. R. Norster (ed.), Pergamon Press (1969), pp. 169-182.

32. Jermanok, J., "The MS6001 - A New Gas Turbine for Power Generation," Gas Turbine Reference Library publication no. GER-222L, the General Electric Company (1979).

33. Dixon, S. L., Fluid Mechanics, Thermodynamics of Turbomachinery, 3rd ed., Pergamon Press (1978), chap. 4.

APPENDIX

CYCLE ANALYSIS OF SINGLE-SHAFT SIMPLE-CYCLE COMBUSTION TURBINE ENGINE

Appendix Nomenclature

English Symbols

a_k	constants in eqs. (A.5-A.8)
B	turbine blockage factor
c_{p0i}	Specific heat for gas at station i
e	compressor air flow fraction used for turbine cooling
e_1	compressor air flow fraction used for first-stage turbine cooling
f	fuel/air ratio
f	symbol indicating mathematical function
HR	engine net heat rate
$\dot{m}$	mass flow rate
N	engine rotational speed
p_{0i}	stagnation pressure at station i
q_f	lower heating value of fuel
q_{34}	heat transfer per unit mass in turbine first stage nozzle
T_{0i}	stagnation temperature at station i
$\dot{W}$	power

Greek Symbols

γ_{ij}	specific heat ratio used for process from stations i to j
η	efficiency

Subscripts

a	air
b	burner (combustor)
c	compressor
d	design
max	maximum
min	mass flow corresponding to maximum pressure ratio in compressor
net	net output for engine
o	combined mechanical and auxiliary
p	combustion products
t	turbine

A. Air-Cooled Turbine

A schematic diagram of the single-shaft, simple-cycle combustion turbine engine with an air-cooled turbine is shown in Fig. A1. The numbering scheme used for the state points is as shown in the figure. The following assumptions were made for the cycle analysis:

1. The working substances (air and combustion products) were assumed to be ideal gases. Variable specific heats were used, although a fixed value was used at each state point. The specific heat values were chosen to yield the appropriate gas enthalpies at rated engine conditions.

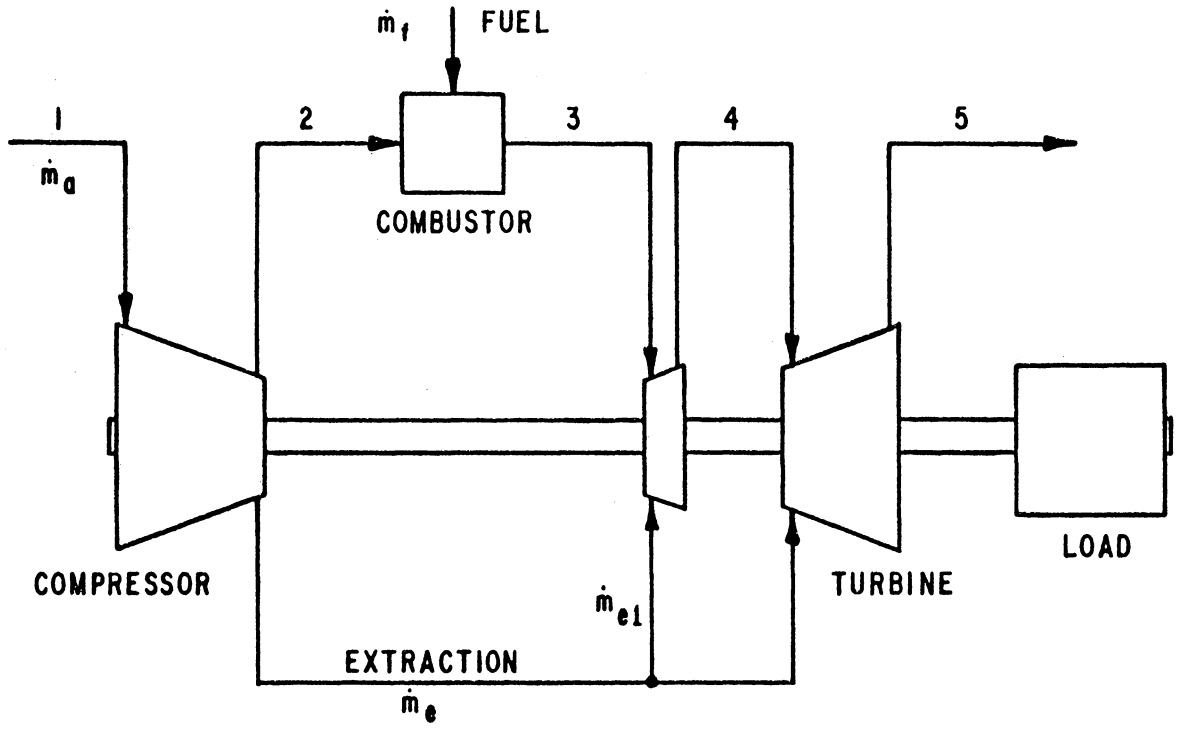

FIGURE A1

AIR-COOLED COMBUSTION TURBINE ENGINE SCHEMATIC

2. Stagnation temperature and pressure losses between engine components were divided such that for the analysis they became part of the component performance characteristics. As a result, only one state point exists between the compressor and combustor, the combustor and turbine, etc.

3. Stagnation pressure losses in the compressor inlet and the turbine exhaust diffuser were assumed to be included in the total-to-total efficiencies of the compressor and turbine, respectively. The compressor inlet conditions were thus the temperature and pressure of the atmospheric air, and the turbine exhaust pressure is atmospheric.

4. Both the compressor and turbine are assumed to be adiabatic.

The performance characteristics of the compressor and turbine must be known. These are generally of the form

For compressor:

$$\frac{P_{02}}{P_{01}} = f_1 \left(\frac{\dot{m}_a \sqrt{T_{01}}}{P_{01}}, \frac{N}{\sqrt{T_{01}}} \right) \qquad \text{(A.1)}$$

$$\eta_c = f_2 \left(\frac{\dot{m}_a \sqrt{T_{01}}}{P_{01}}, \frac{N}{\sqrt{T_{01}}} \right) \qquad \text{(A.2)}$$

For turbine:

$$\frac{P_{03}}{P_{05}} = f_3 \left(\frac{\dot{m}_p \sqrt{T_{03}}}{P_{03}}, \frac{N}{\sqrt{T_{03}}} \right) \tag{A.3}$$

$$\eta_t = f_4 \left(\frac{\dot{m}_p \sqrt{T_{03}}}{P_{03}}, \frac{N}{\sqrt{T_{03}}} \right) \tag{A.4}$$

For the cases of interest, the engine speed is a constant and the component performance characteristics become functions only of the "dimensionless" mass flow rates. Algebraic approximations were made given by the following equations:

for compressor:

$$\frac{P_{02}}{P_{01}} = \left\{ 1 - a_1 \left[\frac{(\dot{m}_a \sqrt{T_{01}}/P_{01})}{(\dot{m}_a \sqrt{T_{01}}/P_{01})_d} - \frac{(\dot{m}_a \sqrt{T_{01}}/P_{01})_{min}}{(\dot{m}_a \sqrt{T_{01}}/P_{01})_d} \right]^2 \right\} \left[\frac{P_{02}}{P_{01}} \right]_{max} \tag{A.5}$$

$$\eta_c = \left\{ 1 - a_2 \left[\frac{(\dot{m}_a \sqrt{T_{01}}/P_{01})}{(\dot{m}_a \sqrt{T_{01}}/P_{01})_d} - 1 \right]^2 \right\} (\eta_{c,d}) \tag{A.6}$$

for turbine:

$$\frac{\dot{m}_p \sqrt{T_{03}}}{P_{03}} = a_3 (1 - B) \sqrt{1 - \left(\frac{P_{05}}{P_{03}}\right)^2} \left[\frac{\dot{m}_p \sqrt{T_{03}}}{P_{03}} \right]_d \tag{A.7}$$

$$\eta_t = a_4 \tag{A.8}$$

With the compressor and turbine characteristics quantified, the cycle analysis can be performed. The procedure is as follows.

1. The operating conditions for the combustion turbine engine are chosen. These are the inlet conditions (T_{01}, p_{01}), the turbine exhaust control temperature T_{05}, and the ash-affected turbine parameters (the blockage B and efficiency η_t).

2. A compressor mass flow is assumed. The compressor pressure ratio is then determined using eq. (A.5) and the efficiency is determined using eq. (A.6). The compressor discharge temperature and power requirement are then determined using

$$T_{02} = T_{01} \left[1 + \frac{1}{\eta_c} \left[\left(\frac{p_{02}}{p_{01}} \right)^{\frac{\gamma_{12}-1}{\gamma_{12}}} - 1 \right] \right] \tag{A.9}$$

$$\dot{W}_c = \dot{m}_a \left(c_{p01} T_{01} - c_{p02} T_{02} \right) \tag{A.10}$$

3. The turbine inlet pressure and turbine pressure ratio are determined using the assumed combustor pressure loss.

$$p_{03} = \left[1 - \left(\frac{p_{02} - p_{03}}{p_{02}} \right) \right] p_{02} \tag{A.11}$$

$$\frac{p_{03}}{p_{05}} = \frac{p_{03}}{p_{01}} \tag{A.12}$$

4. A fuel/air ratio is assumed for the combustor. From this the mass flow rate of combustion products is determined.

$$\dot{m}_p = (1 + f)\, \dot{m}_a \tag{A.13}$$

Equation (A.7), in rearranged form, is then used to determine the turbine inlet temperature.

$$T_{03} = \left[\frac{P_{03}}{\dot{m}_p} a_3 (1 - B) \sqrt{1 - \left(\frac{P_{05}}{P_{03}} \right)^2} \right]^2 \tag{A.14}$$

5. From an energy balance of the combustor, the assumed value of the fuel/air ratio may be checked.

$$f = \frac{c_{p03} T_{03} - c_{p02} T_{02}}{\eta_b q_f - c_{p03} T_{03}} (1 - e) \tag{A.15}$$

Steps 4 and 5 are repeated to obtain convergence of the fuel/air ratio.

6. The turbine exit temperature is determined using

$$T_{05} = T_{03} \left[1 - \eta_t \left[1 - \left(\frac{P_{05}}{P_{03}} \right)^{\frac{\gamma_{35}-1}{\gamma_{35}}} \right] \right] \tag{A.16}$$

This value is checked against the chosen control value. If agreement is not obtained, the air flow (step 2) is adjusted. Steps 2 through 6 are repeated to obtain convergence of the turbine exhaust temperature.

7. The turbine firing temperature is determined from an energy balance of the turbine first-stage nozzle.

$$T_{04} = \frac{(1 + f - e)\, c_{p03}\, T_{03} + e_1\, c_{p02}\, T_{02}}{(1 + f - e + e_1) c_{p04}} \tag{A.17}$$

8. The turbine power output, engine net power output, and engine heat rate are determined as follows:

$$\dot{W}_t = \dot{m}_a\, [(1 + f - e)\, c_{p03}\, T_{03} + e c_{p02}\, T_{02} - (1 + f)\, c_{p05}\, T_{05}] \tag{A.18}$$

$$\dot{W}_{net} = \eta_o\, (\dot{W}_c + \dot{W}_t) \tag{A.19}$$

$$HR = \frac{f \dot{m}_a q_f}{\dot{W}_{net}} \tag{A.20}$$

The cycle analysis for the chosen operation conditions in step 1 is now complete.

B. Water-Cooled Turbine

A schematic diagram of a single-shaft simple cycle combustion turbine engine with a water-cooled first-stage turbine nozzle is shown in Fig. A2. The engine was assumed to have the same component performance characteristics as the air-cooled MS7001B engine. The turbine firing temperature (T_{04}) was taken to be the same as for the previous

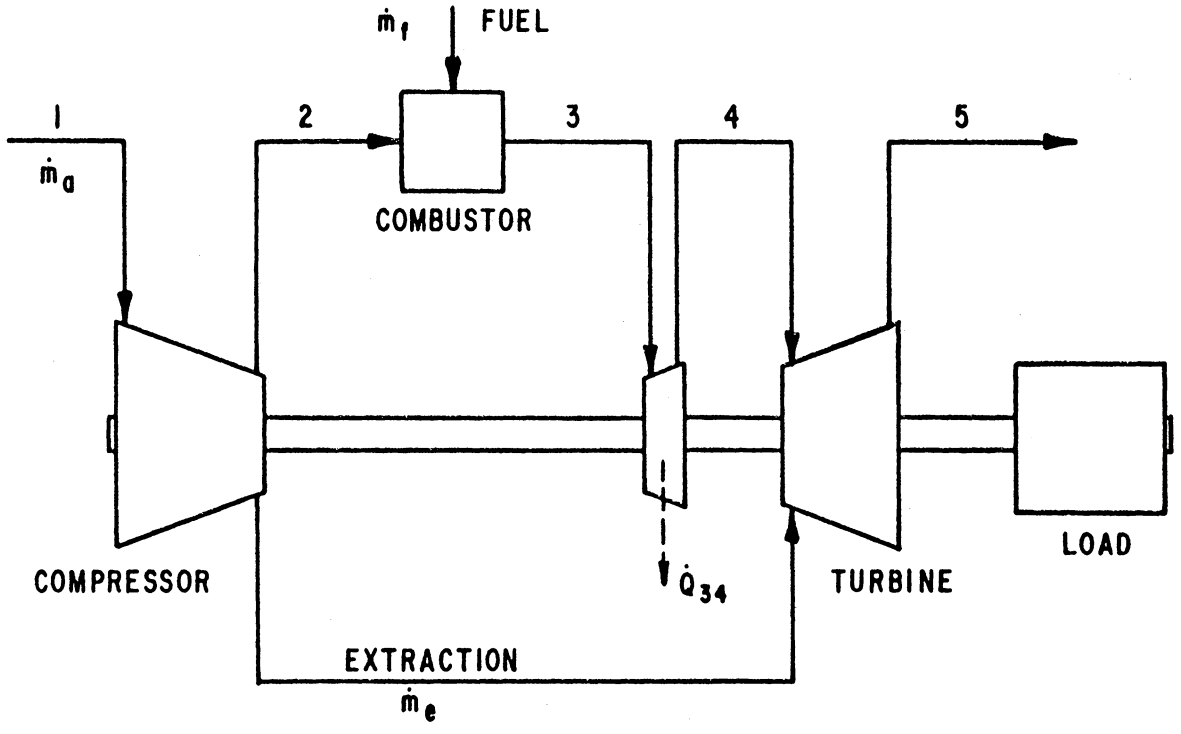

FIGURE A2

WATER-COOLED COMBUSTION TURBINE ENGINE SCHEMATIC

case. The remainder of the turbine beyond the first-stage nozzle was assumed to be cooled exactly as the previous case.

The cycle analysis for the water-cooled turbine engine proceeds under the same assumptions as the air-cooled turbine engine, and steps 1 through 6 of the analysis are the same. In step 7 the turbine firing temperature is evaluated by considering the heat transfer by water-cooling:

$$T_{04} = \frac{c_{p03} T_{03} - q_{34}}{c_{p04}} \tag{A.21}$$

The turbine power in step 8 is evaluated using:

$$\dot{W}_t = \dot{m}_a [(1 + f - e) c_{p03} T_{03} + e c_{p02} T_{02} - (1 + f) c_{p05} T_{05} - (1 + f - e) q_{34}] \tag{A.22}$$

Net engine power and heat rate are determined as before.

The two page vita has been removed from the scanned document. Page 1 of 2

The two page vita has been removed from the scanned document. Page 2 of 2

AN INVESTIGATION OF RESIDUAL FUEL OIL ASH DEPOSIT FORMATION AND REMOVAL IN COOLED GAS TURBINE NOZZLES

by

John Clisby Blanton

(ABSTRACT)

Results are reported from a series of experiments simulating the combustion and expansion processes of a heavy-duty combustion turbine engine burning a heavy residual fuel oil. The tests were carried out in a turbine simulator device, consisting of a combustion chamber and a turbine first-stage nozzle cascade sector. Both film, air-cooled and closed-circuit, water-cooled nozzle sectors were tested. These sectors were four-vane, three-throat sections with throat cross-sectional areas of approximately 50 (10^{-4}) m^2. The test fuel was simulated by adding the appropriate contaminants to no. 2 fuel oil.

A series of seven full-length tests were performed, ranging in length from 22.5 to 88.2 hours. Four of the tests involved the water-cooled nozzle sector and the remaining three used the air-cooled nozzle. The principle objectives of the tests were to assess the rate at which ash accumulates in the turbine nozzle and the relative difficulty in removing these deposits. The variable used to evaluate the extent of the ash deposit on the nozzle was the effective throat area, determined using the calculated gas flow rates, turbine nozzle inlet temperature, and the measured combustion chamber pressure. The parameters varied in

the test program, other than the nozzle sectors, were the gas temperature and the gas pressure. The gas pressure variations served to vary the gas path surface temperatures at constant gas temperature.

The test conditions were nominal turbine firing (nozzle exit) temperatures of 1283 and 1394 K and combustor pressures of 3 and 6 atmospheres. A 2-to-1 pressure ratio was maintained across the nozzle to insure sonic conditions at the throat sections. With the exception of one test, the data show that the deposit rates in the water-cooled turbine nozzle were lower than in the air-cooled nozzle. The effect of increasing the gas temperature was to dramatically increase the ash deposition rates. Decreased gas pressures (and hence surface temperatures) resulted in reduced deposition rates. Ash cleanability was enhanced by water-cooling.

Heat transfer data were analyzed from the water-cooled tests and gave significant insight into the ash deposit formation and removal phenomena. One of the more significant conclusions drawn from these data was that the major portion of the effective area decrease observed in a turbine nozzle because of ash deposits is due to the pressure face deposits.

A computer simulation of a combustion turbine engine was developed to aid in the evaluation of the turbine simulator test data. Results from field tests of full-sized production engines burning residual oil were used in the simulation to determine the relationship between the extent of ash deposition (throat area reduction) and turbine efficiency. This result was then combined with data from the turbine simulator tests

to produce a real-time computer simulation of full-sized combustion turbine engines having air- and water-cooled first-stage turbine nozzles. It was found that water-cooling of the turbine nozzle would result in an increase in engine availability of 27 per cent when operating on heavy residual fuel oil.